Image Processing for Enhancement of Ischemic Stroke in Computed Tomography Examinations

Allan Felipe Fattori Alves

UNIVERSITÉ D'ORLÉANS

ÉCOLE DOCTORALE SANTE, SCIENCES BIOLOGIQUES ET CHIMIE DU VIVANT

Laboratoire Imagerie Multimodale Multiéchelle et Modélisation du Tissu Osseux et articulaire

THÈSE présentée par :

Allan Felipe FATTORI ALVES

soutenue le : **25 février 2019**

pour obtenir le grade de : **Docteur de l'université d'Orléans**

Discipline/ Spécialité : **Traitement du Signal et des Images**

Image Processing for Enhancement of Ischemic Stroke in Computed Tomography Examinations

THÈSE dirigée par:

Rachid JENNANE Professeur, Université d'Orléans
Diana Rodrigues PINA Professeur, São Paulo State University

RAPPORTEURS:

Odemir Martinez BRUNO MCF-HDR, University of São Carlos
Antoine VACAVANT MCF-HDR, Université Clermont-Auvergne

JURY:

Sergio Barbosa DUARTE Professeur, Centro Brasileiro de Pesquisa Física, Président du jury
Rachid JENNANE Professeur, Université d'Orléans, directeur de thèse
Diana Rodrigues PINA Professeur, São Paulo State University, Directeur de thèse
Odemir Martinez BRUNO MCF-HDR, University of São Carlos
Antoine VACAVANT MCF-HDR, Université Clermont-Auvergne

This research was conducted in the Department of Imaging Diagnosis in Botucatu Medical School (São Paulo State University-Brazil), located at Instituto de Biociências de Botucatu, Departamento de Física e Biofísica, UNESP—São Paulo State University, P.O. BOX 510, Distrito de Rubião Junior S/N, Botucatu, São Paulo 18618-000,Brazil.

It was also conducted in the I3MTO Laboratory, located at University of Orléans, 5 Rue de Chartres, BP 6744, 45072 Orléans, France.

The Research Ethics Committee according to Brazilian regulations (CAAE: 52457315.3.0000.5411) approved all images and patient information used in this research.

The retrospective examinations of computed tomography used in this study were all obtained from Botucatu Medical School.

Abstract

Stroke is one of the highest causes of death worldwide. In Brazil, stroke is the leading cause of death, and in 2009, it was responsible for 10.2% of deaths recorded. Non-enhanced computed tomography (CT) and nuclear magnetic resonance imaging (MRI) are the two main imaging techniques used to detect stroke. CT has a lower cost and greater accessibility of the population, so it is still the main method used. In most cases, the assessment of the compromised brain area is performed subjectively and may lead to difficulties in diagnosis. This research work proposes an approach based on a computational algorithm, highlighting regions of ischemic stroke. Different image processing methods were used to enhance ischemic tissues. A set of 41 retrospective CT scans from Botucatu Medical School (Brazil) was used, divided into 25 cases of acute ischemic stroke and 16 normal patients. Stroke cases were obtained within 4.5 h of symptom onset. After selection of CT slices, image averaging was performed to reduce the noise. This was followed by a variational decomposition model and the expectation maximization method was applied to generate enhanced images. We determined a test to evaluate the performance of observers in a clinical environment with and without the aid of enhanced images. The overall sensitivity of the observer's analysis was 64.5 % and increased to 89.6 % and specificity was 83.3 % and increased to 91.7 %. These results show the importance of a computational tool to assist neuroradiology decisions, especially in critical situations such as the diagnosis of ischemic stroke.

Key words: Stroke . Brain . Algorithms . Computed Tomography . Early diagnosis

Resumo

O acidente vascular cerebral (AVC) é uma das maiores causas de morte em todo o mundo. No Brasil, o AVC é a principal, sendo que em 2009, foi responsável por 10,2% das mortes registradas. A tomografia computadorizada (TC) e a ressonância magnética nuclear (RMN) são as duas principais técnicas de imagem usadas para detectar o AVC. A TC tem um custo menor e maior acessibilidade da população, por isso ainda é o principal método de avaliação do acidente vascular cerebral. A avaliação do cérebro comprometido é realizada de forma subjetiva e pode levar à dificuldades no diagnóstico. Esta pesquisa propõe a implementação de um algoritmo computacional, destacando regiões de AVC isquêmico. Diferentes métodos de processamento de imagem foram utilizados para melhorar a visualização do tecido isquêmico. Um conjunto de 41 tomografias retrospectivas obtidas na Faculdade Medicina de Botucatu foram utilizadas, divididas em 25 casos de AVC isquêmico e 16 pacientes controle. Os casos de AVC foram obtidos dentro de 4,5 horas após os primeiros sintomas. Após a seleção dos *slices* com a possível presença de AVC, tais *slices* foram somados resultando em um único *slice* com valores médios de forma a reduzir o ruído. Isto foi seguido por um modelo de decomposição variacional onde se mantiveram componentes de interesse da imagem. O método de maximização de expectativas foi aplicado para gerar imagens melhoradas. Determinamos um teste de desempenho de observadores em um ambiente clínico. A sensibilidade geral da análise observacional foi de 64,5% e aumentou para 89,6% e especificidade foi de 83,3% e aumentou para 91,7% quando usadas imagens originais e realçadas, respectivamente. Estes resultados mostram a importância de uma ferramenta computacional para auxiliar as decisões de neuroradiologia, especialmente em situações críticas, como o diagnóstico de AVC isquêmico.

Palavras-chave: acidente vascular cerebral, processamento de imagens, tomografia computadorizada, diagnóstico precoce

Résumé

Traitement d’images pour le rehaussement de l'AVC ischémique sur des examens de tomographie

L’Accident Vasculaire Cérébral (AVC) est l'une des principales causes de décès dans le monde. Au Brésil, les AVC sont la cause principale de décès. En 2009, ils étaient responsables de 10,2% des décès enregistrés. Le scanner et l'Imagerie par Résonance Magnétique (IRM) sont les deux principales techniques d'imagerie utilisées pour détecter les AVC. L’examen par scanner a un coût inférieur et une plus grande accessibilité à la population, il reste donc la principale méthode de diagnostic. Dans la plupart des cas, l'évaluation de la région cérébrale compromise est effectuée de manière subjective et peut entraîner des difficultés pour déterminer la région atteinte. Ce travail de thèse propose une approche basée sur un algorithme permettant de mettre en évidence les régions atteintes d’AVC ischémique dans les examens de scanner rétrospectifs. Différentes méthodes de traitement des images ont été utilisées pour réhausser les régions des tissus ischémiques. Afin de permettre aux médecins moins expérimentés de détecter de manière fiable les signes précoces AVC, une nouvelle approche est proposée pour améliorer la perception visuelle de l’accident ischémique cérébral sur des images scanner. Une série de 41 images scanner rétrospectifs ont été utilisées, réparties en 25 cas d’AVC ischémiques et 16 patients normaux. Les cas d'AVC ont été obtenus dans les 4,5 heures suivant l'apparition des symptômes. Après la sélection des coupes importantes, une moyenne d'image est effectuée pour réduire le bruit. Ensuite, un modèle de décomposition variationnelle est appliqué afin de conserver la composante pertinente de l'image. Enfin, un algorithme d’espérance-maximisation est appliqué afin de générer des images rehaussées. Un test est proposé afin d’évaluer la performance des observateurs dans un environnement clinique avec et sans l'aide d'images rehaussées. La sensibilité globale de l'analyse de l'observateur a été améliorée de 64,5% à 89,6% et la spécificité de 83,3% à

91,7%. Ces résultats montrent l'importance d'un outil informatique d'aide à la décision en neuroradiologie, notamment dans les situations critiques telles que le diagnostic d'accident ischémique cérébral.

Mots clés: Accident vasculaire cérébral. Cerveau. Algorithmes. Scan tomographique. Diagnostic précoce.

Acknowledgments

This research is dedicated to all those people and families who suffered from stroke and their consequences.

I wish to thank my parents, Olavo Alves Filho and Nádia Maria Fattori, and my sister Allana Caroline Fattori Alves for providing support, care and eternal love.

I wish to thank Associate Professor Diana Rodrigues de Pina for her excellent guidance, patience, dedication, effort and friendship during all her years as my advisor. Thank you.

I wish to thank Full Professor José Ricardo de Arruda Miranda for his wisdom and dedication during all this years of partnership.

I wish to thank Professor Rachid Jennane, for having welcomed me with such dedication in France and for having contributed immeasurably in this research.

I wish to thank Professor Odemir Bruno and Prof Antoine Vacavant for their great revision of this manuscript and for their participation in the defense jury. I also wish to thank Professor Sergio Barbosa Duarte for his participation in the defense jury, and for his support in this research.

I wish to thank all my colleagues, Fouad, Masnsen, Nourhene and all the others in the I3MTO Laboratory in Université d'Orléans. You made my staying in France very pleasant and happy. Moreover, a special thank, for my greatest friend Mohamed Hafri, for saving my life more times than I could count. Thank you, mate.

I wish to thank Professor Carlos Clayton Macedo de Freitas for his friendship and dedication in this research.

I wish to thank Professor Nitamar Abdala and Professor João Altemani for their support and dedication ever since the beginning of this research.

I wish to thank all my dearest friends from LAFAR and BIOMAG Laboratories at São Paulo State University for their excellent companionship and essential aid in this work. A special thanks for my dearest friends Ana Luiza Menegatti Pavan, Fernando Bacchim Neto, Guilherme Giacomini and Maria Eugênia Dela Rosa, for their effort in helping me in all those years of partnership. Thank you.

I wish to thank all of those who directly or indirectly collaborated to the conclusions of this research.

I wish to thank the Brazilian foundation, *Fundação de Amparo à Pesquisa do Estado de São Paulo* (FAPESP), for all the financial support in this research.

Summary

Figure List

Table List

Abbreviation List

ASPECTS – Alberta Stroke Program Early CT Score

CT – Computed Tomography

CAD – Computer Aided-Diagnosis

CPU – Central Processing Unit

CBF – Cerebral Blood Flow

DICOM – Digital Imaging and Communications in Medicine

EM – Expectation Maximization

E1 – Experienced Radiologist 1

E2 – Experienced Radiologist 2

HCFMB- Botucatu Medical School

I3MTO – Imagerie Multimodale Multiéchelle et Modélisation du Tissu Osseux et articulaire

LAFAR – Laboratory of Physics Applied to Radiodiagnosis

MCA - Middle Cerebral Artery

MRI – Magnetic Resonance Imaging

MS – Mean-shift

NECT – Non-enhanced Computed Tomography

NIHSS - National Institute of Stroke Scale

VM – Variational Model

HU – Hounsfield Units

TP – True Positive

TN – True Negatives

FP – False Positives

FN – False Negative

rt-PA - Tissue Plasminogen Activator

R1 – Resident 1st Year

R2 – Resident 1st Year

R3 – Resident 2nd Year

R4 – Resident 3rd Year

UNESP – São Paulo State University

Chapter 1

1. Introduction

This thesis is the result of a joint supervision agreement between São Paulo State University (UNESP) in Brazil and the University of Orleans in France. The research was developed at Botucatu Medical School (HCFMB-UNESP) under the guidance of Associated Professor Diana Rodrigues de Pina, and at the I3MTO Laboratory of the University of Orleans, France, under the guidance of Professor Rachid Jennane.

Prof. Diana Pina is a Professor in medical imaging and coordinator of the Laboratory of Applied Physics in Radiodiagnosis (LAFAR) of Botucatu Medical School (Brazil). Botucatu Medical School has a service coverage that includes the Regional Health Department (DRS VI) with a population of approximately 1,623,027 inhabitants. The Diagnostic Imaging Section of Botucatu Medical School has a vast infrastructure of diagnostic imaging equipment such as computed tomography (CT) scanners, which generated images for this research. The HCFMB-UNESP has two Toshiba Activion 16-channel CT scanners and one General Electric 64-channel CT scanner. All retrospective examinations of CT in this study were obtained from the Diagnostic Imaging Department of Botucatu Medical School (UNESP).

Prof. Rachid Jennane is a full Professor of image processing at the University of Orleans (France) where he is affiliated to the I3MTO (Imagerie Multimodale Multiéchelle et Modélisation du Tissu Osseux et Articulaire) Laboratory.

This research also counted on the clinical and scientific support of Prof. Carlos Clayton Macedo de Freitas (neurosurgeon HCFMB-UNESP), from Prof. Nitamar Abdala, Head of the Diagnostic Imaging Department of the Paulista School of Medicine (UNIFESP) and President of the Institute of Diagnostic Imaging Foundation, and Dr. João Altemani, radiologist of the Department of Radiology of UNICAMP. All those Brazilian physicians participated actively in the study design as well as in the image evaluation, discussion of cases, and in the writing of the scientific paper related to the results presented in this thesis.

This research proposes the implementation of an image segmentation system, highlighting areas of ischemic stroke in CT scans. A computational tool has been developed that can assist radiologists and neuroradiologists to make a safer and more accurate decisions in the detection of stroke. Computational algorithms were developed to improve image contrast, to reduce noise, and to highlight the regions affected by ischemic stroke. There was a comparison analysis between original images and those highlighted by the computational algorithm, named enhanced images, which resulted in a better visualization of stroke signs when analyzed by different radiologists.

The great differential of this proposal is to associate different methods of image processing and to optimize them to improve the visualization and to perform the enhancement of stroke. In this sense, we still propose a comparison between the objective analysis of the radiologists with and without the use of enhanced images of stroke cases. All these factors will contribute to a more accurate and safe diagnosis of stroke. This research was possible due to the interdisciplinary team composed of neurologists, neurosurgeons, radiologists, and medical physicists. The following is a summary of the chapters of this PhD thesis.

Chapter 1 is composed of the introduction to the thesis and describes the primary and specific objectives addressed in this research.

Chapter 2 depicts the theoretical foundations for a better understanding of the subsequent chapters. Some concepts that will be addressed in Chapter 2 are stroke characteristic's and diagnostic modalities used for diagnosing it; digital imaging concepts and some computational methods applied in the last 20 years to enhance the visual perception of ischemic stroke in different imaging methods.

Chapter 3 brings the material and methods since it describes all image-processing methods used in this research, and presents the database and image selection criteria that resulted in the cohort of patients. Each step of our proposed approach is also detailed, and a section is dedicated to experiments with observers that analyzed enhanced images and compared them with raw images of stroke and control cases.

Chapter 4 brings all detailed results from the application of the computational algorithm in CT scan images, as well as the results from the observer's evaluation both before and after the use of enhanced images to diagnose stroke and control cases. Still, in Chapter 4 we compared the results achieved with previous results found in literature, together with other aspects relevant to the discussion.

In addition, in Chapter 5 brings the major and minor conclusion to this research, responding to all the steps proposed in the objectives section. And also the perspectives for future studies concerning stroke detection.

Chapter 6 is dedicated to the bibliography used in this research.

Furthermore, there are five appendices in this thesis.

Appendix 1 brings the document from the approval of the Brazilian Ethics Committee.

Appendix 2 and 3 summarize the tables with the complete results from the subjective evaluations for all observers both before and after the analysis of enhanced images.

Appendix 4 shows the final paper of this research published in April of 2018 in European Radiology, named "Ischemic Stroke Enhancement using a Variational Model and the Expectation Maximization Method."

Appendix 5 brings all the other papers published by the author during the period of the PhD.

1.1 Objectives

This research aims to contribute to the detection of stroke in CT scans through image processing techniques to improve image quality, to objectively highlight and enhance areas affected by ischemic stroke.

This primary objective is divided into specific objects cited below:

- Construction of a database with retrospective CT examinations of patients with confirmed ischemic stroke. The database was obtained in the Computed Tomography Department of Botucatu Medical School.
- Development of computational algorithms in Matlab® environment to enhance brain areas of interest (normal brain, ischemic stroke) and improve their visualization in the previously selected CT exams;
- Comparison of three different segmentation methods (Expectation Maximization, K-means, and Mean-shift) to achieve the best enhancement in ischemic stroke cases;

- Comparison of the results obtained between the developed computational algorithm and the subjective diagnostic evaluation of the stroke performed by radiologists both with and without the aid of enhanced images.

Chapitre 1 - Résumé

Le chapitre 1 introduit et décrit les chapitres suivants ainsi que les objectifs principaux de la thèse.

Ce travail de recherche vise à contribuer à la détection des accidents vasculaires cérébraux dans les scans tomographiques (CT: Computed Tomography) en utilisant des techniques de traitement d'images. Pour ce faire, quatre objectifs principaux ont été fixés :

- Construction d'une base de données avec examens CT rétrospectifs ;
- Développement d'algorithmes sous l'environnement Matlab® pour améliorer les zones d'intérêt du cerveau et améliorer leur visualisation ;
- Etude comparative entre trois méthodes de segmentation différentes ;
- Comparaison entre les résultats obtenus à l'aide de l'algorithme proposé et de l'évaluation diagnostique subjective effectuée par les radiologues.

Chapter 2

2. Context and Theoretical Fundaments

The subjects dealt with in this section will be briefly reviewed in order to introduce necessary theoretical foundations for understanding objectives and methodology developed in this research.

2.1. Stroke

The human brain has a limited supply of nutrients such as oxygen and glucose. The average brain function relies mostly on adequate perfusion by the cerebral circulation. It is for this reason that cerebral vascular tone is intensely regulated, and alterations in mechanisms that modulate cerebral vessel function can predispose to cerebrovascular disease and stroke (James C. Grotta, 2016).

Stroke occurs with an abrupt onset of focal or global neurologic symptoms caused by ischemia or hemorrhage. The terminology ‘stroke’ comprises several cerebrovascular diseases from thromboembolic events and aneurysmal subarachnoid hemorrhage to sinovenous occlusions (Osborn, 1999).

Stroke mainly affects individuals over 60 years of age. It is considered the most significant cause of death worldwide (Health, 2007, Garritano et al., 2012). Between November 2011 and October 2012, approximately 170 thousand individuals were admitted in Brazilian hospitals with stroke symptoms. In Brazil, stroke is the leading

cause of death, and it was responsible for 10.2% of all deaths registered (Abreu et al., 2010, Garritano et al., 2012, Lavados et al., 2007).

The global impact of stroke on the years of life free of functional disability is significant, occupying the sixth place among all diseases, and is expected to occupy the fourth place in 2020 (Yusuf et al.al., 2001). Studies estimate that 70% of stroke patients do not return to their work and that 30% will require help even to walk afterward, which represents a high socioeconomic impact in society. The high degree of disability is directly related to the poor quality of life in individuals that survived stroke (Cerniauskaite et al., 2012).

There are four major types of stroke mostly caused by acute occlusion of a cerebral artery. Table 1 depicts the most common types of stroke with its corresponding frequency.

Table 1 - Etiology of stroke with its frequency of occurrence.

Type	***Percentage (%)***
Cerebral ischemia	80-85
Primary intracranial hemorrhage	15
Nontraumatic subarachnoid hemorrhage (aneurysm)	5
Cerebral venous thrombosis (sinovenous occlusion)	1

Ischemia describes the condition where blood flow decreases with the temporary or permanent loss of organ functions. Cerebral ischemia occurs with diminished blood flow

to all brain parts or selected regions (regional or focal). Ischemic stroke, which corresponds to more than 80% of all cases, is a result of blockage or obstruction of vessels that supply blood to the brain (Association, 2014, Tajiri et al., 2012).

Figure 1 illustrates the main arteries that supply blood to the brain, and a foreign mass traveling through the bloodstream until it stops in a small artery causing an ischemic stroke. This occurrence deprives the brain of oxygen and nutrients and initiates a dynamic sequence of pathophysiological events. When the interruption of blood flow occurs, it causes cell death and an irreversibly injured infarct core (Powers William et al., 2015).

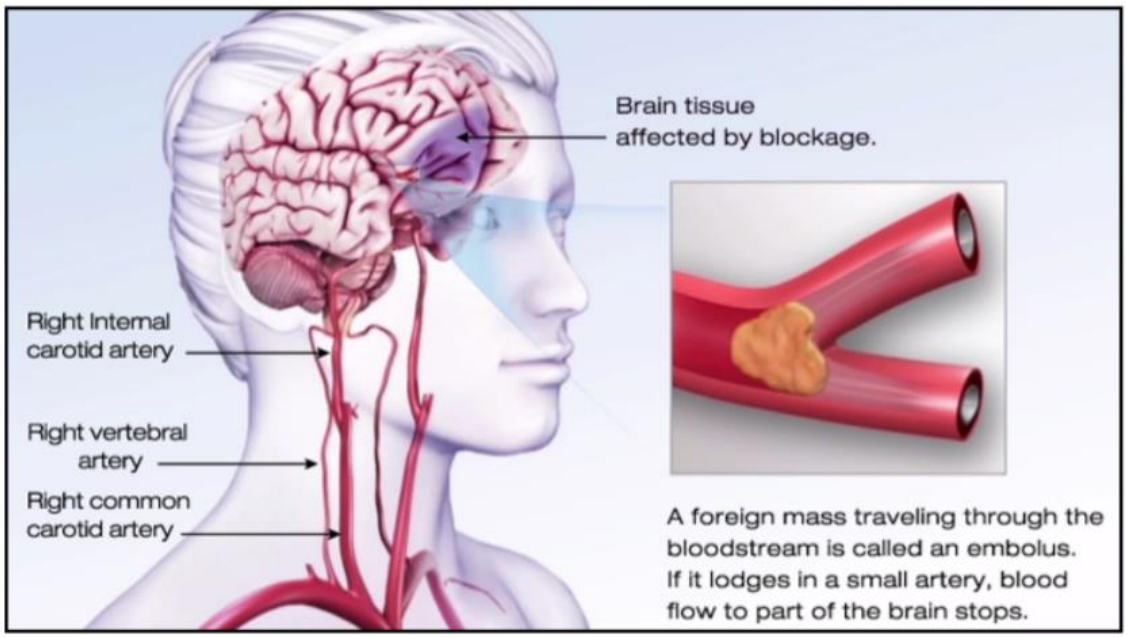

Figure 1 - Ischemic stroke illustration (Powers William et al., 2015).

If the blood supply is not that severe or it lasts for a short period, then the brain tissue may be recovered. Brain tissue may survive when blood flow restores quickly enough. Ischemic penumbra accounts for this potentially reversibly damaged brain tissue that surrounds the ischemic lesion core (TD, 1980). When blood flow is not restored the penumbral tissue will proceed to infarction, and the original core lesion will grow. When

a more substantial portion of the brain is affected, functional disability might appear and be permanently damaged (Powers William et al., 2015).

Cerebral ischemia manifestations include some predictors including the duration of the event, its location, tissue volume affected and how much the flow decreases Due to an ischemic event, an area of coagulation necrosis can occur, which is called infarct. The process by which an infarct develops is the infarction. There are two different areas in acute infarcts: the central ischemic core, and the ischemic penumbra, lying in the peripheral zone (Osborn, 1999).

The region of low perfusion (core) in which cells have lost their membrane potential is surrounded by the penumbra where intermediate perfusion prevails, and cells depolarize intermittently ("peri-infarct depolarization"), as can be seen in Figure 2.

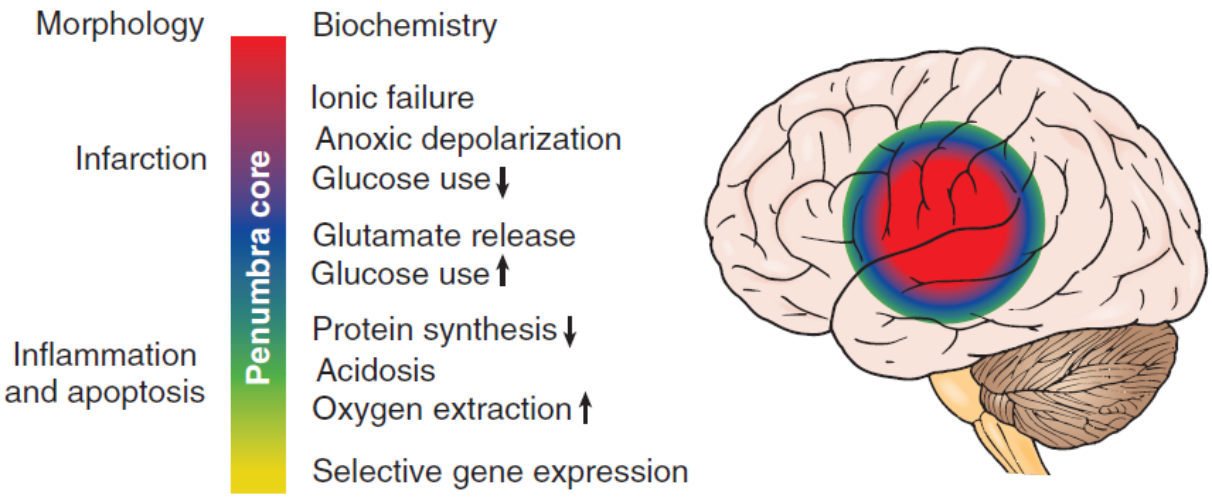

Figure 2 – Representation of the core and penumbra of ischemic stroke accompanied by pathophysiological events occurring in both regions (James C. Grotta, 2016, Longa et al., 1989).

Hemorrhagic stroke, which occurs in 13% of cases, is caused by the rupture of a vessel followed by the diffusion of the blood through brain tissues. This type of stroke accounts

for 37% of all deaths reported by this disease. Even when it does not lead to death, stroke can cause sequelae that compromise life quality in most patients (Association, 2014).

Early diagnosis of stroke is essential as brain morphological damage increases within a few hours of symptom's onset (Amar, 2011). When the Cerebral Blood Flow (CBF) is reduced to 30-35% of normal, it causes functional suppression, mostly because of the lack of energy-requiring ion pump mechanisms in brain cells (Osborn, 1999). Blood flow obstructions of 5 to 10 minutes to areas of the brain can cause irreversible damage (Astrup et al., 1981).

Most damage occurs in the infarcted core and spreads into the ischemic penumbra. The penumbra is metabolically unstable with CBF of approximately 20-40% of normal. If perfusion returns in a suitable period, it is still possible to recover the penumbra (Astrup et al., 1981, Osman et al., 2011). There are some cases where more extended periods of poor perfusion can recover without permanent injury. Those cases depend mainly on the collateral circulation surrounding the stroke core (Ginsberg, 1997).

Effective stroke treatments are considered a difficult challenge since penumbral tissues are only salvageable within few hours after its start (Wardlaw,2010). Therefore, the primary therapeutic decisions are to quickly reestablish the main blocked artery to prevent the infarct expansion. This was made possible with the advent of the thrombolytic agent (alteplase, rt-PA, Tissue Plasminogen Activator) for the treatment of ischemic stroke.

When the early signs of ischemic areas with the potential to be preserved are detected it increases the chances of using rt-PA. The treatment window for venous thrombolysis with rt-PA is approximately 3 hours after the first symptoms (Jauch et al., 2013). Some authors even reinforce that this treatment window can be expanded to 4,5 hours with good

results (Tekle et al., 2012). The choice for rt-PA or other treatments depends on factors such as size, location, vascular distribution of the infarcted region and presence or absence of bleeding. This stage of diagnosis is fundamental because the detection of hemorrhagic points in the middle of ischemic areas leads to entirely different choices of treatment. Also, after thrombolytic therapy, the hemorrhagic transformation is a frequent complication of ischemic stroke (Zhang et al., 2014).

In summary, the interactions between plasminogen activators and ischemic cerebral tissue are not completely konwn. However, it is clear that thrombus dissolution in the central nervous system can be achieved with the use of Pas and there are increased intracerebral hemorrhage risks with its use (James C. Grotta, 2016).

In this research thesis, the greatest motivation was to develop a computational tool to aid physicians in the early detection of ischemic stroke in CT examinations. This tool could be possibly used within the thrombolytic treatment window and increase the chances of tissue recovery. We aimed to contribute with a computational tool that could provide more clearly the signs of ischemic stroke especially to those physicians with less experience or that are not specialists in neuroradiology.

2.2. Diagnostic Modalities

This early stage diagnosis of stroke occurs through different imaging modalities. Because time is critical to establish the diagnosis, a limited number of essential diagnostic tests are recommended (Jauch et al., 2013). Stroke protocols and pathways must be clearly defined before acute treatment decisions. Magnetic Resonance Imaging (MRI), Non-enhanced computed tomography (CT), and computed tomography with perfusion are the

main choices for diagnosing stroke (Amar, 2011). Since this research computed tomography was the only modality used for image processing, it will be discussed in more details. Other modalities such as MRI and computed tomography with perfusion will be briefly explained below with their main advantages and disadvantages for the stroke diagnosis.

2.2.1. Computed Tomography

After its introduction in 1971, CT has developed from an X-ray modality limited to the generation of axial images of the brain in neuroradiology in a versatile 3D image mode, allowing the generation of images of the whole human body. It currently covers a wide range of applications, including oncology, vascular radiology, cardiology, traumatology and interventional radiology (Dance et al., 2014, Hendee and Ritenour, 2002). The TC concept refers to the creation of cross-section images of an object from the transmission of data collected in various directions (Bushberg, 2002). The CT image acquisition process involves the measurement of the X-ray transmission profile through the patient, from a large number of projections. These projections are obtained by rotating the X-ray tube and the detectors around the patient, as shown in Figure 3. The transmission profiles are used to reconstruct the CT image, composed of an array of pixels (Dance et al., 2014, Bushberg, 2002, Hendee and Ritenour, 2002).

Figure 3 - An example of the method of computed tomography imaging where the whole X-ray and the detectors rotate around the patient (Dance et al., 2014).

The assigned values to the pixels in a CT image are associated with the attenuation of the corresponding tissue, or, more specifically, the linear attenuation coefficient (μ). The linear attenuation coefficient depends on the composition and density of the tissue, as well as the energy of the photon. The attenuation of the X-ray beam is described by Equation 1 (Dance et al., 2014).

$$I(x) = I_0 e^{-\mu x} \tag{1}$$

Where *I(x)* is the intensity of the attenuated X-ray beam, I_0 is the original beam intensity, and *x* is the thickness of the material. When an X-ray beam transmitts through a patient, different tissues have different linear attenuation coefficients. If the path through the patient ranges from 0 to *d*, then the intensity of the attenuated X-ray beam, transmitted at distance *d*, can be expressed by Equation 2 (Dance et al., 2014, Bushberg, 2002, Hendee and Ritenour, 2002).

$$I(d) = I_0 e^{-\int_0^d \mu(x)dx} \tag{2}$$

Since a CT image is composed of an array of pixels, the scanned patient are represented by an array of different linear attenuation coefficient volume elements (voxels). Figure 4 shows a 4*x*4 matrix representing the measured transmission across a line. For such discretization, the attenuation is expressed in Equation 3 (Dance et al., 2014, Bushberg, 2002, Hendee and Ritenour, 2002).

$$I(d) = I_0 e^{-\sum_{i=1}^{i=n} \mu_i \Delta x} \tag{3}$$

where *n* represents the size of the matrix in the sense of the analysis.

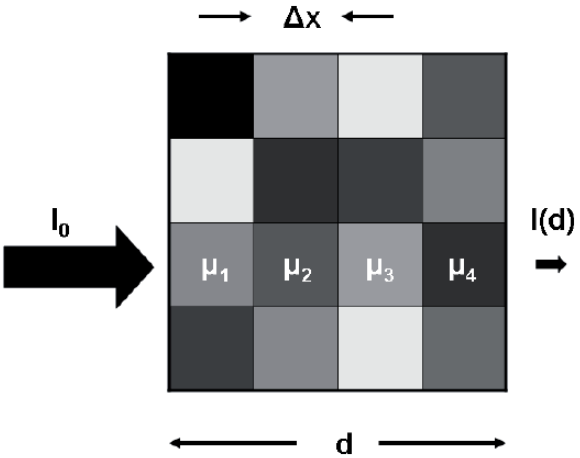

Figure 4 - The principle of an X-ray beam attenuation in a simplified 4 × 4 matrix. Each element of the matrix may have an associated linear attenuation coefficient (Dance et al., 2014).

Therefore, the underlying data necessary to generate a CT image are the intensities of attenuated and non-attenuated X-ray beams, respectively *I(d)* and I_0. The image reconstruction techniques can then be applied to derive the matrix of linear attenuation coefficients, which is the basis of the CT image (Dance et al., 2014).

In a CT image, the reconstructed linear attenuation coefficient matrix ($\mu_{material}$) is transformed into a corresponding matrix of Hounsfield Units (HU), where the HU scale express the relation to the linear water attenuation coefficient (μ_{water}), as shows Equation 4 (Dance et al., 2014, Bushberg, 2002).:

$$HU_{material} = \frac{\mu_{material} - \mu_{água}}{\mu_{água}} x\ 1000 \quad (4)$$

It can be seen that HU_{water} = 0 ($\mu_{material} = \mu_{água}$), HU_{air} = -1000 ($\mu_{material}$ = 0) e HU = 1 is associated with 0.1% of the linear attenuation coefficient of water. From the definition of HU, for all substances other than air and water, variations in HU values occur when different voltages are used in the X-ray tube. The reason is that, as a function of photon energy, different substances have a non-linear relationship of its linear attenuation coefficients relative to that of water. This effect is most notable for substances that have relatively higher effective atomic numbers, such as contrasting blood and bones (Dance et al., 2014).

CT has excellent sensitivity to detect intracranial hemorrhage and to distinguish non-vascular problems caused by neurological symptoms. Non-enhanced CT definitively excludes parenchymal hemorrhage (The European Stroke Organisation Executive and the, 2008). Its capacity is limited to the detection of ischemic areas due to the small difference between ischemic tissue density and healthy tissue. However, CT continues to be the primary modality for the rapid evaluation and diagnosis of patients with potentially ischemic lesions (Jauch et al., 2013). The option for CT is due to its lower cost compared to other methods, greater accessibility of the population, shorter execution time and compatibility with prostheses, implants and metallic equipment (Amar, 2011, Adams et al., 2007, Srinivasan et al., 2006b).

Due to its significant advantages, CT exams are still the first option for emergency decisions concerning acute ischemic stroke. Therefore, in this research, we aim to contribute to the early diagnosis of stroke in retrospective examinations of CT. All techniques developed here and all results presented in the next sections were entirely applied in CT examinations.

2.2.2. Magnetic Resonance Imaging

MRI is a technique that has excellent detection of ischemic tissues in the brain (van Everdingen et al., 1998). This method of diagnosis in relation to CT better detects regions with cytotoxic edema, better distinguishes acute ischemic regions from chronic ones, has better spatial resolution and does not use ionizing radiation. However, MRI has disadvantages such as the long examination time and the high sensitivity to movement artifacts, which often makes it difficult to perform in patients with stroke. Its high financial cost limits its use to the general population, making it difficult to use on a large scale, especially in countries such as Brazil. In addition, another disadvantage is its incompatibility with patients who have dentures and metal implants (Jauch et al., 2013).

2.2.3. Computed Tomography with perfusion

Perfusion computed tomography also has good sensitivity for ischemic stroke detection. This method consists of the sequential acquisition of images in a specific CT scan slice during contrast injection (Allmendinger et al., 2012). CT perfusion can be used to generate functional perfusion maps, the most used being: cerebral blood volume, blood flow, mean transit time (the difference between arterial and venous contrast passage), and

time to peak contrast enhancement. Each of these produces a different-sized lesion, with the processing algorithm also influencing the lesion size, even when the same parameter is estimated. Figure 5 shows an example of a CT scan with perfusion. In Figure 5a, no abnormalities are seen. However, the use of CT with perfusion reveals a deficit in the mean transit time (Figure 5b) as well as in the regional blood volume map (Figure 5c) and on the regional cerebral blood flow map (Figure 5d). Furthermore, a digital subtraction technique may be used to enhance the occlusion of an artery, as shown in Figures 4e-f.

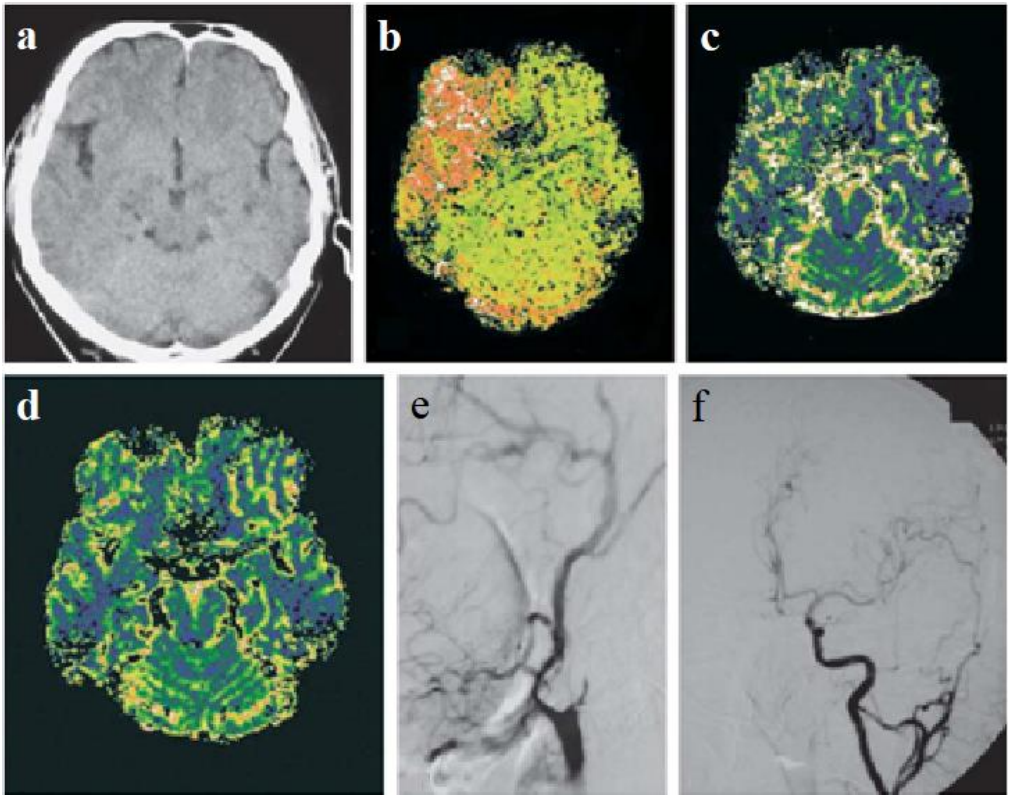

Figure 5 – a) A CT scan of a 63-year-old patient with a left-sided hemiparesis revealed no abnormalities. (b) Perfusion-weighted CT showed a perfusion deficit in the mean transit time parameter maps as well as on (c) the regional cerebral blood volume map and on (d) the regional cerebral blood flow map. Digital subtraction angiography (e and f) on the right-hand side shows occlusion of the internal carotid artery (Marincek and Dondelinger, 2007).

Identifying which perfusion parameter should be used is essential to achieve the best possible diagnosis. Similarly, raw diffusion-weighted acquisitions can be post-processed to provide diffusion-weighted images, apparent diffusion coefficient (ADC) maps, fractional anisotropy (FA) or the diffusion tensors (DT). CT perfusion main advantage in relation to other diagnostic methods is to allow both qualitative and quantitative evaluations. When compared to CT, it has essential disadvantages such as increased radiation dose, longer time for image acquisition and processing, higher financial cost and also a high dependence on qualified professionals for the diagnosis (Srinivasan et al., 2006a, Jauch et al., 2013).

2.3. Digital Image

An image can be represented by a two-dimensional function, $f(x, y)$, where x and y are spatial coordinates (plane), and the value of f in any pair of coordinates (x, y) is named the gray level of the image. When x and y and the intensity values of f are finite and discrete quantities, we have a digital image. In this case, each element of the image is called a pixel (Gonzalez and Woods, 2008, Bovik, 2005). The digitization of the coordinate values is named sampling, while the digitization of the amplitude values is called quantization (Gonzalez and Woods, 2008, Bovik, 2005).

Digital image processing relates to the process of manipulation of an image by a computer so that the output of the process is an image with different characteristics according to the user's necessity (Gonzalez and Woods, 2008). Image processing generally applies to methods that receive an image as input and generate a modified image (enhancing characteristics), measures (analyzing regions of interest), or classifications (aiding human visual perception) as output (Zarinbal and Zarandi, 2014).

Image processing methods aim to improve the visualization of an image or to convert them into a more suitable form for analysis of humans or computational systems. There are various methods for image processing proposals. Usually, a combination of techniques is combined to achieve the output image (Zarinbal and Zarandi, 2014).

Segmentation are essential in image processing (Lin et al., 2006), which comprises a process of separation between objects and the background. The segmentation divides the image into different regions so that each region is homogeneous in relation to some property, such as the value of the pixel or texture (Roerdink and Meijster, 2000, Khokher et al., 2012).

2.4. Thresholding

Due to its inherent properties, the simplicity of implementation and computational speed, image thresholding has a central position in image processing applications, especially in segmentation approaches. This process consists in separating the gray intensities of an image in different ranges. A gray intensity value, called threshold, is determined to separate parts of the image according to the pixels values. A pixel with a value greater than the threshold is called the point of the object. Any pixel with a value smaller than the threshold is called a background point. This can be exemplified in Equation 5 (Gonzalez and Woods, 2008, Bovik, 2005):

$$g(x,y) = \begin{cases} 1 \; if \; f(x,y) > threshold \\ 0 \; if \; f(x,y) < threshold \end{cases} \quad (5)$$

Where g(x, y) represents the pixels of the threshold image, and f(x, y) represents the pixels of the original image. After the thresholding process, the final image has only two possible pixel values.

When the pixel intensity distributions from background and objects are sufficiently different, it is possible to use a single threshold applicable to the whole image and is called the overall threshold. However, in some specific cases, it is necessary to use a variable threshold, where the threshold value changes throughout the image. The use of these thresholds depends on the type of image to work on and the region to be segmented (Gonzalez and Woods, 2008).

In this study, a thresholding technique was implemented in one of the first algorithm steps in order to segment different regions of interest.

2.5. Histogram Stretching

The histogram of an image is composed by a set of numbers indicating the percentage of pixels in a specific gray level. These values are generally represented by a graph bar that provides for each level of gray, the number (or percentage) of corresponding pixels in the image. Through the visualization of the histogram of an image, one can obtain an indication of its quality as to the level of medium brightness (if the image is predominantly light or dark) (MARQUES FILHO, 1999).

When analyzing one image histogram, the measure of its dynamic range it is named contrast. The dynamic image range is defined as the entire range of intensity values contained within an image, thus the maximum pixel value minus the minimum pixel value. For example, an 8-bit image has a dynamic range of 256, and a 12-bit image has a dynamic range of 4096 (Gonzalez and Woods, 2008).

Contrast stretching or histogram stretching is a technique that attempts to improve an image by stretching the range of its intensity values. Contrast stretching is restricted to a linear mapping of the input image before conversion to the output. The initial step

determines the limits of the new image intensity extension. The original image histogram is examined first. If the original range covers the full possible set of values, straightforward contrast stretching will not change the contrast (Gonzalez and Woods, 2008).

This technique must be used when the restricted range of pixel intensities can be stretched linearly, to the full limit of the extended output. Then for each pixel, the original value is mapped to a new output value using Equation 6:

$$s = (r - c)\left(\frac{b-a}{d-c}\right) + a \quad (6)$$

Where s is the new value of the pixel, and r is the old value. These lower and upper limits are called a and b, respectively (for standard 8-bit grayscale images, these limits are usually 0 and 255). The limits value of the original histogram are determined by the lower = c and upper = d.

2.6. Variational Decomposition Model

Variational models have been used in a variety of image processing problems, usually for image denoising and or texture identification (Bergounioux, 2016, Bergounioux et al., 2016, Bergounioux and Piffet, 2010). The variational model (VM) provides a decomposition of the image at different scales, in which noise and texture may be modelled as oscillating components.

In this work, we used the mathematical formulation described in (Bergounioux, 2016). One can assume that the image to recover belongs to the $L_2(\Omega)$ space and that it can be

decomposed. The image P was modeled as the sum of three terms, as can be seen in Equation 7:

$$P = u + v + w \tag{7}$$

The components w, v and u belong to different functional spaces: $v \in BH(\Omega)$ which is the (smooth) second-order part, u is a $BV(\Omega)$ component, and $w \in L2(\Omega)$ is the remainder term. We also consider that the space $BV(\Omega)$ is the classical Banach space of functions of bounded variation. The *BV*-part are related to the contours of the image, and the *BH*-part is continuous (at least for $d \leq 2$) and it gives the image dynamic. We consider the following cost function defined on $BV(\Omega) \times BH(\Omega)$ as shown in Equation 8:

$$F_{\lambda,\mu}(u,v) = \frac{1}{2}\|P - u - v\| + \lambda TV(u) + \mu TV^2(\mathrm{v}) \tag{8}$$

Where $\|P - u - v\|$ is the fitting data term, $TV(u)$ is the first order total variation of u, $TV^2(v)$ is the second order total variation of v, and λ and μ are two real numbers fixed empirically for contours and homogeneity ($\lambda > 0$ and $\mu > 0$). More information on the methods can be found elsewhere in the following papers (Bergounioux, 2016, Bergounioux et al., 2016, Bergounioux and Piffet, 2010). In this study, the variational decomposition model was used to enhance the contrast of the image; highlighting the ischemic stroke region more clearly.

2.7. Expectation Maximization

Expectation Maximization (EM) is a popular iterative method for maximum likelihood parameter estimation and image segmentation (Jong-Kae and Djuric, 1997). This technique consists of the generalization of the maximum likelihood estimate from a given

data set. First, we recall the definition of the maximum-likelihood estimation problem (Bilmes, 1997).

One can assume a density function $p(x|\theta)$ regulated by some parameters. If we consider a set of Gaussians, those parameters are means and covariances. We also have a data set of size N, from the distribution $X = \{x_1, \dots, x_N\}$. We must assume that these data vectors are independent and identically distributed with distribution *p*. The resulting density for the samples is achieved through Equation 9:

$$p(x|\theta) = \prod_{i=1}^{N} p(x_i|\theta) = L(\theta|X) \tag{9}$$

This function $L(\theta|X)$ is the likelihood of the parameters from the data. In maximum likelihood problems, our goal is to find the value of θ that maximizes L.

The EM algorithm can be applied to find the maximum-likelihood estimate of those parameters. We assume that X is the observed data and therefore it is somehow incomplete. We assume that a complete data set exist, named $Z = (X, Y)$ with the following joint density function in Equation 10:

$$p(z|\theta) = p(x, y|\theta) = p(y|x, \theta)p(x|\theta) \tag{10}$$

In this manner, one can assume a joint relationship between missing and observed data. With a new density function, we define a new complete-data likelihood function as in Equation 11:

$$L(\theta|Z) = L(\theta|X, Y) = p(X, Y|\theta) \tag{11}$$

The EM algorithm finds the expected value of the complete-data log-likelihood of the unknown data *Y* given the observed data *X* and the current parameter estimates. That is, we define in Equation 12:

$$Q(\theta, \theta') = E[\log p(X, Y|\theta|X, \theta')] \quad (12)$$

The evaluation of expectation is named the E-step of the algorithm. Notice the meaning of the two arguments in the function $Q(\theta, \theta')$. The first argument θ corresponds to the parameters that ultimately will be optimized in an attempt to maximize the likelihood. The second argument θ'corresponds to the parameters used to evaluate the expectation. The second step (the M-step) of the EM algorithm is to maximize the expectation computed in the first step. That is, we find in Equation 13:

$$Q(\theta') = argmax_{\theta}\, Q(\theta, \theta') \quad (13)$$

These two steps are repeated as long as it is necessary. Each iteration increases the log-likelihood, and the algorithm converges to a local maximum of the likelihood function.

2.8. K-means

The K-Means algorithm, as well as the EM algorithm, can both be used to find natural clusters within given data based in input parameters (MacQueen, 1967). Clusters can be found based on pixel intensity, color, texture, location, or some combination of these features. In K-Means, the starting locations of the partitions used are critical to achieving the optimal solution. K-Means is susceptible to termination when achieving a local maximum as opposed to the global maximum.

K-Means relies the on the assignment of information to a given set of partitions. At every pstep of the algorithm, each data value is assigned to the nearest partition based

upon some similarity parameter such as Euclidean distance. The partitions are then recalculated based on these assignments. With each successive step, a data value can switch to another partition, thus altering the values of the partitions. K-Means algorithms typically converge to a quick solution as opposed to other clustering algorithms (Hartigan, 1979, Yizong, 1995).

Unsupervised classification method such as K-means aims to minimize the sum of the quadratic error on all groups. For this, it requires three specific parameters: the number of groups, the initialization of the group and the metric of the distance. The quadratic errors, $J(C_k)$ between μ_k and the points in a group C_k are defined in Equation 14:

$$J(C_k) = \sum_{x_i \in C_k} \|x_i - \mu_k\|^2 \quad (14)$$

Where $i = 1, .., C = ck, k = 1, ..., K$ is the set of K clusters and μ_k is the average of C_k clusters. As the goal is to minimize the sum of the square error on all clusters, the Equation 6 is rewritten as Equation 15:

$$J(C) = \sum_{k=1}^{K} \sum_{x_i \in C_k} \|x_i - \mu_k\|^2 \quad (15)$$

One of the most complex parameters in cluster analysis is the definition of the number of groups (k) to be found in the data set. K-means was one of the methods tested for the final step of our approach, in the segmentation (Yizong, 1995, Hartigan, 1979).

2.9. Mean Shift

Mean Shift (MS) is a non-parametric feature-space analysis technique for locating the maximum of a density function, initially presented in 1975 (Fukunaga and Hostetler, 1975). MS algorithm is an unsupervised clustering segmentation method, where the

number and the shape of the data are unknown at start and it can be applied to discontinuity preserving smoothing (Comaniciu and Meer, 2002). The segmentation process is based on a region-merging technique applied to the filtered image, and the number of regions after segmentation is determined by the minimum number of pixels in a region, denoted by *M* (i.e., regions containing less than *M* pixels will be eliminated and merged into its neighboring region). An appropriate value of *M* can be chosen to yield an accurate region representation of segmented regions.

We present a brief summary of the MS method based on the results published by (Comaniciu and Meer, 2002, Yizong, 1995, Comaniciu, 2003, Tao et al., 2007). Mean-shift operates through finding the maximum of a density function given discrete data sampled. It is an iterative method, which starts with an initial estimate. Consider a radially symmetric kernel in Equation 16:

$$k(x) = c_{k,d} k(\|x\|^2) \tag{16}$$

Where constant $c_{k,d} > 0$, such that:

$$\int_0^\infty K(x)dx = \int_0^\infty c_{k,d} k(\|x\|^2)\, dx = 1 \tag{17}$$

k(x) is a monotonically decreasing function, and it is kernel profile. Given the function $g(x) = -k'(x)$ for profile, we define a new kernel *G(x):*

$$G(x) = c_{g,d} g(\|x\|^2) \tag{18}$$

Where constant $c_{g,d} > 0$, for *n* data points x_i, $i=1, \ldots, n$ in the d-dimensional space R^d, MS is defined as:

$$m_{h,G}(x) = \frac{\sum_{i=1}^{n} x_i \, g\left(\left\|\frac{x-x_i}{h}\right\|^2\right)}{\sum_{i=1}^{n} g\left(\left\|\frac{x-x_i}{h}\right\|^2\right)} - x \tag{19}$$

Where *x* is the center of the kernel window, and *h* is the bandwidth. MS is obtained as the difference between the weighted mean, obtained through the kernel *G* as the weights and *x* as the center of the kernel.

MS image filtering algorithm can be estimated with the equations above. First, an image represented by a 2-D lattice of p-dimensional vectors (pixels) is used, where p = 1 for gray-level intensities. The space of the lattice is known as the spatial domain, while the graph level information are represented in the range domain. For both domains, we assume Euclidean metrics. Let x_i and z_i, $i = 1, \ldots, n$, respectively, be the d-dimensional (d = p + 2) input image and the filtered pixels in the joint spatial-range domain.

The segmentation is achieved through a merging process performed on a region produced by the MS filtering application. MS segmentation requires the selection of the bandwidth parameter *h = (hr, hs)*, which controls the size of the kernel and determines the resolution of the mode detection.

2.10. Diagnosing Stroke

The diagnosis of ischemic stroke depends heavily on the radiologist's experience and manner that images are viewed, such as the correct centering and width of the windowing in CT scan images (Mainali et al., 2014). All these factors must be adjusted so that the diagnostic evaluation of the stroke is done correctly and within the window of treatment with the thrombolytic treatment (Jauch et al., 2013). Some score classification based on visual assessment of image was introduced to facilitate the diagnosis of stroke and the

establishment of the patient's condition, such as the ASPECTS scoring system and the NIHSS score.

2.10.1. ASPECTS

The diagnosis of ischemic stroke in CT improves with the use of a structured score system such as the ASPECTS (Alberta Stroke Program Early CT Score). The ASPECTS scale uses a scoring system to identify areas of the brain that indicate regions of ischemia. Two axial CT slices obtained between the thalamus and at the upper margin of the ganglion structures are used. The scale divides the region of the middle cerebral artery (MCA) into 10 regions of interest. The neuroradiologist subtracts a single point of the score for each area of ischemic change. Thus a score of 10 corresponds to a healthy brain, and a score of 0 to a brain with ischemic stroke diffused to the entire region of the middle cerebral artery (Huisa et al., 2010). Figure 6 identifies the positions to be evaluated during ASPECTS used in clinical routine.

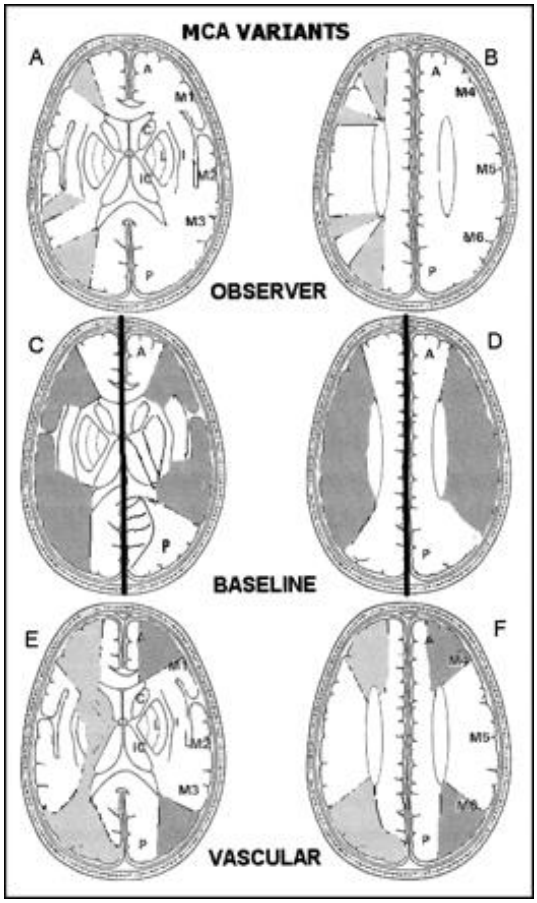

Figure 6- ASPECTS study form. A and B, Right hemisphere, observer variations: lower and upper ASPECTS slices show as shaded areas the minimal and maximal variations in size of the cortical areas of the MCA (M1–M6) chosen by six expert observers. Left hemisphere, ASPECTS study form: A = anterior circulation; P = posterior circulation; C = caudate head; L = lentiform nucleus; IC = internal capsule; I = insular ribbon; MCA = middle cerebral artery; M1 = anterior MCA cortex; M2 = MCA cortex lateral to insular ribbon; M3 = posterior MCA cortex; M4, M5, and M6 are anterior, lateral, and posterior MCA territories, respectively, approximately 2 cm superior to M1, M2, and M3, respectively, rostral to basal ganglia. C and D, Cortical MCA area variations with change of baseline (Pexman et al., 2001)

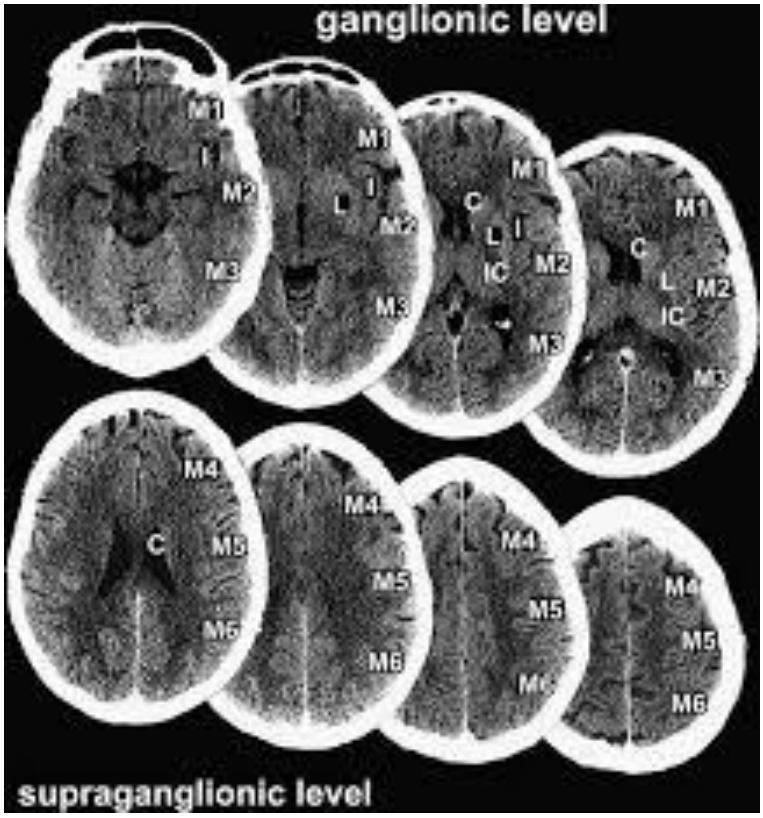

Figure 7 - Another representation of the ASPECTS evaluation in CT scan slices for diagnosing ischemic stroke in the MCA territory.

In this research, all our patients were evaluated with the ASPECTS scale. Those data are essential to understanding our cohort of stroke patients. The complete data of ASPECTS are available in Appendix 2.

2.10.2. NIHSS score

A standardized neurological examination ensures that the major components of a neurological examination are performed in the correct form. Evaluation scores such as National Institute of Stroke Scale (NIHSS) may be performed rapidly, since they demonstrated its utility, and may be used by a broad spectrum of healthcare providers (Jauch et al., 2013).

Several institutions use NIHSS for the diagnosis and treatment of stroke in the first 24 hours after the event. This score evaluates the level of consciousness, degree of muscular strength, language, facial paralysis, visual field, sensitivity, attention and presence of ataxia. This scale presented significant evidence of reliability and applicability. It consists of 11 domains being scored between 0 and 4. Table 2 exemplifies all the aspects evaluated in NIHSS.

Table 2 - National Institute of Stroke Scale.

Tested Item	Title	Responses and Scores
1A	Level of consciousness	0 – Alert 1 – Drowsy 2 – Obtuned 3 – Coma/unresponsive
1B	Orientation questions (2)	0 – Answers both correctly 1 – Answers 1 correctly 2 – Answers neither correctly
1C	Response do commands (2)	0 – Performs both tasks correctly 1 – Performs 1 task correctly 2 – Performs neither
2	Gaze	0 – Normal 1 – Partial gaze palsy 2 – Complete gaze palsy
3	Visual Fields	0 – No visual field detect 1 – Partial hemianopia 2 – Complete hemianopia 3 – Bilateral hemianopia
4	Facial movement	0 – Normal 1 – Minor facial weakness 2 – Partial facial weakness 3 – Complete unilateral palsy
5	Motod function (arm) a. Left	0 – No drift 1 – Drift before 5 seconds

	b. Right	2 – Falls before 10 seconds
		3 – No effort against gravity
		4 – No movement
		0 – No drift
	Motor function (leg)	1 – Drift before 5 seconds
6	a. Left	2 – Falls before 5 seconds
	b. Right	3 – No effort against gravity
		4 – No movement
		0 – No movement
7	Limb ataxia	1 – Ataxia in 1 limb
		2 – Ataxia in 2 limbs
		0 – No sensory loss
8	Sensory	1 – Mild sensory loss
		2 – Severe sensory loss
		0 – Normal
9	Language	1 – Mild aphasia
		2 – Severe aphasia
		3 – Mute or global aphasia
		0 – Normal
10	Articulation	1 – Mild dysarthria
		2 – Severe dysarthria
		0 – Absent
11	Extinction or inattention	1 – Mild (loss 1 sensory modality lost)
		2 – Severe (loss 2 modalities lost)

The higher the sum, the greater the level of neurological impairment. A slight impairment is considered from 0 to 5 points; from 6 to 13, moderate impairment and above 14 points, severe impairment (Caneda et al., 2006). NIHSS assessment helps to quantify the degree of neurological deficits and facilitate communication. It is also possible to identify the location of vessel occlusion, provide an early prognosis, and select patients for various interventions, and identify those with potential for complications (Jauch et al., 2013). In

this research, all our patients were evaluated with the NIHSS scale. Those data are essential to understanding our cohort of stroke patients. The complete data of NIHSS are available in Appendix 2.

2.11. Computational methods for detecting and enhancing ischemic stroke

Different computational methods were used to improve the visualization of areas affected by stroke. Medical image analysis approaches and statistical tools were highly explored in the last 20 years to identify different tissue states. Those approaches were used to differentiate and spatially localize tissues affected by stroke. Also, to predict the final ischemic tissue outcome, and understand factors that influence the dynamic evolution of the infarct and the penumbra such as lesion swelling, collateral flow pathways and spontaneous reperfusion (Rekik et al., 2012).

In almost all image-processing approaches, the detection of specific regions necessarily involves the segmentation of the image in different regions of interest. Loncaric et al.1999 contributed extensively to the segmentation of medical images using the fuzzy c-means clustering (FCM) technique. The authors were interested in analyzing the intracerebral brain hemorrhage. After segmentation of the brain images, different tissues were identified with basic rule-based systems. The classification of tissues was given the following denominations: background, brain tissue, bone tissue, hemorrhages and calcifications (Loncaric et al., 1999).

Chan 2007 also evaluated stroke in High-Resolution CT (HRCT) images in which the hemorrhagic region was extracted using the top-hat type transform and the comparison

of symmetry between the two cerebral hemispheres (left and right) was applied, being able to identify small hemorrhagic clots (Chan, 2007).

Bradera et al. 2009, proposed the semi-automatic segmentation for cerebral hematoma and edema as well as the measurement of their volumes. The author's combined region-growing techniques to segment the hematoma and also applied the segmentation of the level set to extract the edema (Bradera et al., 2009).

Chawla et al. 2009 presented an automatic method for the detection and classification of ischemic and hemorrhagic stroke in CT scans. This method relied on the observation that stroke causes a disturbance in the contralateral symmetry of the cerebral hemispheres. The areas of stroke were identified through tissue density and texture distribution when compared to the opposite hemispheres (Chawla et al., 2009).

Liao et al. have developed computed aided-diagnosis (CAD) programs that detect changes in brain symmetry, shape, and size of brain hematomas (Liao et al., 2006, Liao et al., 2007). In their most recent work, the authors proposed the automatic detection of intracranial hematomas. First, the regions of the skull are segmented into smaller sized images by applying a maximum filter. Then the intracranial regions are found by connectivity and the possible regions of hematomas through adaptive thresholds. This information is used as input in a multi-resolution binary level set algorithm. This procedure is repeated until the resolution of the original image is reached (Liao et al., 2010).

In summary, a system for automatic stroke detection CT scan images should contain some features that ensure its effectiveness and reproducibility. The pre-processing of the image should be as minimal as possible; deformations of the cerebral anatomy cannot

impair detection as well as movement artifacts. The system should be tested in a large number of clinical cases to assess its adaptability (Liao et al., 2010).

In this research, we propose a methodology to enhance ischemic stroke using a combination of different image processing techniques in CT scan images, producing enhanced images. Those images were tested in a clinical environment with physicians of different level of experience.

2.12. New Perspectives for Stroke Detection

Recent advances in machine learning and deep learning techniques have been used in multiple medical problems. Many authors have explored with review papers the potential use of these new advances in diagnosing and predicting the outcome of stroke lesions (Feng et al., 2018, Liebeskind, 2018, Nielsen et al., 2018, Pinto et al., 2018). Artificial intelligence tools could guide diagnosis of stroke with automated creation of features, image segmentation, and multimodal prognostication (Feng et al., 2018).

Very recently, Tang et al. used an approach with machine learning applied to MRI images of acute ischemic stroke to estimate the tissue outcome in penumbral regions. Authors demonstrated through their artificial intelligence that the administration of intravenous thrombolysis could be successfully applied even in periods greater than the 4,5 hours treatment window (Tang et al., 2018). Abedi et al. developed an artificial neural network model to recognize acute cerebral ischemia and differentiate that from stroke mimics in an emergency setting (Abedi et al., 2017).

The decision-making in stroke will always be a complex task since it involves far more than imaging the lesion. The clinical decision of the human brain cannot be fully replaced by a logical method. As the authors (Feng et al., 2018) said ‘Deep learning is not a

replacement for existing analytical techniques, but rather a new set of powerful tools that have opened up exciting opportunities for data-driven stroke management both for acute intervention and for guiding prognosis.'

Ultimately, deep learning and machine learning tools will become more frequent in the modern stroke specialist's diagnosis, mostly because of their speed and powerful results. We highly trust that those recent technologies will benefit the future clinical scenario of stroke not only with more accurate treatment decisions but also with improved patient outcome.

Chapitre 2 - Résumé

Le chapitre 2 décrit les fondements théoriques pour une meilleure compréhension des chapitres suivants.

Le diagnostic précoce de l'Accident Vasculaire Cérébral (AVC) est essentiel car les dommages morphologiques cérébraux augmentent quelques heures après les premiers symptômes. Ce diagnostic précoce se produit à travers différentes modalités d'imagerie, les deux plus importantes sont la Tomodensitométrie (CT) et l'imagerie par résonance magnétique (IRM). Le chapitre 2 décrit les principaux outils de traitement d'images utilisés pour améliorer l'identification de l'AVC ischémique dans les images CT.

Ces outils sont le seuillage, l'étirement de l'histogramme et la décomposition par modèle variationnel. Nous avons également testé trois méthodes de segmentation : Expectation-Maximization (EM), K-means et Mean-Shift.

Le diagnostic d'accident ischémique cérébral dépend largement de l'expérience du radiologue et de la manière dont les images sont visualisées. Ainsi, nous avons définie certains concepts fondamentaux du diagnostic de l'AVC dans un environnement clinique. L'échelle ASPECTS (Alberta Stroke Program Early CT Score) utilise un système de notation pour identifier les zones du cerveau qui représentent les régions de l'ischémie. Et aussi le score NIHSS (National Institute of Stroke Scale) qui évalue le niveau de conscience, le degré de la force musculaire, la langue, la paralysie faciale, le champ visuel, la sensibilité, l'attention et la présence d'ataxie. Le chapitre 2 se termine avec

quelques méthodes de traitement d’images appliquées au cours des 20 dernières années pour améliorer la perception visuelle de l’accident ischémique cérébral.

Dans le chapitre 2, nous avons également décrit les perspectives de futures études sur la détection des AVC. Nous souhaitons appliquer notre approche en routine clinique dans notre hôpital à tous les nouveaux patients victimes d'un AVC. Dans ce contexte, les outils développés dans le cadre de cette étude pourraient être utilisés non seulement sur les images CT non améliorés, mais également avec d'autres techniques d'imagerie telles que l'IRM et la tomographie avec perfusion. De plus, nos outils pourraient être testés en association avec une technique d'apprentissage profond, notamment à des fins de segmentation. Étant donné que l'AVC est d'abord identifié par ses symptômes cliniques, le diagnostic assisté par ordinateur avec apprentissage profond pourrait constituer un outil efficace pour un diagnostic rapide.

Par ailleurs, les outils d’apprentissage profond et d’apprentissage automatique deviendront de plus en plus fréquents pour le diagnostic de l’AVC, principalement en raison de leur rapidité et de leurs résultats puissants. Nous sommes convaincus que ces technologies récentes bénéficieront au futur scénario clinique d'accident vasculaire cérébral, non seulement grâce à des décisions de traitement plus précises, mais également grâce à des résultats bénéfiques pour les patients.

Chapter 3

3. Materials and Methods

This research was possible due to the Brazilian foundation, *Fundação de Amparo à Pesquisa do Estado de São Paulo* (FAPESP) that provided all the financial support thorough the entire PhD and BEPE scholarship in France, with the following process 2014/22296-1 and 2016/05321-8.

In this research, a novel approach to enhance the visual perception of ischemic stroke in CT scans was proposed. This enhancement aims to enable less experienced viewers, such as radiologists, to reliably detect early signs of stroke in clinical routine. Our new contribution consists in combining efficiently different image processing techniques to enhance the visual insight of ischemic stroke in non-enhanced CT scans.

The image processing techniques were developed in Matlab® software R 2014a. All computational analyzes were performed using the DICOM images (*Digital Imaging and Communications in Medicine*). A computational algorithm was proposed to enhance the ischemic stroke perception and assist the physicians in their diagnosis. Firstly, to reduce noise and redundancies, a projection (summation) of the slices containing the ischemic stroke was realized followed by band-pass filtering. Then, to enhance the contrast of the obtained projection, a Variational Model (VM) decomposition was used. Finally, the expectation maximization (EM) method was applied to the relevant component from the VM decomposition to segment and emphasize the ischemic stroke. Furthermore, two different methodologies to segment and emphasize ischemic stroke were applied and compared (K-Means and Mean-Shift). The performance of observers, such as

experienced radiologists and resident radiologists in diagnosing acute ischemic stroke images was evaluated. We compared their sensitivity and accuracy performances for stroke and control cases both with and without the aid of enhanced images. The proposed approach steps are described in the flowchart in Figure 8

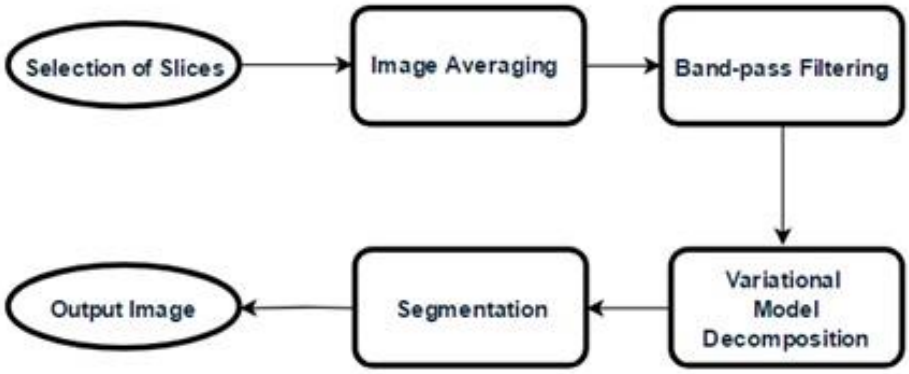

Figure 8 - Flowchart with the main image processing steps performed (Alves et al., 2018) .

3.1. Database

(CAAE: 52457315.3.0000.5411). A database was composed of retrospective CT examinations obtained from sthe Diagnostic Imaging Department of Botucatu Medical School (UNESP - Brazil). Images were acquired from two 16-channel Toshiba Activion scanners and one GE Optima 64-channel tomography scanner from January 2012 to November 2017, thus reaching the sample images foreseen in the preparation of this research project. We evaluated approximately 78 retrospective CT exams previously diagnosed by radiologists and neuroradiologists.

We collected retrospective CT scans of patients submitted to non-enhanced examinations. Patients were selected with the following criteria of inclusion and exclusion.

- Inclusion criteria: patients with confirmed acute ischemic stroke lesions that undergone CT scans examinations until 4,5 hours after the onset of first symptoms.
- Exclusion criteria: patients with previous stroke lesions, intracranial malformations or a history of intracranial hemorrhage.

This study also did not considered cases of hemorrhagic stroke. Since all exams were retrospective, the ground-truths of confirmed stroke cases were checked with the follow up of the patients within the hospital, including clinical reports, histological and pathological analysis, which were further validated by two experienced radiologists.

After this selection, only 25 cases from the initial 78 cases were used. The information presented on patients clinical reports such as the ASPECTS scale evaluation and the NIHSS were included in the final results. Furthermore, 16 normal cases of CT exams were used as a control group. The control group was selected at random from Botucatu Medical School as patients with no radiological findings who underwent CT exams due to headache, known as migraine. This group was necessary to test the reliability of the developed methodology since the control cases were submitted to the same computational approach as the stroke cases. The mean age of patients was 68.89 ± 10.41 years for stroke group and 66.76 ± 9.36 for control. The database information is summarized in Table 3.

Table 3 - Number of exams of the database of this project, and those included in the final study design.

Imaging Modality	Number of evaluated patients		Number of patients that met inclusion and exclusion criteria	
	Ischemic Stroke	Control	Ischemic Stroke	Control
Computed Tomography	78	26	25	16

Using the t-student test, the age difference between the two groups was not significant ($p < 0.05$). CT scans were performed on multislice CT scanners. Scanner acquisition settings were: kVp = 120, automatic exposure control, exposure time = 1 second, matrix size was 512 x 512 and slice thickness = 1 mm. All images were stored using the DICOM format.

3.2.Selection of slices

As a prior step to image processing, it is necessary to select a sequence of CT images in each patient with suspected ischemic stroke. The selection of tomographic slices was performed in the same anatomical region used for the evaluation of the ASPECTS protocol (Huisa et al., 2010). This protocol in the diagnosis of stroke is used in patients submitted to computed tomography, according to international guidelines on the management and treatment of stroke (Jauch et al., 2013, Amar, 2011). The processing starts by opening one sequence of CT scan images of individual patients. A sequence of

slices in the middle cerebral artery territory and basal ganglia is selected. These regions are most commonly affected by stroke (Jauch et al., 2013). This selection of slices was performed by an experienced neuroradiologist. Moreover, all observers analyzed the same sequence of slices for each patient in this study.

Figure 9 represents an example of a sequence of slices from the complete CT scan examination. All patients from our database had their slices selected in the same manner in this step of the approach.

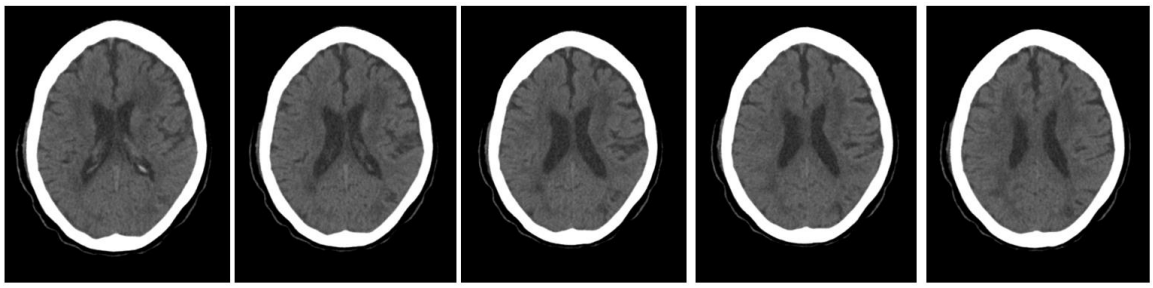

Figure 9 – Sequence of slices in the same patient representing the slices selected by the physician. This patient CT scan sequence had a total of 94 slices, and 5slices were selected.

3.3. Image Averaging

After selecting slices with susceptible ischemic density changes, an image averaging is performed by summing the values of the gray levels in each slice. As a result, a unique image is obtained with the average of pixel intensities from the different selected slices from the previous step. Image averaging is a processing technique often employed to enhance images by reducing random noise. The algorithm operates by computing an arithmetic mean of the intensity values for each pixel position in a set of captured images from subsequent slices using Equation 20:

$$P(i,j) = \frac{\sum_{n=1}^{N} S_n(i,j)}{N} \tag{20}$$

Where $P(i,j)$ is a resulting pixel of the averaging, S_n is the sequence of selected slices, (i,j) are pixel coordinates for each image slice, and N (4 to 9) is the number of slices used in the sequence. Even though CT scans are performed with thin slices, the number of slices used was carefully chosen to avoid averaging slices with many different anatomical structures. This approach was performed to highlight the presence of stroke and also lower the image noise level. All control group images were also averaged using a fixed number of five slices extracted in the middle cerebral artery territory and basal ganglia.

3.4. Thresholding

After the image averaging step, the next step in the image processing algorithm was to remove non-intracranial tissues from the projection image. Figure 10 shows the histogram of the projected image. Intracranial tissues are within the range of 5 to 50 HU. The great peak of pixels around -1000 Hounsfield Units correspond to the air outside of the patient's head. Moreover, all pixels above 50 Hounsfield Units might be considered non-intracranial, such as bone tissues for example. Therefore, pixels out of the [5, 50] range do not correspond to biological tissues and were removed from the image. This thresholding step was performed to facilitate the subsequent step of enhancement and segmentation methods. Thus, we applied a threshold with a lower limit and an upper limit of 5 and 50 HU to remove all the pixels belonging to the bone tissue, to the background and other undesirable structures in the image.

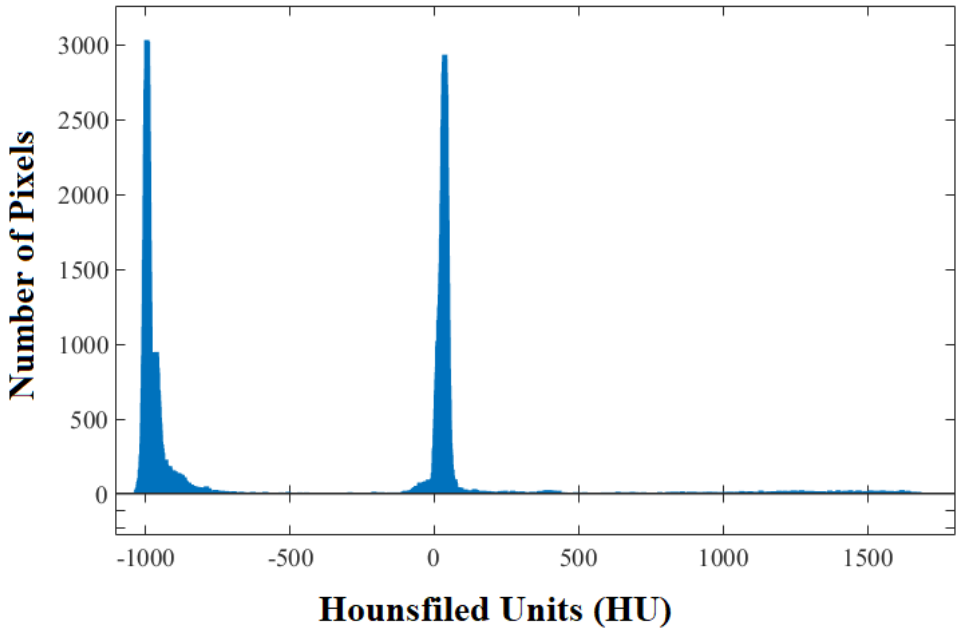

Figure 10 - Original image's histogram. Near the -1000 HU represents pixels from the air around the patients head. Intracranial tissue is found between 5 and 50 HU. In addition, all pixels above 200 HU are considered bone tissue.

After this stage, a histogram normalization was performed by redistributing the pixels intensities. The histogram normalization enabled improving the contrast between adjacent regions. Following the band-pass filtering, we made an operation on the histogram of the image. The operation called histogram stretching changed our range from [5 to 50] and distributed between 0 and 255 grayscale intensities. Therefore, we changed our levels of gray intensity to 256 levels. As a result, all levels of intracranial gray intensity were distributed throughout the histogram, as can be seen in Figure 11.

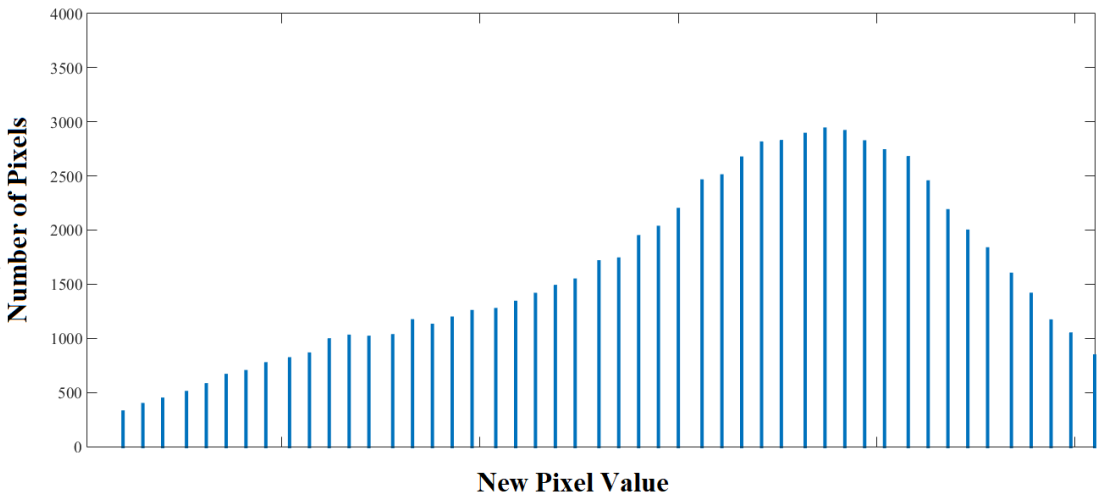

Figure 11 - Histogram after the stretching and normalization process.

This operation allowed to improve the contrast between adjacent regions in the image, slightly increasing the differentiation between the regions of the stroke and the healthy brain tissue that surrounds it. As an example of the application of this step in a stroke patient, we can observe the original image in Figure 12, and the image with the improved contrast after the removal of undesirable pixels in Figure 13.

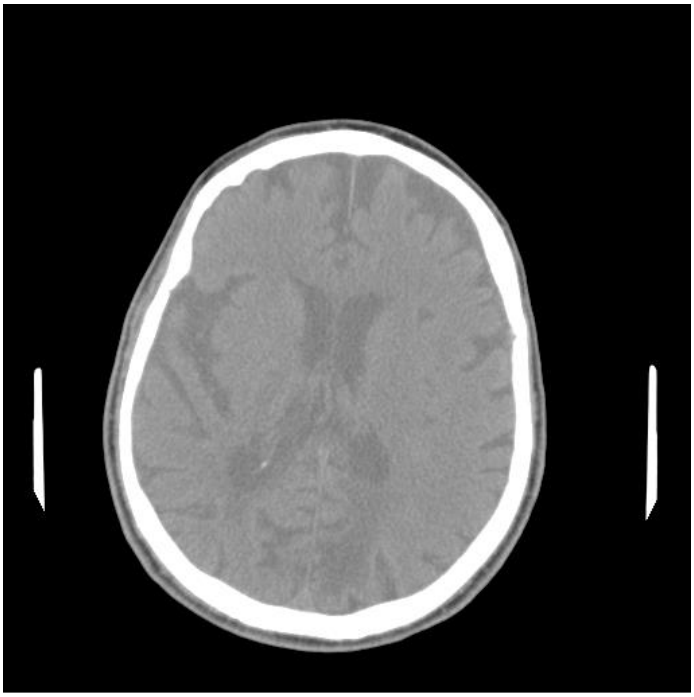

Figure 12 – Original image from a stroke patient before the removal of undesirable pixels.

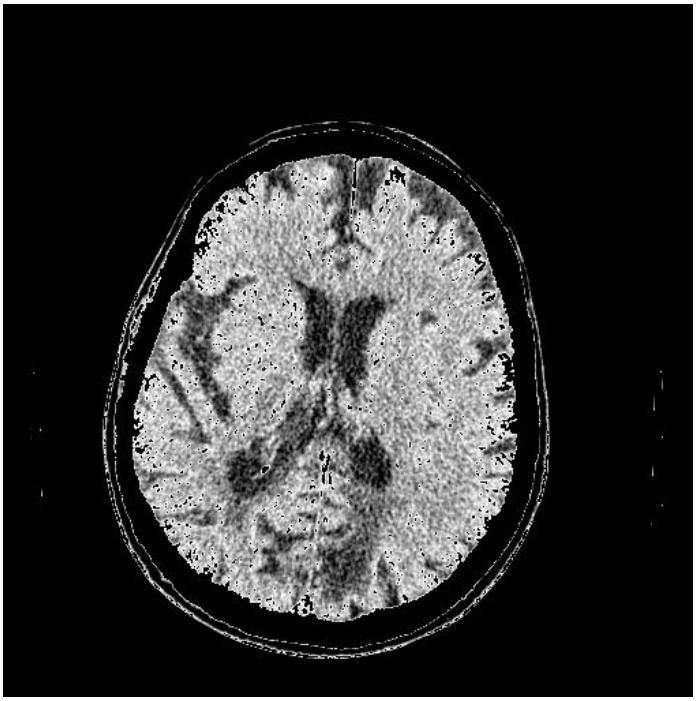

Figure 13 – Image contrast image after the application of the thresholding step.

3.5.Variational Model Decomposition

To better enhance the contrast of the image, a Variational Model (VM) decomposition was applied to decompose the image into different components (Bergounioux, 2016, Bergounioux et al., 2016). We recall that the image P was modeled as the sum of three terms: $P = u + v + w$. In this model, v is the smooth second order part, u is related to contours and w is linked to fine textures. Our primary interest is in the v component since it is related to the contrast and brightness of the image. Ischemic stroke region was more clearly enhanced using the values of λ and μ equal to 1 and 10, respectively.

3.6. Segmentation

The next step concerned the image segmentation, which was applied to the v component after the VM decomposition. Different segmentation methods were tested to enhance ischemic stroke for the whole database. Three different methods were compared: Expectation Maximization, K-Means and Mean Shift.

3.6.1. Expectation Maximization Method

The Expectation Maximization (EM) is iterative and starts from some initial estimate and then proceeds to an iteratively update until convergence is detected. Each iteration consists of an Expectation (*E*-step) and a Maximization (*M*-step) step (Bilmes, 1997), as it was described in Chapter 2. Each pair of *E* and *M* steps is considered one iteration. Thus, in the final assignment, each pixel of the final image will belong to only one cluster.

3.6.2. K-means

K-Means is a clustering segmentation method similar to EM. The goal is to choose cluster centers that minimize the total squared distance between each point and its closest center. Each data value is assigned to the nearest partition based upon a similarity parameter, in this approach the Euclidean distance of intensity (Hartigan, 1979). At every step of the algorithm, partitions are then recalculated based on these hard assignments. The values of the partitions can alter at each successive step. K-Means algorithms are typically faster when compared to other clustering algorithms (Spath, 1985).

3.6.3. Mean Shift

In the Mean Shift segmentation method each pixel was associated with a joint domain located in its neighborhood. The algorithm delineates the cluster by grouping all pixels that are closer than *hs,* which is the spacial domain bandwidth and *hr*, the range domain bandwidth. After the application of this approach, each pixel element will be assigned to a partition. The Mean Shift generates partitions characterized by a nonparametric model. We used the approach described by Comaniciu *et al.* with a different selection of spatial and range domains. The best results were achieved with (*hs, hr*) = (16, 4) (Comaniciu and Meer, 2002).

3.7. Observers Evaluation

Previously selected stroke exams were subjectively evaluated by neuroradiology specialists. Evaluations were performed in conjunction with the neurosurgeon Prof. Carlos Clayton, a professor at Botucatu Medical School-UNESP. Another experienced

radiologist and some radiology residents participated in the assessments. The evaluation of CT images followed the recommendations of the "*Guidelines for the Early Management of Patients with Acute Ischemic Stroke*" (Jauch et al., 2013).

This publication provides guidance on the evaluation of ischemic stroke areas through ASPECTS scale, and regarding the correct choice of center and width of the windowing of the images, search for changes in symmetry between the cerebral hemispheres and assessment of the increase of density in the region of the middle cerebral artery (Bhadauria and Dewal, 2014).

In this present research, a test was established to evaluate the performance of observers in a clinical environment based on a scoring system used by Tang *et al.* (Tang et al., 2011). We selected our set of examinations, being 16 normal cases and 25 confirmed cases of acute ischemic stroke. Four resident radiologists from first, second and third year of residence and two experienced radiologists with ten and twenty years of experience in radiology, worked as observers in this study. All radiologists were from Botucatu Medical School in Brazil. They had no previous knowledge regarding the history of the patients, thus always blind if the patient had or not the presence of ischemic stroke.

First, the set of raw images (with no processing) was analyzed. Observers were allowed to adjust contrast, brightness, and magnification of images according to their own experience in diagnosing stroke in clinical routine. For each case, each observer was required to give a score relating to the presence of acute stroke (definitely absent: 1, absent: 2, uncertain: 3, present: 4 and definitely present: 5). Then a new set of enhanced images was created resulting from our proposed approach, and observers repeated their evaluation and scored all images, again. The change of the score in diagnosis was tracked after the observation of enhanced images. Improvement changes were considered when

the observer changed his evaluation to the desired score. These analyses permitted to test the confidence of the diagnosis both before and after image enhancement.

We also measured both sensitivity and accuracy of the performance of the observers before and after the enhanced images. Sensitivity is the true positive fraction, given that the subject has the ischemic stroke. Accuracy is the probability that a diagnostic evaluation is correctly performed. The Equations for both quantitative measures are given in Equations 21 and 22. The scores 1, 2 and 3 were considered as negative evaluations, and the scores 4 and 5 were considered as positive.

$$\text{Sensitivity} = \frac{TP}{(TP+FN)} \tag{21}$$

$$\text{Accuracy} = \frac{(TP+TN)}{(TP+FP+FN+TN)} \tag{22}$$

where *TP* are true positives, *TN* are true negatives, *FP* are false positives and *FN* are false negatives. We also determined the confidence intervals for both sensitivity and accuracy measurements through the Wilson score method (Newcombe, 1998).

We tracked the difference in scores that resulted from the analysis of the original images compared to the enhanced images. For the difference scores, one can consider a positive score when the observer changes his previous score from any given value to a higher one. For example, the original score was 3 (uncertain), and the observer changed after analyzing the enhanced image to a score of 4, which means that the stroke can now be visualized. Moreover, changes of the score from 4 to 5 which means a higher certainty in the location and determination of stroke. Additionally, negative scores represent false negative cases when observing the enhanced images.

Chapitre 3 - Résumé

Le chapitre 3 concerne le matériel et les méthodes. Le comité d'éthique institutionnel local a approuvé le protocole de cette étude. Nous avons ainsi construit une base de données composée d'examens CT rétrospectifs obtenus au département d'imagerie diagnostique de l'école de médecine de Botucatu. Des critères d'inclusion et d'exclusion ont permis de sélectionner 25 cas sur 78 patients. Les informations présentées sur les rapports cliniques des patients, telles que l'évaluation par les échelles ASPECTS et le NIHSS, ont été incluses dans les résultats.

Un algorithme est proposé pour améliorer la perception visuelle des accidents ischémiques. Après sélection des coupes d'images, une étape de seuillage et une projection sont appliquées pour réduire le bruit et les informations redondantes. Ensuite, une décomposition par modèle variationnel est utilisée sur la projection obtenue pour conserver la composante pertinente pour notre analyse.

L'étape suivante concerne la segmentation de l'image. Différentes méthodes de segmentation ont été testées pour améliorer les accidents vasculaires cérébraux ischémiques pour l'ensemble de la base de données. Trois méthodes différentes ont été comparées : Expectation maximisation (EM), K-means et le décalage moyen (Mean shift).

La méthode d'EM est très populaire en imagerie médicale. EM regroupe les pixels de l'image en différents groupes en utilisant une distribution gaussienne probabiliste. Le modèle de mélange est composé d'une somme de K distributions gaussiennes, chaque distribution ayant ses propres paramètres. L'algorithme commence à partir d'une estimation initiale avant de procéder à une mise à jour itérative jusqu'à la convergence. Chaque itération comprend une évaluation (E-step) et une maximisation (M-step). Toutes les étapes ont été effectuées à l'aide du logiciel Matlab R2014a.

Ensuite, un test d'évaluation est mis en place pour évaluer la performance des observateurs dans un environnement clinique basé sur un système de notation. Quatre radiologistes résidents de $1^{ère}$, $2^{ème}$ et $3^{ème}$ années de résidence et deux radiologues expérimentés avec dix et vingt ans d'expérience en radiologie en tant qu'observateurs.

Aucune connaissance préalable concernant les antécédents des patients n'a été fournie aux observateurs.

Tout d'abord, l'ensemble des images sans traitement a été analysé. Les observateurs ont ajusté le contraste, la luminosité et le grossissement des images en fonction de leur propre expérience. Pour chaque cas, chaque observateur devait donner un score relatif à la présence d'un accident vasculaire cérébral aigu (définitivement absent: 1, absent: 2, incertain: 3, présent: 4 et définitivement présent: 5). Ensuite, le même processus d'observation pour chaque radiologue a été répété sur un nouvel ensemble d'images améliorées. Le changement du score dans le diagnostic a été observé après visualisation des images améliorées par les radiologues. Les changements d'amélioration ont été pris en compte lorsque l'observateur a modifié son évaluation pour obtenir le score souhaité. Ces analyses ont permis de tester la confiance du diagnostic avant et après l'amélioration des images. Nous avons également mesuré la sensibilité et la précision des performances des observateurs avant et après les images améliorées.

Chapter 4

4. Results and Discussion

In this thesis, we proposed an approach to enhance the visual perception of ischemic stroke in Non-Enhanced CT scans. The selected stroke cases were imaged with four or less hours after the symptom's onset. Two experienced radiologists selected all ground through stroke cases both clearly evident cases as well as complicated cases. However, those two specialists did not participate in the observer's evaluation section.

In this study, the mean age of patients was 68.89 ± 10.41 years for stroke and 66.76 ± 9.36 for control. No significant difference was found between stroke patients and controls for age (*p-value* = 0.1735) using Student's t-test. Stroke patients had a mean NIHSS of 13 ± 7 and mean ASPECTS of 7 ± 2. The complete results of NIHSS and ASPECTS are presented in Appendix 2.

Although 78 stroke patients were selected at the beginning of this study, only 23 were included in the final analysis. This occurred because many of the patients had previous brain lesions that could be confused with acute stroke regions. Another reason that led to the non-inclusion of some cases was when computed tomography was performed outside the therapeutic window of 4.5 hours after the first symptoms, which was one of our exclusion criteria.

After the selection of the 23 stroke cases, as well as the 16 control cases, all sequence of analyzed images passed through the image processing steps described in the flowchart of Figure 8. Figure 14A-E illustrate the ischemic density changes in adjunct CT slices of

the same patient. While Figure 14F presents the resulting image after computing the projection using slices A to E.

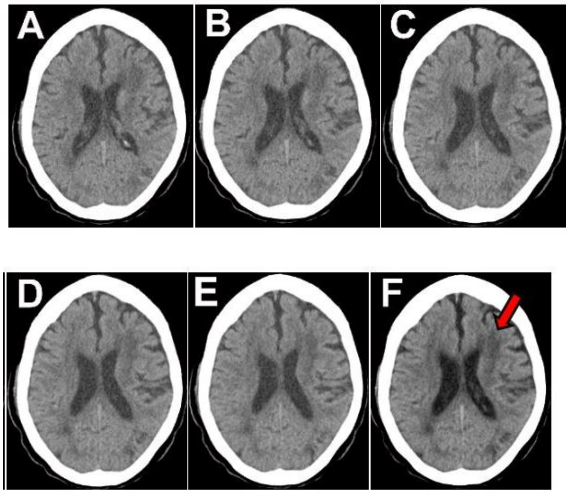

Figure 14- A-E)- Adjunct slices sequence with the presence of the subtle density changes in the same patient. F is the result of the projection involving slices A, B, C, D and E. Stroke is present in the left frontal lobe of the brain, as indicated by the red arrow.

The image averaging technique was used to reduce noise and improve the perception of stroke while using subsequent slices with slightly different anatomical structures (Figure 14). This was considered an acceptable tradeoff by the physician's analysis.

After this stage, the Variational Model decomposition helped to enhance the contrast and the brightness of the images. Representative examples of enhanced final images from different patients are presented in Figure 15. On the top, corresponding to letters A, B, C and D are presented the images resulting from the image averaging step of three different patients with stroke and one control case. On the second, third and fourth rows are presented the enhanced images according to our proposed approach accounting the band-pass filtering, followed by the VM decomposition and the segmentation methods. The difference between second, third and fourth row are accounted from the segmentation method used, being EM, K-Means, and Mean-Shift respectively. For the EM, images

correspond to letters E, F, G and H. For K-Means, the images are I, J, K and L. For the Mean-Shift method, images correspond to letters M, N, O, and P.

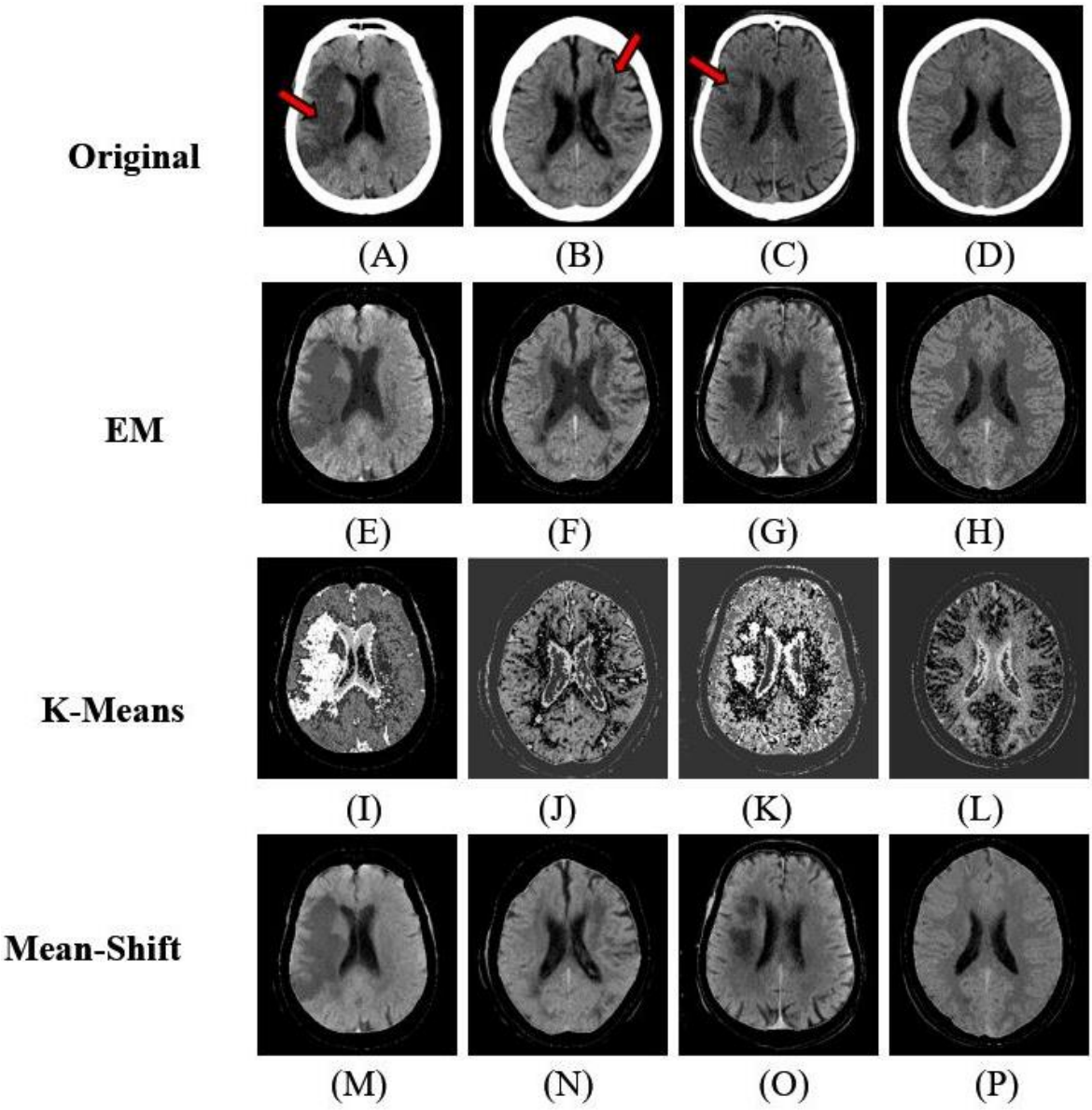

Figure 15 - Average images for three different patients with stroke (A, B, C) and one control (D). Red arrows indicate the region of ischemic stroke in images A, B and C. Enhanced images are shown in second, third and fourth rows. EM approach (E, F, G, H), followed by K-Means (I, J, K, and L) and Mean-Shift (M, N, O, P). Six clusters are highlighted after the segmentation process with the EM and K-Means methods. For Mean-Shift we used hs = 16 and ht = 4, in which hs *is the spacial domain bandwidth and* hr is *the range domain bandwidth.*

The purpose of the segmentation was to enhance the visual perception of ischemic stroke for the physician's subjective analysis. It was not the intention of the authors to perform a complete automatic segmentation of the stroke region. A key question for the EM and k-means approach is to choose the number of clusters that will segment the pixel intensities.

In this case, our target was to achieve a number that would both benefit the visual enhancement of the regions of interest with no additional cost in computational time. This is an important issue since the main goal is to apply this algorithm in a medical diagnosis workstation since available workstations do not possess necessarily high-end computer processors. If the number of clusters is too large, the model will increase the computational cost vastly and highly comprise the diagnosis time, which is a crucial point in detecting early signs of ischemic stroke.

For the EM and K-Means methods, a different number of clusters were tested to achieve the best-enhanced image possible. This was determined in a previous evaluation of those images with an experienced radiologist. Stroke was more clearly enhanced when the number of clusters, K was equal to six in both methods.

The average elapsed time for each patient analysis is 141.6 ± 1.5 seconds. Our experiments were performed on machines running Intel® processors with 2.4GHz CPU frequency and having 32 GB of memory. Table 4 shows the table of sensitivity and overall specificity of the three targeting segmentation methods.

Table 4 - Sensitivity and Accuracy using the three segmentation methods Maximization of Expectation (EM), K-Means and Mean-shift. The values are in percentage followed by the confidence interval.

	Sensitivity (%)		**Accuracy (%)**	
Method	**Original**	**Enhanced**	**Original**	**Enhanced**
EM	64,5	89,6	83,3	91,7
K-Mean	64,5	74,2	83,3	71,5
Mean-shift	64,5	69,5	83,3	72,3

When comparing the three segmentation methods, EM was superior to both K-Means and Mean-Shift methods in the majority of evaluated cases for the observer's performance. Then, all following results considered the observer's evaluation in enhanced images with the EM approach only. The complete assessment of all selected cases of ischemic stroke and control cases by all observers are summarized in Table 5. The results show the sensitivity and accuracy obtained for each observer both before and after evaluating the enhanced images.

Table 5 - Observer's evaluation before and after the enhanced images. R1 to R4 are resident physicians of radiology. E1 and E2 are the experienced radiologists. Parameters evaluated were sensitivity and specificity. For both of them, we evaluated the mean values and the confidence interval.

Observers	Sensitivity (%)				Accuracy (%)			
	Original		Enhanced		Original		Enhanced	
	Mean	**CI**	**Mean**	**CI**	**Mean**	**CI**	**Mean**	**CI**
R1	26.1	(12.5 - 46.7)	60.9	(40.8 - 77.8)	81.3	(57.0 - 93.4)	87.5	(63.9 - 96.5)
R2	52.2	(32.9 - 70.7)	78.3	(58.1 - 90.4)	93.7	(71.7 - 98.9)	93.7	(71.7 - 98.9)
R3	65.2	(44.9 - 81.2)	82.6	(62.9 - 93.0)	93.7	(71,7 - 98.9)	93.7	(71,7 - 98.9)
R4	78.3	(58.1 - 90.4)	87.0	(67.9 - 95.5)	100	(80.7 - 100)	100	(80.7 - 100)
E1	73.9	(53.3 - 87.5)	91.3	(73.2 - 97.6)	75.0	(50.5 - 89.8)	75.0	(50.5 - 89.8)
E2	91.3	(73.2 - 97.6)	100	(85.7 - 100)	93.7	(71.7 - 98.9)	100	(80.7 - 100)
Overall	**64.5**	**(56.2 - 72.0)**	**89.6**	**(81.8 - 94.2)**	**83.3**	**(76.3 - 88.7)**	**91.7**	**(84.4 - 95.7)**

The choice for the confidence interval to represent both sensitivity and accuracy was made because this estimate is relatively close to the data itself, being on the same scale of all the measurements. We also compared the difference scores for all observers analyzing the original images and then the enhanced images for stroke cases. For a better visualization of scores, the observers R1, R2 and R3 were joined in the graph of Figure 16 and observers R4, E1, and E2 in the graph of Figure 17. As can be seen, for the majority of cases, enhanced images by our approach, enable better diagnosis of the presence of stroke.

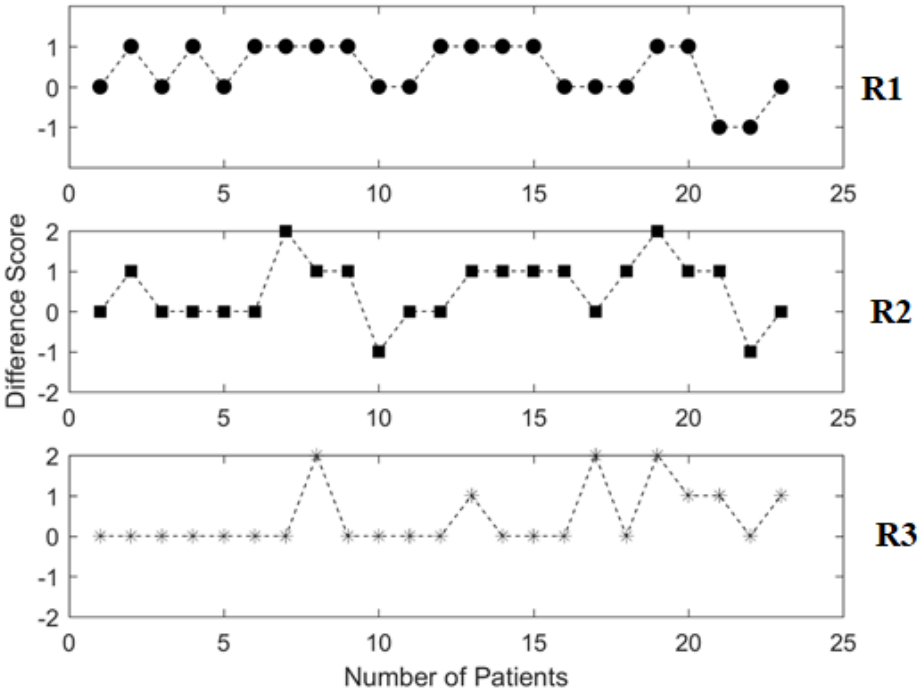

Figure 16 - Difference scores for the observers R1, R2, and R3 are represented in the graphs above from top to bottom respectively. The difference was obtained when the score given for the enhanced images are compared to the score given for the original images. Positive values indicate an enhancement in diagnosis. Negative changes indicate false negative cases.

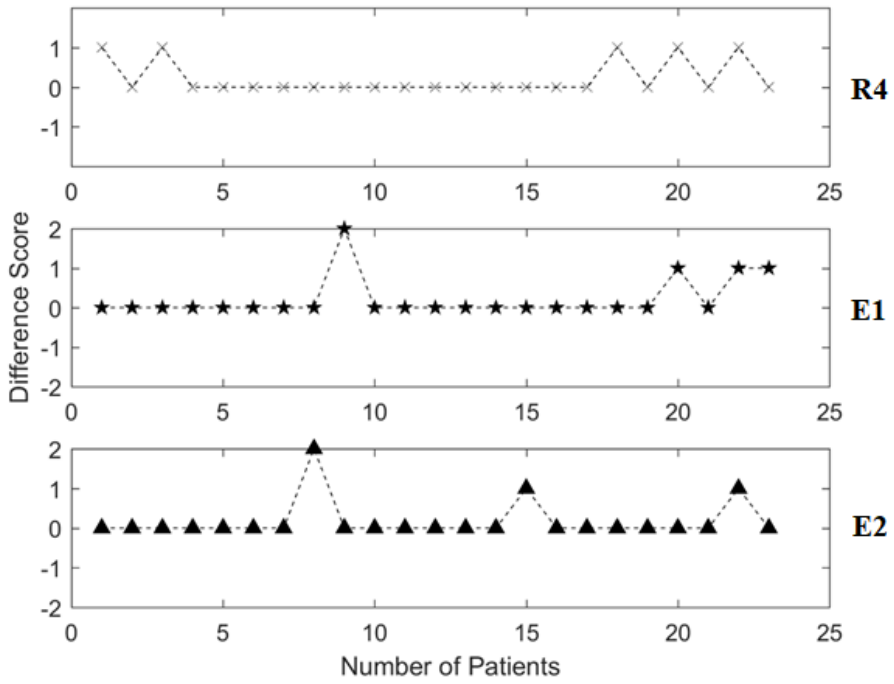

Figure 17- Difference scores for the observers R4, E1, and E2 are represented in the graphs above from top to bottom respectively. The difference was obtained when the score given for the enhanced images are compared to the score given for the original images. Positive values indicate an enhancement in diagnosis. Negative changes indicate false negative cases. The resident 4 was included in this analysis since its results were more similar to the experienced radiologists.

With the observer's evaluation, we examined the impact of enhanced images on the score of diagnosis. The overall sensitivity of the observer's analysis was 63.9% and changed to 78.9% after the evaluation of the enhanced images. The overall accuracy was of 67.4% and increased to 78.2%. Considering the three least experienced the improvement was even more remarkable from 46.2% to 69.9% for sensitivity and from 57.6% to 71% for accuracy. This great improvement was also showed in the difference score graphs. The maximum difference score was 2 (Figure 16 and Figure 17), since the maximum changes occurred when observers first assigned the score 3 and then changed to score 5 after analyzing the enhanced images. In general, all observers agreed that the proposed approach helps to clarify difficult cases of acute ischemic stroke.

One of the great advantages of our approach is that it can be easily implemented in any workstation to aid clinical diagnosis since we have a low computational cost. This tool can be a great help for inexperienced physicians. One limitation of our approach is that it is not entirely automatic since it depends on the physician selection of the slices before the application of the algorithm. After this stage, all subsequent steps are entirely automatic.

Chapitre 4 - Résumé

Le chapitre 4 présente tous les résultats de l'application de notre approche sur des images CT. Les résultats de l'évaluation des observateurs avant et après rehaussement des images sont aussi décrits. Notre technique a fourni des images améliorées qui ont permis aux médecins d'établir un diagnostic plus fiable de l'AVC ischémique lors des examens de tomodensitométrie. Des exemples représentatifs de ces images améliorées pour différents patients sont aussi présentés.

La sensibilité globale de l'analyse de l'observateur est passée de 64,5% à 89,6% après évaluation des images améliorées. La spécificité globale était de 83,3% et a augmenté à 91,7%. En comparant les trois méthodes de segmentation, EM était supérieure aux méthodes K-Means et Mean-Shift dans la majorité des cas évalués pour la performance de l'observateur. Ainsi, pour la suite, l'évaluation des observateur s'est effectuée uniquement avec les images améliorées par l'algorithme EM.

Nous avons également comparé les scores de différence de tous les observateurs analysant les images d'origine, puis les images améliorées pour les cas d'accident vasculaire cérébral. De cette manière, on pouvait tester si les images améliorées permettaient un diagnostic plus fiable. L'amélioration de la sensibilité était plus remarquable pour les trois médecins les moins expérimentés. Cette grande amélioration a également été montrée dans les graphiques de score de différence. Pour ces cas, les images améliorées ont permis une plus grande fiabilité dans le diagnostic de l'AVC ischémique.

Néanmoins, au chapitre 4, nous avons comparé les résultats obtenus avec les résultats précédents trouvés dans la littérature, ainsi qu'avec d'autres aspects pertinents pour la discussion.

Chapter 5

5. Conclusion

In this research, a novel approach based on a Variational Model and the Expectation Maximization method was used to enhance the ischemic stroke perception in non-enhanced computed tomography examinations. All proposed objectives were achieved as described below:

- We constructed a database with retrospective CT examinations of patients with confirmed ischemic stroke from Botucatu Medical School. Seventy-eight stroke cases were pre-selected, and twenty five were included in the final approach after inclusion and exclusion criteria assessment.
- We developed a computational algorithm in Matlab® environment to enhance ischemic stroke areas in CT images to improve their visualization when compared to the healthy brain tissue;
- We compared three different segmentation methods (Expectation Maximization, K-means, and Mean-shift) to achieve the best enhancement in ischemic stroke cases; our results indicated that the EM method resulted in the best enhancement of ischemic stroke in our database.
- We performed a test to evaluate the performance of observers in a clinical environment with a subjective evaluation of the stroke cases performed by radiologists. They evaluated both original and enhanced images, and we showed through sensitivity and accuracy scores that enhanced images provided a more reliable stroke diagnosis. Thus, we demonstrated that enhanced images improved physician's performance to diagnose early signs of acute stroke.

- All those results showed the importance of a computational tool to assist neuroradiology decisions, especially in critical situations such as institutions that do not have stroke specialists.
- As future perspectives for our work, the tools developed in our research could be used not only in non-enhanced CT scanners but also with other imaging techniques such as MRI and computed tomography with perfusion.
- Our tools could be tested in association with a deep learning technique especially for segmentation purposes. Computer-assisted diagnosis with deep learning could provide an effective tool of rapidly diagnosing it.
- We proved that enhanced images with our approach might mainly increase the potential candidates for thrombolysis treatment since they increase the chances of finding early signs of ischemic stroke in patients submitted to CT scans.
- Our final paper of this thesis named “Ischemic Stroke Enhancement using a Variational Model and the Expectation Maximization Method” was published in April 2018 in European Radiology journal (Alves et al., 2018), and it can be found in Appendix 4.

Chapitre 5 - Résumé

Dans cette étude, une nouvelle approche a été proposée pour améliorer la perception de l'AVC ischémique lors d'examens de CT non améliorés. Tous les objectifs proposés ont été atteints :

- Nous avons construit une base de données d’examens CT rétrospectifs de patients chez lesquels un AVC ischémique était confirmé,

- Nous avons développé une approche sous l'environnement Matlab pour améliorer les zones d'AVC ischémiques dans les images CT,
- Une étude comparative a été effectuée entre trois méthodes de segmentation différentes (EM, K-means et Mean-shift) pour obtenir la meilleure amélioration dans les cas d'accident ischémique cérébral,
- Un test a été proposé pour évaluer la performance des observateurs dans un environnement clinique avec une évaluation subjective des cas d'AVC,
- Nous avons démontré que les images rehaussées amélioraient les performances du médecin pour diagnostiquer les premiers signes d'un AVC aigu.

Tous ces résultats ont montré l'importance d'un outil informatique facilitant la prise de décision en neuroradiologie.

Notre dernier article intitulé « Ischemic Stroke Enhancement using a Variational Model and the Expectation Maximization Method » a été publié en avril 2018 dans la revue European Radiology (Alves et al., 2018). Vous le trouverez à l'annexe 4.

5. Bibliography

ABEDI, V., GOYAL, N., TSIVGOULIS, G., HOSSEINICHIMEH, N., HONTECILLAS, R., BASSAGANYA-RIERA, J., ELIJOVICH, L., METTER JEFFREY, E., ALEXANDROV ANNE, W., LIEBESKIND DAVID, S., ALEXANDROV ANDREI, V. & ZAND, R. 2017. Novel Screening Tool for Stroke Using Artificial Neural Network. *Stroke,* 48**,** 1678-1681.

ABREU, D. M. X. D., SAKURAI, E. & CAMPOS, L. N. 2010. A evolução da mortalidade por causas mal definidas na população idosa em quatro capitais brasileiras, 1996-2007. *Revista Brasileira de Estudos de População,* 27**,** 75-88.

ADAMS, H. P., DEL ZOPPO, G., ALBERTS, M. J., BHATT, D. L., BRASS, L., FURLAN, A., GRUBB, R. L., HIGASHIDA, R. T., JAUCH, E. C., KIDWELL, C., LYDEN, P. D., MORGENSTERN, L. B., QURESHI, A. I., ROSENWASSER, R. H., SCOTT, P. A. & WIJDICKS, E. F. M. 2007. Guidelines for the Early Management of Adults With Ischemic Stroke: A Guideline From the American Heart Association/ American Stroke Association Stroke Council, Clinical Cardiology Council, Cardiovascular Radiology and Intervention Council, and the Atherosclerotic Peripheral Vascular Disease and Quality of Care Outcomes in Research Interdisciplinary Working Groups: The American Academy of Neurology affirms the value of this guideline as an educational tool for neurologists. *Stroke,* 38**,** 1655-1711.

ALLMENDINGER, A. M., TANG, E. R., LUI, Y. W. & SPEKTOR, V. 2012. Imaging of stroke: Part 1, Perfusion CT--overview of imaging technique, interpretation pearls, and common pitfalls. *AJR Am J Roentgenol,* 198**,** 52-62.

ALVES, A. F. F., JENNANE, R., DE MIRANDA, J. R. A., DE FREITAS, C. C. M., ABDALA, N. & DE PINA, D. R. 2018. Ischemic stroke enhancement using a variational model and the expectation maximization method. *Eur Radiol,* 28**,** 3936-3942.

AMAR, A. P. 2011. Brain and vascular imaging of acute stroke. *World Neurosurg,* 76**,** S3-8.

ASSOCIATION, A. H. 2014. Heart Disease and Stroke Statistics-2014 Update: A Report from the American Heart Association. *Journal of Consumer Health on the Internet.*

ASTRUP, J., SIESJÖ, B. K. & SYMON, L. 1981. Thresholds in cerebral ischemia - the ischemic penumbra. *Stroke,* 12**,** 723-5.

BERGOUNIOUX, M. 2016. Mathematical Analysis of a Inf-Convolution Model for Image Processing. *Journal of Optimization Theory and Applications,* 168**,** 1-21.

BERGOUNIOUX, M., CAILLAU, J.-B., HABERKORN, T., PEYRÉ, G. & SCHNÖRR, C. (eds.) 2016. *Variational methods in imaging and geometric control,* France: de Gruyter.

BERGOUNIOUX, M. & PIFFET, L. 2010. A Second-Order Model for Image Denoising. *Set-Valued and Variational Analysis,* 18**,** 277-306.

BHADAURIA, H. S. & DEWAL, M. L. 2014. Intracranial hemorrhage detection using spatial fuzzy c-mean and region-based active contour on brain CT imaging. *Signal, Image and Video Processing,* 8**,** 357-364.

BILMES, J. A. 1997. A Gentle Tutorial of the EM Algorithm and its Application to Parameter Estimation for Gaussian Mixture and Hidden Markov Models.

BOVIK, A. C. 2005. *Handbook of image and video processing,* Amsterdam ; Boston, MA, Elsevier Academic Press.

BRADERA, A., BOADA, I., FEIXAS, M., REMOLLO, S., BLASCO, G., SILVA, Y. & PEDRAZA, S. 2009. Semi-Automatic Method for Brain Hematoma and Edema Quantification Using Computed Tomography. *Int. J. Comput. Med. Imaging Graph***,** 304-311.

BUSHBERG, J. T. 2002. *The essential physics of medical imaging,* Philadelphia, Lippincott Williams & Wilkins.

CANEDA, M. A. G. D., FERNANDES, J. G., ALMEIDA, A. G. D. & MUGNOL, F. E. 2006. Confiabilidade de escalas de comprometimento neurológico em pacientes com acidente vascular cerebral. *Arquivos de Neuro-Psiquiatria,* 64**,** 690-697.

CERNIAUSKAITE, M., QUINTAS, R., KOUTSOGEORGOU, E., MEUCCI, P., SATTIN, D., LEONARDI, M. & RAGGI, A. 2012. Quality-of-life and disability in patients with stroke. *Am J Phys Med Rehabil,* 91**,** S39-47.

CHAN, T. 2007. Computer aided detection of small acute intracranial hemorrhage on computer tomography of brain. *Comput Med Imaging Graph,* 31**,** 285-98.

CHAWLA, M., SHARMA, S., SIVASWAMY, J. & KISHORE, L. 2009. A method for automatic detection and classification of stroke from brain CT images. *Conf Proc IEEE Eng Med Biol Soc,* 2009**,** 3581-4.

COMANICIU, D. 2003. An algorithm for data-driven bandwidth selection. *IEEE Transactions on Pattern Analysis and Machine Intelligence,* 25**,** 281-288.

COMANICIU, D. & MEER, P. 2002. Mean shift: a robust approach toward feature space analysis. *IEEE Transactions on Pattern Analysis and Machine Intelligence,* 24**,** 603-619.

DANCE, D., CHRISTOFIDES, S., MAIDMENT, A., MCLEAN, I. & NG, K. 2014. *Diagnostic Radiology Physics: A Handbook for Teachers and Students,* International Atomic Energy Agency.

FENG, R., BADGELEY, M., MOCCO, J. & OERMANN, E. K. 2018. Deep learning guided stroke management: a review of clinical applications. *Journal of NeuroInterventional Surgery,* 10**,** 358-362.

FUKUNAGA, K. & HOSTETLER, L. 1975. The estimation of the gradient of a density function, with applications in pattern recognition. *IEEE Transactions on Information Theory,* 21**,** 32-40.

GARRITANO, C. R., LUZ, P. M., PIRES, M. L., BARBOSA, M. T. & BATISTA, K. M. 2012. Analysis of the mortality trend due to cerebrovascular accident in Brazil in the XXI century. *Arq Bras Cardiol,* 98**,** 519-27.

GINSBERG, M. D. 1997. The new language of cerebral ischemia. *AJNR Am J Neuroradiol,* 18**,** 1435-45.

GONZALEZ, R. C. & WOODS, R. E. 2008. *Digital image processing,* Upper Saddle River, NJ, Pearson/Prentice Hall.

HARTIGAN, J. A. W., M. A. 1979. Algorithm AS 136: A K-Means Clustering Algorithm. *J Applied Statistics,* 28.

HEALTH, N. I. O. 2007. Why population aging matters: a global perspective. US Departament of Health and Human Services.

HENDEE, W. R. & RITENOUR, E. R. 2002. *Medical imaging physics,* New York, Wiley-Liss.

HUISA, B. N., RAMAN, R., ERNSTROM, K., TAFRESHI, G., STEMER, A., MEYER, B. C. & HEMMEN, T. 2010. Alberta Stroke Program Early CT Score (ASPECTS) in patients with wake-up stroke. *J Stroke Cerebrovasc Dis,* 19**,** 475-9.

JAMES C. GROTTA, M., GREGORY W ALBERS, MD, JOSEPH P BRODERICK, MD, SCOTT E KASNER, MD, MSCE, FRCP, ENG H LO, PHD, A DAVID MENDELOW, MB BCH, FRCS, PHD, RALPH L SACCO, MD MS FAHA FAAN AND LAWRENCE KS WONG, MD 2016. *Stroke: Pathophysiology, Diagnosis, and Management,* Elsevier.

JAUCH, E. C., SAVER, J. L., ADAMS, H. P., JR., BRUNO, A., CONNORS, J. J., DEMAERSCHALK, B. M., KHATRI, P., MCMULLAN, P. W., JR., QURESHI, A. I., ROSENFIELD, K., SCOTT, P. A., SUMMERS, D. R., WANG, D. Z., WINTERMARK, M., YONAS, H., AMERICAN HEART ASSOCIATION STROKE, C., COUNCIL ON CARDIOVASCULAR, N., COUNCIL ON PERIPHERAL VASCULAR, D. & COUNCIL ON CLINICAL, C. 2013. Guidelines for the early management of patients with acute ischemic stroke: a guideline for healthcare professionals from the American Heart Association/American Stroke Association. *Stroke,* 44**,** 870-947.

JONG-KAE, F. & DJURIC, P. M. 1997. EM algorithm for image segmentation initialized by a tree structure scheme. *IEEE Transactions on Image Processing,* 6**,** 349-352.

KHOKHER, M. R., GHAFOOR, A. & SIDDIQUI, A. M. 2012. Image segmentation using multilevel graph cuts and graph development using fuzzy rule-based system. *IET Image Process,* 7**,** 201-211.

LAVADOS, P. M., HENNIS, A. J., FERNANDES, J. G., MEDINA, M. T., LEGETIC, B., HOPPE, A., SACKS, C., JADUE, L. & SALINAS, R. 2007. Stroke epidemiology, prevention, and management strategies at a regional level: Latin America and the Caribbean. *Lancet Neurol,* 6**,** 362-72.

LIAO, C.-C., FUREN, X., JAU-MIN, W. & CHIANG, I. J. A simple genetic algorithm for tracing the deformed midline on a single slice of brain CT using quadratic Bezier curves. Data Mining Workshops, 2006. ICDM Workshops 2006. Sixth IEEE International Conference on, 18-22 Dec. 2006 2006. 463-467.

LIAO, C.-C., XIAO, F., WONG, J.-M. & CHIANG, I. J. 2007. A Knowledge Discovery Approach to Diagnosing Intracranial Hematomas on Brain CT: Recognition, Measurement and Classification. *In:* ZHANG, D. (ed.) *Medical Biometrics.* Springer Berlin Heidelberg.

LIAO, C.-C., XIAO, F., WONG, J.-M. & CHIANG, I. J. 2010. Computer-aided diagnosis of intracranial hematoma with brain deformation on computed tomography. *Computerized Medical Imaging and Graphics,* 34**,** 563-571.

LIEBESKIND, D. S. 2018. Artificial intelligence in stroke care: Deep learning or superficial insight? *EBioMedicine,* 35**,** 14-15.

LIN, Y. C., TSAI, Y. P., HUNG, Y. P. & SHIH, Z. C. 2006. Comparison Between Immersion-Based and Toboggan-Based Watershed Image Segmentation. *IEEE Trans on Image Processing,* 15**,** 632-641.

LONCARIC, S., DHAWAN, A. P., COSIC, D., KOVACEVIC, D., BRODERICK, J. & BROTT, T. Quantitative intracerebral brain hemorrhage analysis. 1999. 886-894.

LONGA, E. Z., WEINSTEIN, P. R., CARLSON, S. & CUMMINS, R. 1989. Reversible middle cerebral artery occlusion without craniectomy in rats. *Stroke,* 20**,** 84-91.

MACQUEEN, J. Some methods for classification and analysis of multivariate observations. Proceedings of the Fifth Berkeley Symposium on Mathematical Statistics and Probability, Volume 1: Statistics, 1967 1967 Berkeley, Calif.: University of California Press, 281-297.

MAINALI, S., WAHBA, M. & ELIJOVICH, L. 2014. Detection of Early Ischemic Changes in Noncontrast CT Head Improved with "Stroke Windows". *ISRN Neurosci,* 2014**,** 654980.

MARINCEK, B. & DONDELINGER, R. F. 2007. *Emergency radiology : imaging and intervention,* Berlin, Springer.

MARQUES FILHO, O. V. N., HUGO. 1999. *Processamento Digital de Imagens,* Rio de Janeiro,

Brasport.

NEWCOMBE, R. G. 1998. Two-sided confidence intervals for the single proportion: comparison of seven methods. *Stat Med,* 17**,** 857-72.

NIELSEN, A., HANSEN MIKKEL, B., TIETZE, A. & MOURIDSEN, K. 2018. Prediction of Tissue Outcome and Assessment of Treatment Effect in Acute Ischemic Stroke Using Deep Learning. *Stroke,* 49**,** 1394-1401.

OSBORN, A. G. 1999. *Diagnostic Cerebral Angiography,* Philadelphia, Lippincott Williams & Wilkins.

OSMAN, M. M., LULIC, D., GLOVER, L., STAHL, C. E., LAU, T., VAN LOVEREN, H. & BORLONGAN, C. V. 2011. Cyclosporine-A as a neuroprotective agent against stroke: its translation from laboratory research to clinical application. *Neuropeptides,* 45**,** 359-68.

PEXMAN, J. H. W., BARBER, P. A., HILL, M. D., SEVICK, R. J., DEMCHUK, A. M., HUDON, M. E., HU, W. Y. & BUCHAN, A. M. 2001. Use of the Alberta Stroke Program Early CT Score (ASPECTS) for Assessing CT Scans in Patients with Acute Stroke. *American Journal of Neuroradiology,* 22**,** 1534-1542.

PINTO, A., MCKINLEY, R., ALVES, V., WIEST, R., SILVA, C. A. & REYES, M. 2018. Stroke Lesion Outcome Prediction Based on MRI Imaging Combined With Clinical Information. *Frontiers in Neurology,* 9.

POWERS WILLIAM, J., DERDEYN COLIN, P., BILLER, J., COFFEY CHRISTOPHER, S., HOH BRIAN, L., JAUCH EDWARD, C., JOHNSTON KAREN, C., JOHNSTON, S. C., KHALESSI ALEXANDER, A., KIDWELL CHELSEA, S., MESCHIA JAMES, F., OVBIAGELE, B. & YAVAGAL

DILEEP, R. 2015. 2015 American Heart Association/American Stroke Association Focused Update of the 2013 Guidelines for the Early Management of Patients With Acute Ischemic Stroke Regarding Endovascular Treatment. *Stroke,* 46**,** 3020-3035.

REKIK, I., ALLASSONNIÈRE, S., CARPENTER, T. K. & WARDLAW, J. M. 2012. Medical image analysis methods in MR/CT-imaged acute-subacute ischemic stroke lesion: Segmentation, prediction and insights into dynamic evolution simulation models. A critical appraisal. *NeuroImage: Clinical,* 1**,** 164-178.

ROERDINK, J. B. T. M. & MEIJSTER, A. 2000. The Watershed transform: Definitions, algorithms and parallelization strategies. *Fundamenta Informaticae,* 41**,** 187-228.

SPATH, H. 1985. *The Cluster Dissection and Analysis Theory FORTRAN Programs Examples,* Prentice-Hall, Inc.

SRINIVASAN, A., GOYAL, M., AL AZRI, F. & LUM, C. 2006a. State-of-the-art imaging of acute stroke. *Radiographics,* 26 Suppl 1**,** S75-95.

SRINIVASAN, A., GOYAL, M., AZRI, F. A. & LUM, C. 2006b. State-of-the-Art Imaging of Acute Stroke. *RadioGraphics,* 26**,** S75-S95.

TAJIRI, N., LAU, T., GLOVER, L. E., SHINOZUKA, K., KANEKO, Y., VAN LOVEREN, H. & BORLONGAN, C. V. 2012. Cerebral aneurysm as an exacerbating factor in stroke pathology and a therapeutic target for neuroprotection. *Curr Pharm Des,* 18**,** 3663-9.

TANG, F.-H., NG, D. K. S. & CHOW, D. H. K. 2011. An image feature approach for computer-aided detection of ischemic stroke. *Computers in Biology and Medicine,* 41**,** 529-536.

TANG, T.-Y., JIAO, Y., CUI, Y., ZENG, C.-H., ZHAO, D.-L., ZHANG, Y., PENG, C.-Y., YIN, X.-D., GAO, P.-Y., YANG, Y.-J., JU, S.-H. & TENG, G.-J. 2018. Development and validation of a penumbra-based predictive model for thrombolysis outcome in acute ischemic stroke patients. *EBioMedicine,* 35**,** 251-259.

TAO, W., JIN, H. & ZHANG, Y. 2007. Color Image Segmentation Based on Mean Shift and Normalized Cuts. *IEEE Transactions on Systems, Man, and Cybernetics, Part B (Cybernetics),* 37**,** 1382-1389.

TD, L. S. 1980. THE RELATIONSHIP BETWEEN CBF, EVOKED POTENTIALS AND THE CLINICAL FEATURES IN CEREBRAL ISCHAEMIA. *Acta Neurologica Scandinavica,* 62**,** 175-190.

TEKLE, W. G., CHAUDHRY, S. A., FATIMA, Z., AHMED, M., KHALIL, S., HASSAN, A. E., RODRIGUEZ, G. J., SURI, F. K. & QURESHI, A. I. 2012. Intravenous Thrombolysis in Expanded Time Window (3-4.5 hours) in General Practice with Concurrent Availability of Endovascular Treatment. *Journal of vascular and interventional neurology,* 5**,** 22-26.

THE EUROPEAN STROKE ORGANISATION EXECUTIVE, C. & THE, E. S. O. W. C. 2008. Guidelines for Management of Ischaemic Stroke and Transient Ischaemic Attack 2008. *Cerebrovascular Diseases,* 25**,** 457-507.

VAN EVERDINGEN, K. J., VAN DER GROND, J., KAPPELLE, L. J., RAMOS, L. M. & MALI, W. P. 1998. Diffusion-weighted magnetic resonance imaging in acute stroke. *Stroke,* 29**,** 1783-90.

YIZONG, C. 1995. Mean shift, mode seeking, and clustering. *IEEE Transactions on Pattern Analysis and Machine Intelligence*, 17**,** 790-799.

ZARINBAL, M. & ZARANDI, M. H. F. 2014. Type-2 fuzzy image enhancement: Fuzzy rule based approach. *Journal of Intelligent & Fuzzy Systems*, 26**,** 2291-2301.

ZHANG, J., YANG, Y., SUN, H. & XING, Y. 2014. Hemorrhagic transformation after cerebral infarction: current concepts and challenges. *Annals of translational medicine*, 2**,** 81-81.

Appendix 1

The document below refers to the approval of this research with accordance to The Research Ethics Committee according to Brazilian regulations (CAAE: 52457315.3.0000.5411). This document approved the use of all images and patient information in this research obtained from Botucatu medical School (Brazil).

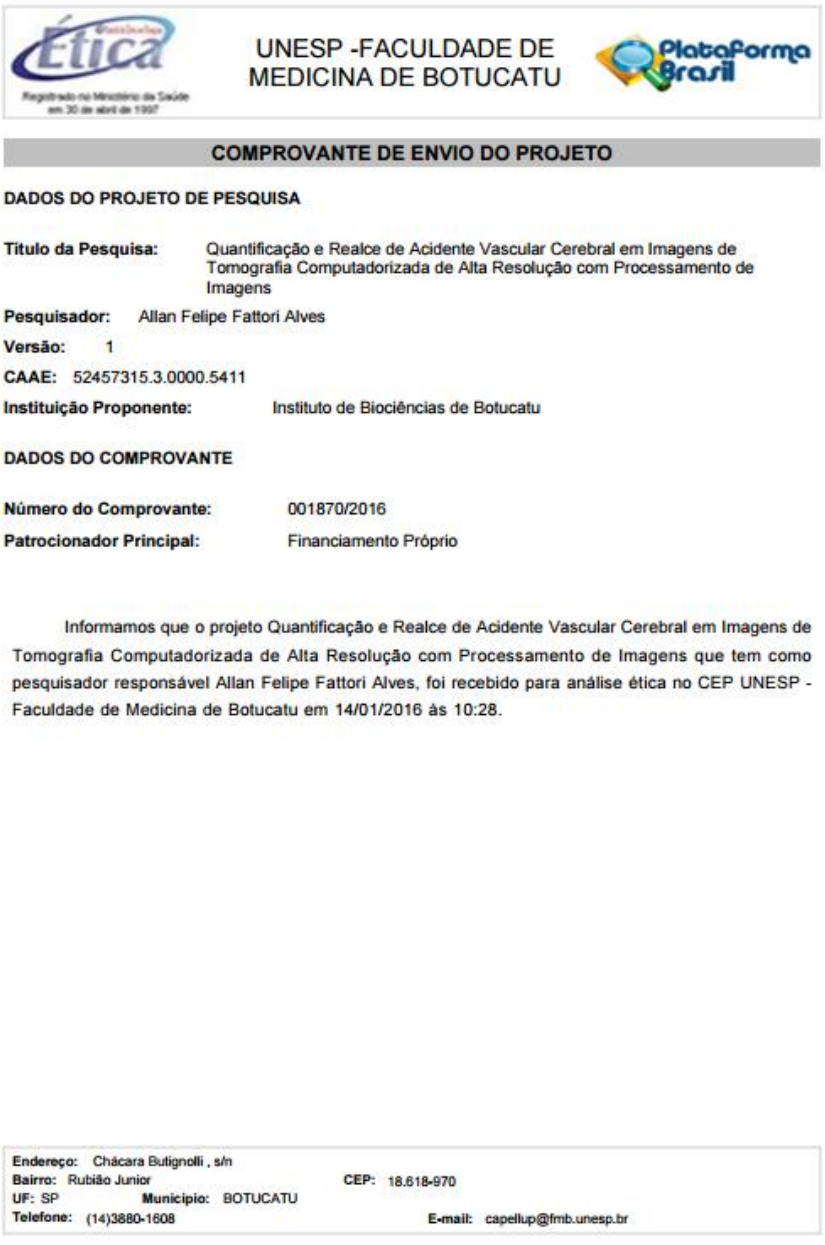

UNESP -FACULDADE DE MEDICINA DE BOTUCATU

COMPROVANTE DE ENVIO DO PROJETO

DADOS DO PROJETO DE PESQUISA

Título da Pesquisa: Quantificação e Realce de Acidente Vascular Cerebral em Imagens de Tomografia Computadorizada de Alta Resolução com Processamento de Imagens

Pesquisador: Allan Felipe Fattori Alves

Versão: 1

CAAE: 52457315.3.0000.5411

Instituição Proponente: Instituto de Biociências de Botucatu

DADOS DO COMPROVANTE

Número do Comprovante: 001870/2016

Patrocinador Principal: Financiamento Próprio

Informamos que o projeto Quantificação e Realce de Acidente Vascular Cerebral em Imagens de Tomografia Computadorizada de Alta Resolução com Processamento de Imagens que tem como pesquisador responsável Allan Felipe Fattori Alves, foi recebido para análise ética no CEP UNESP - Faculdade de Medicina de Botucatu em 14/01/2016 às 10:28.

Endereço: Chácara Butignolli , s/n
Bairro: Rubião Junior **CEP:** 18.618-970
UF: SP **Município:** BOTUCATU
Telefone: (14)3880-1608 **E-mail:** capellup@fmb.unesp.br

Appendix 2

Table 6 - - presents the group of patient with stroke with their NIHSS score, ASPECTS previous evaluation, and the subjective evaluation for all observers (1 – 6). Subjective evaluation 1 (E1) refers to the evaluation of original images, and the subjective evaluation 2 (E2) refers to the evaluation of enhanced images. Difference scores (Dif) represents the score in E2 minus E.

Patient	NIHSS	ASPECTS	O1			O2			O3			O4			O5			O6		
			E1	E2	Dif	E1	E2	Dif	E1	E2	Dif	E1	E2	Dif	E1	E2	Dif	E1	E2	Dif
1	14	9	4	4	0	4	4	0	4	4	0	3	4	1	5	5	0	5	5	0
2	16	6	3	4	1	4	5	1	5	5	0	5	5	0	5	4	0	5	5	0
3	19	9	4	4	0	4	4	0	4	4	0	4	5	1	5	5	0	5	5	0
4	16	5	4	5	1	5	5	0	5	5	0	5	5	0	5	5	0	5	5	0
5	13	9	4	4	0	5	5	0	4	4	0	5	5	0	5	5	0	5	5	0
6	22	6	3	4	1	4	4	0	5	5	0	5	5	0	5	5	0	5	5	0
7	4	8	3	4	1	2	4	2	4	4	0	4	4	0	3	3	0	5	5	0
8	6	10	2	3	1	2	3	1	2	4	2	4	4	0	5	5	0	3	5	2
9	21	9	3	4	1	3	4	1	4	4	0	5	5	0	3	5	2	5	5	0
10	3	9	2	2	0	5	4	-1	4	4	0	5	5	0	5	5	0	5	5	0
11	15	9	3	3	0	5	5	0	4	4	0	4	4	0	3	3	0	5	5	0
12	2	9	3	4	1	4	4	0	4	4	0	5	5	0	5	5	0	5	5	0
13	21	6	2	3	1	3	4	1	3	4	1	4	4	0	5	5	0	5	5	0
14	20	3	3	4	1	4	5	1	5	5	0	5	5	0	5	5	0	5	5	0
15	24	9	3	4	1	4	5	1	4	4	0	2	2	0	5	5	0	3	4	1
16	12	9	3	3	0	4	5	1	4	4	0	4	4	0	5	5	0	5	5	0
17	21	6	2	2	0	3	3	0	2	4	2	3	3	0	5	5	0	5	5	0
18	15	7	4	4	0	3	4	1	3	3	0	4	5	1	5	5	0	5	5	0
19	4	8	4	5	1	2	4	2	2	4	2	3	3	0	4	4	0	5	5	0
20	3	9	3	4	1	4	5	1	2	3	1	4	5	1	3	4	1	5	5	0
21	17	5	2	1	-1	2	3	1	2	3	1	2	2	0	4	4	0	5	5	0
22	7	8	3	2	-1	2	1	-1	2	2	0	3	4	1	3	4	1	4	5	1
23	3	6	3	3	0	3	3	0	3	4	1	4	4	0	3	4	1	5	5	0

Appendix 3

Table 7 - Group of control patient with the subjective evaluation for all observers (1 – 6). Subjective evaluation 1 (E1) refers to the evaluation of original images, and the subjective evaluation 2 (E2) refers to the evaluation of enhanced images. Difference scores (Dif) represents the score in E2 minus E1.

Patient	O1			O2			OB3			OB4			OB5			OB6		
	E1	E2	Dif	E1	E2	Dif	E1	E2	Dif	E1	E2	Dif	E1	E2	Dif	OR	PR	Diff
1	2	2	0	1	1	0	1	1	0	2	1	1	3	3	0	1	1	0
2	2	3	-1	3	3	0	4	4	0	2	2	0	3	3	0	3	3	0
3	2	2	0	2	1	1	2	2	0	2	1	1	4	4	0	2	2	0
4	2	2	0	3	2	1	1	1	0	2	1	1	3	1	2	3	3	0
5	2	1	1	2	1	1	2	1	1	2	3	-1	2	3	-1	3	1	2
6	3	4	-1	3	1	2	3	2	1	3	2	1	3	3	0	1	1	0
7	2	1	1	2	1	1	1	2	-1	2	2	0	3	4	-1	1	1	0
8	2	2	0	2	1	1	2	2	0	2	2	0	3	3	0	1	1	0
9	1	2	-1	2	3	-1	2	2	0	3	3	0	3	2	1	1	1	0
10	3	1	2	2	1	1	2	1	1	2	2	0	2	2	0	4	1	3
11	4	3	1	2	2	0	2	2	0	2	2	0	3	3	0	1	1	0
12	4	3	1	4	2	2	2	2	0	3	3	0	5	5	0	3	1	2
13	4	3	1	3	1	2	2	1	1	3	3	0	3	2	1	1	1	0
14	3	4	-1	2	4	-2	2	2	0	2	2	0	3	3	0	1	1	0
15	2	2	0	3	1	2	3	2	1	2	2	0	3	3	0	1	1	0
16	2	1	1	2	1	1	1	1	0	3	3	0	3	3	0	1	1	0

Appendix 4

European Radiology (2018) 28:3936–3942
https://doi.org/10.1007/s00330-018-5378-2

COMPUTED TOMOGRAPHY

Ischemic stroke enhancement using a variational model and the expectation maximization method

Allan Felipe Fattori Alves[1] · Rachid Jennane[2] · José Ricardo Arruda de Miranda[1] · Carlos Clayton Macedo de Freitas[3] · Nitamar Abdala[4] · Diana Rodrigues de Pina[5]

Received: 20 November 2017 / Revised: 18 January 2018 / Accepted: 7 February 2018 / Published online: 4 April 2018

Abstract

Objectives In order to enable less experienced physicians to reliably detect early signs of stroke, A novel approach was proposed to enhance the visual perception of ischemic stroke in non-enhanced CT.

Methods A set of 39 retrospective CT scans were used, divided into 23 cases of acute ischemic stroke and 16 normal patients. Stroke cases were obtained within 4.5 h of symptom onset and with a mean NIHSS of 12.9±7.4. After selection of adjunct slices from the CT exam, image averaging was performed to reduce the noise and redundant information. This was followed by a variational decomposition model to keep the relevant component of the image. The expectation maximization method was applied to generate enhanced images.

Results We determined a test to evaluate the performance of observers in a clinical environment with and without the aid of enhanced images. The overall sensitivity of the observer's analysis was 64.5 % and increased to 89.6 % and specificity was 83.3 % and increased to 91.7 %.

Conclusion These results show the importance of a computational tool to assist neuroradiology decisions, especially in critical situations such as the diagnosis of ischemic stroke.

Key Points

- *Diagnosing patients with stroke requires high efficiency to avoid irreversible cerebral damage.*
- *A computational algorithm was proposed to enhance the visual perception of stroke.*
- *Observers' performance was increased with the aid of enhanced images.*

Keywords Stroke · Brain · Algorithms · Tomography · Early diagnosis

Abbreviations

ASPECTS	Alberta Stroke Program Early CT Score
CPU	Central Processing Unit
CT	Computed tomography
DICOM	Digital Imaging and Communications in Medicine

Electronic supplementary material The online version of this article (https://doi.org/10.1007/s00330-018-5378-2) contains supplementary material, which is available to authorized users.

✉ Diana Rodrigues de Pina
drpina@fmb.unesp.br

[1] Instituto de Biociências de Botucatu, Departamento de Física e Biofísica, UNESP—Universidade Estadual Paulista, P.O. BOX 510, Distrito de Rubião Junior S/N, Botucatu, São Paulo 18618-000, Brazil

[2] Laboratory I3MTO – University of Orleans, 5 Rue de Chartres, BP 6744, 45072 Orléans, France

[3] Departamento de Neurologia, Psicologia e Psiquiatria, Faculdade de Medicina de Botucatu, UNESP—Universidade Estadual Paulista, Distrito de Rubião Junior S/N, Botucatu, São Paulo 18618-000, Brazil

[4] Departamento de Diagnóstico por Imagem, Escola Paulista de Medicina – UNIFESP, Rua Napoleão de Barros, 800, São Paulo 04024-002, Brazil

[5] Departamento de Doenças Tropicais e Diagnóstico por Imagem, Faculdade de Medicina de Botucatu, UNESP—Universidade Estadual Paulista, Distrito de Rubião Junior S/N, Botucatu, São Paulo 18618-000, Brazil

E1	Evaluation 1
E2	Evaluation 2
FN	False negative
FP	False positive
HU	Hounsfield units
MRI	Magnetic resonance image
NECT	Non-enhanced computed tomography
O1-6	Observer 1-6
TN	True Negative
TP	True Positive
VM	Variational Model

Introduction

Stroke is a cardiovascular disease that currently ranks in the fifth position among all causes of death [1]. The evaluation and initial treatment of patients with stroke symptoms require a high efficiency to avoid irreversible cerebral damage [2, 3]. Multiple medical imaging modalities appear as alternatives in the diagnosis of early signs of stroke such as magnetic resonance image (MRI) and computed tomography (CT) [4]. CT is more accessible, less expensive and faster. Non-enhanced CT (NECT) is the first radiological examination performed in emergency decisions and it is sufficient in most cases for identifying contraindications to fibrinolysis treatment [5]. The earliest signs of ischemic stroke are quite subtle on NECT. Usually, after 1–3 h of symptom onset, a slight hypodense area of infarction in either the cortices or the basal ganglia can become visible [6].

The image enhancement may aid physicians in diagnosing early signs of acute ischemic stroke. Previous studies have demonstrated approaches for enhancing ischemic stroke. Przelaskowski et al. [7] used a wavelet-based processing method for improving acute stroke detection. Chawla et al. [8] proposed an algorithm based on the contralateral symmetry to detect stroke in CT. Tang et al. [9] presented a computer-aided detection scheme for early detection of ischemic stroke using image feature characteristics.

In this paper, a novel approach to enhance the visual perception of ischemic stroke in NECT is proposed. This enhancement aims to enable less experienced viewers to reliably detect early signs of stroke. Our new contribution consists of efficiently combining different image processing techniques. Firstly, to reduce noise and redundancies, a projection of the slices likely to contain the ischemic stroke followed by a band-pass filtering is realized. Then, to enhance the contrast of the projection obtained, a variational model (VM) decomposition is used. Finally, the expectation maximization method is applied to the relevant component from VM decomposition to segment and emphasize the ischemic stroke. The performance of observers was evaluated. We compared their sensitivity and specificity performances for stroke and control cases.

Materials and methods

Patients and image selection

The study was approved by the local institutional ethics committee. We collected retrospective examinations of patients. Patients were selected using the following criteria for inclusion and exclusion. Inclusion criteria: patients with confirmed acute ischemic stroke lesions who had undergone CT scan examinations within less than 4.5 h of symptom onset [10]. Exclusion criteria: patients with previous stroke lesions, intracranial malformations or haemorrhage. This study also did not consider cases of stroke with haemorrhagic transformation. Certified CT scans of stroke were checked with the clinical reports including histological, pathological and clinical results, and with the follow-up NECT examination acquired in the following days for each patient. Finally, all cases were further validated by two radiologists, and only cases approved by both of them were used. After this selection, a set of 39 CT examinations were used: 23 cases of acute ischemic stroke, and 16 normal cases used as a control group. Normal cases were obtained from the database of our institution from migraine studies in which patients did not have any anatomical or neurological alterations. CT scans were performed on multislice CT scanners. Scanner acquisition settings were: kVp = 120, automatic exposure control, exposure time = 1 s, matrix size = 512 × 512 and slice thickness = 2.5 mm. All images were stored using the DICOM format.

Methods

A computational algorithm was proposed to enhance the ischemic stroke visual perception. After selection of adjunct slices, an average image (called projection) was performed to reduce the noise and redundant information. Then, a VM decomposition was applied on the obtained projection to keep the relevant component for our analysis. Finally, the Expectation Maximization (EM) method was applied to enhance the ischemic stroke. The proposed approach steps are described in the flowchart (Fig. 1). All steps were performed using Matlab software R 2014a.

Selection of slices

The processing starts by opening one sequence of CT scan images of individual patients. The selection of slices was performed in the same region as the ASPECTS score, involving

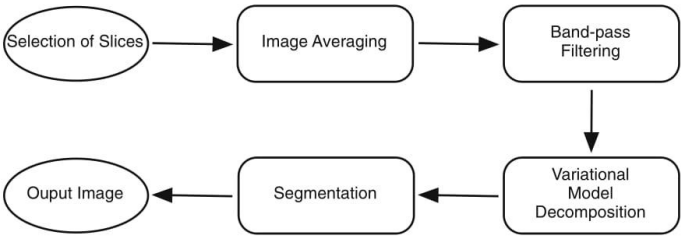

Fig. 1 Flowchart showing the main image processing steps performed

two slices, one at the level of the thalamus and basal ganglion and one adjacent to the most superior margin of the ganglionic structures, such that they were not seen [11]. These regions are most commonly affected by stroke [2]. After selecting slices, a projection is performed by summing the values of the grey levels in each slice, yielding an average image. The algorithm operates by computing an arithmetic mean of the intensity values for each pixel position in a set of captured images from subsequent slices. This approach was performed to highlight the presence of stroke and lower the image noise level. All control group images were also averaged using slices in the same region evaluated for the stroke group.

Band-pass filtering and variational model decomposition

After the projection step, a band-pass filtering was applied between 0 and 50 Hounsfield units (HU) to remove all pixels of bone tissue, background and other unwanted structures. All pixels out of this band were assigned a new value equal to zero HU. After this stage, a histogram normalization was performed by redistributing pixels intensities from [0, 50] to [0, 255] HU. The histogram normalization enabled improving the contrast between adjacent regions.

To further enhance the contrast of the projection, a Variational Model (VM) [12, 13] decomposition was applied to decompose the image into different components. The image p was modelled as the sum of three terms: $p = u + v + w$. Here, v is the smooth second order part, u is related to contours and w is linked to fine textures. Our primary interest is in the v component since it is related to contrast and brightness of the image. More details of the VM decomposition are presented in the Supplementary Material.

Segmentation

The next step concerned the image segmentation, which was applied to the v component after the VM decomposition. The Expectation Maximization (EM) method has been very popular in medical imaging and several variants of the algorithm have been proposed [14, 15]. EM is a segmentation method that assigns pixel intensities into different clusters using a probabilistic Gaussian distribution. The mixture model is composed of a sum of K Gaussian distributions, each distribution with its own parameters. The algorithm is iterative and starts from some initial estimate and then proceeds to iteratively update until convergence. Each iteration consists of an Expectation (E-step) and a Maximization (M-step) step [14]. Each pair of E and M steps are considered one iteration. This EM cycle is repeated until some preset threshold. Thus, in the final assignment each pixel of the final image will belong to only one cluster. More details on the EM method are presented in the supplementary material.

Observers' evaluation

A test was established to evaluate the performance of observers based on a scoring system used by Tang et al. [9]. Four resident radiologists from the first (Observer 1 – O1 and Observer 2 – O2), second (Observer 3 – O3) and third (Observer 4 – O4) years of residence and two experienced radiologists (Observer 5 – O5 and Observer 6 – O6) with 10 and 20 years of experience in radiology, worked as observers. All radiologists were from Botucatu Medical School Hospital, Brazil. They had no previous knowledge regarding the history of the patients. First, the set of original images was analysed in a random order combining stroke and control cases. Observers were allowed to adjust contrast, brightness and magnification of images according to their own experience. Each observer was required to give a score relating to the presence of acute stroke (definitely absent: 1, absent: 2, uncertain: 3, present: 4 and definitely present: 5). Then, as a second step, the observers evaluated the enhanced images that were created from our proposed approach. The change of the score in diagnosis was tracked after the observation of enhanced images. Improvement changes were considered when the observer changed his evaluation to the correct score. These analyses permitted testing the confidence of the diagnosis both before and after the image enhancement.

We also measured both sensitivity and specificity of the performance of the observers before and after the enhanced images. The formula for both quantitative measures is given in Eqs. 1 and 2. The scores 1, 2 and 3 were considered as

negative evaluations and the scores 4 and 5 were considered as positive.

$$\text{Sensitivity} = \frac{TP}{(TP + FN)} \quad (1)$$

$$\text{Specificity} = \frac{(TN)}{(TN + FP)} \quad (2)$$

where TP are true positives, TN are true negatives, FP are false positives and FN are false negatives.

We tracked the difference scores that resulted from the analysis of both original and enhanced images. For the difference scores, one can consider a positive score when the observer changes his previous score from any given value to a higher one. For example, the original score was 3 and the observer changed after analysing the enhanced image to a score of 4, which means that the stroke can now be visualized. Additionally, negative scores represent false-negative cases.

Results

In this study the mean age of patients was 68.45 ± 9.56 years for stroke and 65.12 ± 9.22 for control. No significant difference was found between the stroke patients and controls for age (p-value = 0.1735) using Student's t-test. Stroke patients had a mean NIHSS of 13±7 and mean ASPECTS of 7±2. The complete results of NIHSS and ASPECTS are presented in the Electronic Supplementary Material. All sequence of images analysed passed through the image processing steps described in the flowchart in Fig. 1. Figure 2 A-E illustrates the ischemic density changes in adjunct CT slices of the same patient. Figure 2 F presents the resulting image after computing the projection using slices A–E.

Our approach provided enhanced images that helped physicians to achieve a more reliable diagnosis of ischemic stroke in CT examinations. Representative examples of those enhanced images from different patients are presented in Fig. 3. On the top, corresponding to letters A, B, C and D, are presented the images resulting from the image averaging step of three different patients with stroke and one control case (Fig. 3 D). In the second row, corresponding to letters E, F, G and H, are presented the enhanced images according to our proposed approach accounting the band-pass filtering, followed by the VM decomposition and the EM segmentation method.

The overall sensitivity of the observer's analysis was 64.5 % and changed to 89.6 % after the evaluation of the enhanced images. The overall specificity was 83.3 % and increased to 91.7 %. The sensitivity and specificity obtained for each observer both before and after evaluating the enhanced images are summarized in Table 1. We also compared the difference scores for all observers analysing the original images and then the enhanced images for stroke cases. In this manner, one could see each case in which enhanced images provided a more reliable diagnosis. For a better visualization of scores, the observers O1, O2 and O3 were joined in the graph of Fig. 4 and observers O4, O5, and O6 in the graph of Fig. 5.

The improvement of sensitivity was more remarkable for the three least experienced physicians. This great improvement was also shown in the difference score graphs. The maximum difference score was 2 (Fig. 4 and Fig. 5), since the maximum changes occurred when observers first assigned the score 3 and then changed to score 5 after analysing the enhanced images. For those cases, enhanced images provided greater reliability in the diagnosis of ischemic stroke.

Discussion

In this paper, we proposed an approach to enhance the visual perception of ischemic stroke to be used in clinical routine as a support to the diagnosis of this disease. One limitation of our approach is that it is not entirely automatic, since it depends on the physician selection of the slices before the application of the algorithm. Two experienced radiologists selected all ground through stroke cases with the support of the follow-up CT in the same patient to confirm the occurrence of stroke. The image averaging technique was used to reduce noise and improve the perception of stroke while using subsequent slices with slightly different anatomical structures (Fig. 2). This was considered an acceptable tradeoff by the physician's analysis. The VM decomposition helped to enhance the contrast and the brightness of the images.

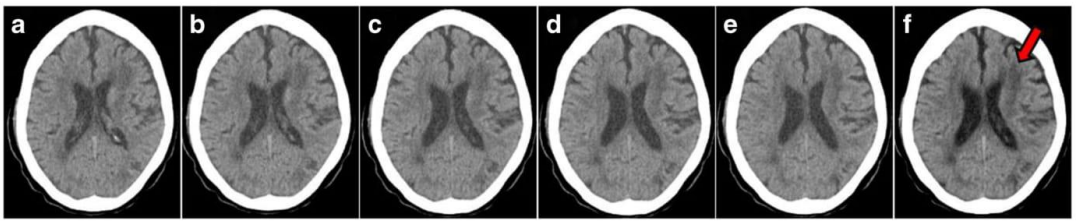

Fig. 2 (**A-E**) Adjunct slices sequence with the presence of the subtle density changes in the same patient. **F** is the result of the projection involving slices **A, B, C, D** and **E**. Stroke is present in the left frontal lobe of the brain, as indicated by the red arrow

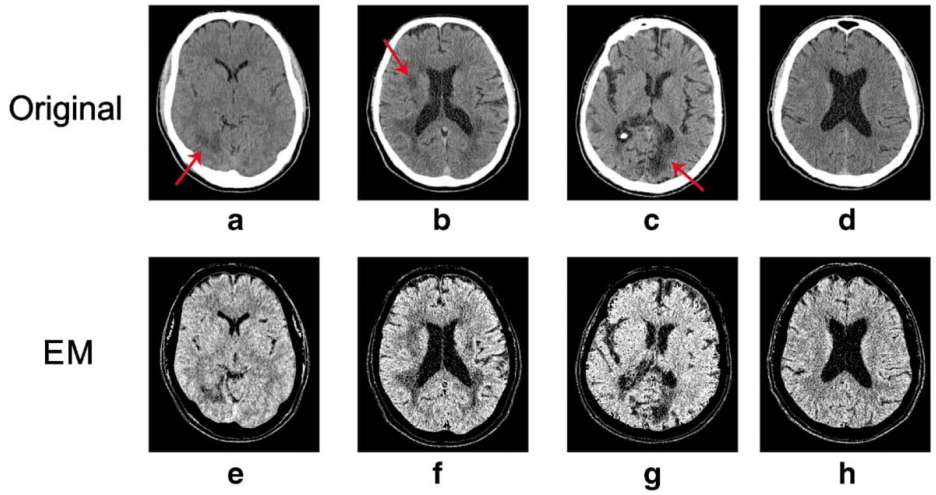

Fig. 3 Average images for three different patients with strokes (**A, B, C**) and one control (**D**). Enhanced images are shown in second row with the Expectation Maximization (EM) approach (**E, F, G, H**).

The purpose of the EM segmentation was to enhance the visual perception of ischemic stroke. A key aspect for the EM approach is to choose the number of clusters for segmentation. Our target was to achieve a number that would both benefit the visual enhancement and have no additional cost in computational time. This is an important issue since the main goal is to apply this algorithm to a medical diagnosis workstation. The best achieved results were found for six clusters. The average elapsed time for each patient analysis is 141.6 ± 1.5 s. Our experiments were performed on machines running Intel® processors with 2.4 GHz CPU frequency and having 32 GB of memory.

Regarding previous studies, Przelaskowski et al. [7] proposed a method to enhance the subtle signs of ischemic stroke in NECT. They analysed a small cohort of 11 CT examinations and improved the sensitivity of two observers from 12.5 % to 56.3 %. Tang et al. [9] proposed a method with a Circular Adaptive Region of Interest to analyse stroke in NECT scans. With a cohort of 40 examinations, they showed a significant improvement in sensitivity and specificity for three observers. They also demonstrated a great correlation between the experience of physicians and its performance. Our results corroborate that the ability of observers to detect early signs of ischemic stroke highly depend on their experience. With the aid of the enhanced images, inexperienced physicians achieved the ability to diagnose stroke, very close to the average or even higher when compared to other published papers. Patel et al. [17] found 31 % sensitivity for these early infarct signs, while von Kummer et al. [18] found that this rate increases to 82 % 6 h after symptoms onset. In general, the observers' ability to detect stroke in NECT without enhancement is less than 67 % in cases imaged within 3 h [19]. Our results indicate an initial sensitivity of 63.9 % with an improvement to 78.9 %.

Table 1 Observers' sensitivity and specificity before (evaluation 1– E1) and after (evaluation 2 – E2) of the enhanced images. Confidence intervals (CIs) for sensitivity and specificity are calculated with the Wilson score method [16]

Observers	Sensitivity				Specificity			
	E1		E2		E1		E2	
	Mean	CI	Mean	CI	Mean	CI	Mean	CI
O1	26.1	(12.5–46.7)	60.9	(40.8–77.8)	81.3	(57.0–93.4)	87.5	(63.9–96.5)
O2	52.2	(32.9–70.7)	78.3	(58.1–90.4)	93.7	(71.7–98.9)	93.7	(71.7–98.9)
O3	65.2	(44.9–81.2)	82.6	(62.9–93.0)	93.7	(71.7–98.9)	93.7	(71.7–98.9)
O4	78.3	(58.1–90.4)	87.0	(67.9–95.5)	100	(80.7–100)	100	(80.7–100)
O5	73.9	(53.3–87.5)	91.3	(73.2–97.6)	75.0	(50.5–89.8)	75.0	(50.5–89.8)
O6	91.3	(73.2–97.6)	100	(85.7–100)	93.7	(71.7–98.9)	100	(80.7–100)
Overall	64.5	(56.2–72.0)	89.6	(81.8–94.2)	83.3	(76.3–88.7)	91.7	(84.4–95.7)

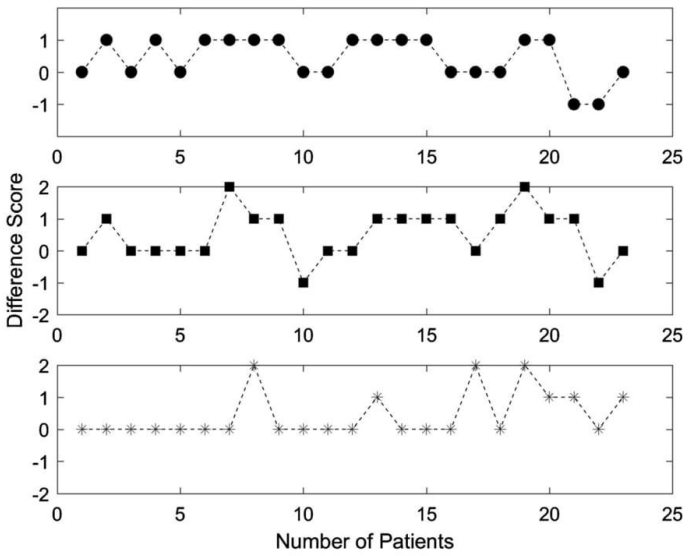

Fig. 4 Difference scores for the observers O1 (circle), O2 (square) and O3 (asterisk). The difference was obtained when the scores given for the enhanced images are compared to the scores given for the original images. Positive values indicate an enhancement in diagnosis. Negative changes indicate false-negative cases

Chawla et al.'s [8] method used the dissimilarity between the left and right hemispheres of the brain, which was used it to classify different types of stroke. According to the authors, this approach fails when the same type of stroke occurs symmetrically in both hemispheres. The same applies for Tang et al. [9], whose proposed scheme is not applicable when the brain is asymmetrical. Our proposed approach does not rely on brain symmetry. Most patients with stroke symptoms are agitated and there is a high risk that their heads were tilted during image acquisition, which compromises hemisphere comparison. According to the opinion of the observers who participated in this study, the enhanced images were particularly useful when displayed together with the original images. We strongly suggest that the enhanced images be displayed in association with the original images instead of standalone.

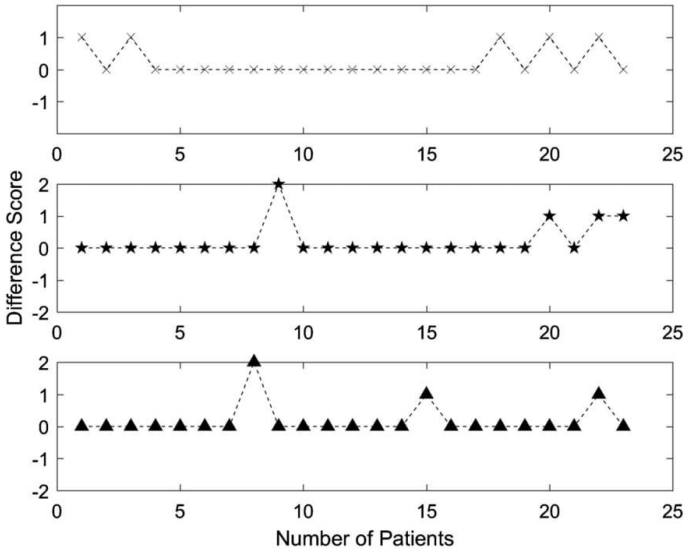

Fig. 5 Difference scores for the observers O4 (cross), O5 (star) and O6 (triangle). The difference was obtained when the scores given for the enhanced images are compared to the scores given for the original images. Positive values indicate an enhancement in diagnosis. Resident 4 results were included in this analysis since they were more similar to the experienced radiologists

A novel approach based on a VM and EM method was used to enhance the ischemic stroke perception in non-enhanced CT examinations. We demonstrated that enhanced images improved physicians' performance to diagnose early signs of acute ischemic stroke. These results show the importance of a computational tool to assist neuroradiology decisions, especially in critical situations such as institutions that do not have stroke specialists. Enhanced images may largely increase the potential candidates for thrombolysis treatment.

Acknowledgements The authors wish to thank all clinical personnel of the Botucatu Medical School Radiodiagnostic facility. We also thank the Laboratories I3MTO from University of Orleans and LAFAR from São Paulo State University.

Funding Financial support was provided by Fundação de Amparo à Pesquisa do Estado de São Paulo (FAPESP).

Compliance with ethical standards

Guarantor The scientific guarantor of this publication is José Ricardo de Arruda Miranda from São Paulo State University, Brazil.

Conflict of interest The authors of this manuscript declare no relationships with any companies whose products or services may be related to the subject matter of the article.

Statistics and biometry No complex statistical methods were necessary for this paper.

Informed consent Written informed consent was not required for this study because all CT scans used were retrospective and no confidential patient information was used throughout this study.

Ethical approval Institutional Review Board approval was obtained.

Methodology
- retrospective
- diagnostic or prognostic study
- performed at one institution

References

1. Benjamin EJ, Blaha MJ, Chiuve SE et al (2017) Heart disease and stroke statistics—2017 update: a report from the American Heart Association. Circulation. https://doi.org/10.1161/cir.0000000000000485
2. Jauch EC, Saver JL, Adams HP Jr et al (2013) Guidelines for the early management of patients with acute ischemic stroke: a guideline for healthcare professionals from the American Heart Association/American Stroke Association. Stroke 44:870–947
3. Amar AP (2011) Brain and vascular imaging of acute stroke. World Neurosurg 76:S3–S8
4. Mohr JP, Biller J, Hilal SK et al (1995) Magnetic resonance versus computed tomographic imaging in acute stroke. Stroke 26:807–812
5. Wu H-Q, Wu H, Shi L-L et al (2017) The association between retinal vasculature changes and stroke: a literature review and meta-analysis. Int J Ophthalmol 10:109–114
6. Barber PA, Demchuk AM, Zhang J, Buchan AM (2000) Validity and reliability of a quantitative computed tomography score in predicting outcome of hyperacute stroke before thrombolytic therapy. Lancet 355:1670–1674
7. Przelaskowski A, Sklinda K, Bargieł P, Walecki J, Biesiadko-Matuszewska M, Kazubek M (2007) Improved early stroke detection: wavelet-based perception enhancement of computerized tomography exams. Comput Biol Med 37:524–533
8. Chawla M, Sharma S, Sivaswamy J, Kishore L (2009) A method for automatic detection and classification of stroke from brain CT images. Conf Proc IEEE Eng Med Biol Soc 2009:3581–3584
9. Tang F-h, Ng DKS, Chow DHK (2011) An image feature approach for computer-aided detection of ischemic stroke. Comput Biol Med 41:529–536
10. Hacke W, Kaste M, Bluhmki E et al (2008) Thrombolysis with alteplase 3 to 4.5 hours after acute ischemic stroke. N Engl J Med 359:1317–1329
11. Huisa BN, Raman R, Ernstrom K et al (2010) Alberta stroke program early CT score (ASPECTS) in patients with wake-up stroke. J Stroke Cerebrovasc Dis 19:475–479
12. Bergounioux M (2016) Mathematical analysis of a inf-convolution model for image processing. J Optim Theory Appl 168:1–21
13. Bergounioux M, Caillau J-B, Haberkorn T, Peyré G, Schnörr C (2016) Variational methods in imaging and geometric control. de Gruyter, France
14. Bilmes JA (1998) A gentle tutorial of the EM algorithm and its application to parameter estimation for Gaussian mixture and hidden Markov models. University of Berkeley, California 94704-1198
15. Zhang Y, Brady M, Smith S (2001) Segmentation of brain MR images through a hidden Markov random field model and the expectation-maximization algorithm. IEEE Trans Med Imaging 20:45–57
16. Newcombe RG (1998) Two-sided confidence intervals for the single proportion: comparison of seven methods. Stat Med 17:857–872
17. Patel SC, Levine SR, Tilley BC et al (2001) Lack of clinical significance of early ischemic changes on computed tomography in acute stroke. JAMA 286:2830–2838
18. von Kummer R, Holle R, Gizyska U et al (1996) Interobserver agreement in assessing early CT signs of middle cerebral artery infarction. Am J Neuroradiol 17:1743–1748
19. Latchaw RE, Alberts MJ, Lev MH et al (2009) Recommendations for imaging of acute ischemic stroke. A scientific statement from the American Heart Association. Stroke 40:3646–3678

Appendix 5

The author, Allan Felipe Fattori Alves, published the following papers during the period of his PhD. We present the first page of those papers in the sequence below.

European Journal of Radiology 84 (2015) 1579–1585

Contents lists available at ScienceDirect

European Journal of Radiology

journal homepage: www.elsevier.com/locate/ejrad

Construction of pediatric homogeneous phantoms for optimization of chest and skull radiographs

Allan Felipe Fattori Alves[a,*], José Ricardo de Arruda Miranda[c,2], Fernando Antonio Bacchim Neto[c,2], Sérgio Barbosa Duarte[d,3], Diana Rodrigues de Pina[b,1]

[a] Instituto de Biociências de Botucatu, P.O. BOX 510, Departamento de Física e Biofísica, UNESP—Universidade Estadual Paulista, Distrito de Rubião Junior S/N, Botucatu, 18618-000 São Paulo, Brazil
[b] Departamento de Doenças Tropicais e Diagnóstico por Imagem, Faculdade de Medicina de Botucatu, UNESP—Universidade Estadual Paulista, Distrito de Rubião Junior S/N, Botucatu, 18618-000 São Paulo, Brazil
[c] Instituto de Biociências de Botucatu, Departamento de Física e Biofísica, UNESP—Universidade Estadual Paulista, Distrito de Rubião Junior S/N, Botucatu, 18618-000 São Paulo, Brazil
[d] Centro Brasileiro de Pesquisas Físicas, Laboratório de Altas Energias, Dr. Xavier Sigaud, 150, Rio de Janeiro, 22290-180 Rio de Janeiro, Brazil

ARTICLE INFO

Article history:
Received 26 September 2014
Received in revised form 6 April 2015
Accepted 8 May 2015

Keywords:
Chest and skull
Pediatric homogenous phantom
Image quality
Dose optimization

ABSTRACT

Objectives: To develop two pediatric patient-equivalent phantoms, the Pediatric Chest Equivalent Patient (PCEP) and the Pediatric Skull Equivalent Patient (PSEP) for children aged 1 to 5 years. We also used both phantoms for image quality evaluations in computed radiography systems to determine Gold Standard (GS) techniques for pediatric patients.
Methods: To determine the simulator materials thickness (Lucite and aluminum), we quantified biological tissues (lung, soft, and bone) using an automatic computational algorithm. To objectively establish image quality levels, two physical quantities were used: effective detective quantum efficiency and contrast-to-noise ratio. These quantities were associated to values obtained for standard patients from previous studies.
Results: For chest radiographies, the GS technique applied was 81 kVp, associated to 2.0 mAs and 83.6 μGy of entrance skin dose (ESD), while for skull radiographies, the GS technique was 70 kVp, associated to 5 mAs and 339 μGy of ESD.
Conclusion: This procedure allowed us to choose optimized techniques for pediatric protocols, thus improving quality of diagnosis for pediatric population and reducing diagnostic costs to our institution. These results could also be easily applied to other services with different equipment technologies.

1. Introduction

Because of increased mitotic activity and longer life expectancy, children are more radiosensitive than middle-aged adults. Children are two- to three-times more susceptible to radiation and the consequent development of leukemia, and adults who are exposed to radiation during childhood have an increased probability of developing breast or thyroid cancer [1]. Chest and skull radiography are the most commonly performed examinations in pediatric patients aged 1 to 5 years because of head trauma [2,3] and pneumonia [4].

The optimization of radiographic techniques for pediatric patients is especially important when using digital systems because of an imperceptible increase in dose with time [5]. Homogeneous phantoms are important tools to establish optimized techniques [6–9], especially in medical departments with restricted resources, which can easily simulate realistic anatomical regions [10]. Two homogeneous phantoms are currently used: LucAl phantom (which provides accurate simulation of primary and scatter transmission through the lung field) [11] and patient equivalent phantom (PEP; also known as the ANSI phantom [6,10,12] for the chest, skull, and extremities). The PEP is lightweight and transportable. It is constructed of readily available materials and accurately simulates the standard patient's attenuation properties [13,14].

The present study presents a methodology for constructing pediatric homogeneous phantoms, namely the Pediatric Chest

* Corresponding author. Tel.: +55 14 3880 0285; fax: +55 14 3880 0285.
E-mail addresses: allan@ibb.unesp.br (A.F.F. Alves), jmiranda@ibb.unesp.br (J.R.d.A. Miranda), fernando.bacchim@gmail.com (F.A. Bacchim Neto), sbd@cbpf.br (S.B. Duarte), drpina@fmb.unesp.br (D.R.d. Pina).
[1] Tel: +55 14 3811 6254, Fax: +55 14 3811 6254.
[2] Tel: +55 14 3880 0285, Fax: +55 14 3880 0285.
[3] Tel: +55 21 2141 7328, Fax: +55 21 2141 7328.

http://dx.doi.org/10.1016/j.ejrad.2015.05.015
0720-048X/

Physica Medica 31 (2015) 1065–1069

Contents lists available at ScienceDirect

Physica Medica

journal homepage: http://www.physicamedica.com

Technical Notes

Quality and dose optimization in hand computed radiography

A.L.M. Pavan [a], A.F.F. Alves [a], S.B. Duarte [b], G. Giacomini [a], T. Sardenberg [c], J.R.A. Miranda [a], D.R. Pina [d,*]

[a] Dept of Physics and Biophysics, Biosciences Institute of Botucatu, São Paulo State University, Distrito de Rubião Junior S/N, Botucatu, São Paulo 18618-000, Brazil
[b] Brasilian Center of Physics Research -CBPF-MCT, Rio de Janeiro 22290-180, Brazil
[c] Dept of Orthopedics and Traumatology, Botucatu Medical School, São Paulo State University, Distrito de Rubião Junior S/N, Botucatu, São Paulo 18618-000, Brazil
[d] Dept of Tropical Diseases and Diagnostic Imaging, Botucatu Medical School, Univ Estadual Paulista, Distrito de Rubião Junior S/N, Botucatu, São Paulo 18618-000, Brazil

ARTICLE INFO

Article history:
Received 7 April 2015
Received in revised form 26 May 2015
Accepted 15 June 2015
Available online 3 July 2015

Keywords:
Phantom
Figure of merit
Visual Grading Analysis
Image optimization

ABSTRACT

The objective of the present study was to optimize a radiographic technique for hand examinations using a computed radiography (CR) system and demonstrate the potential for dose reductions compared with clinically established technique. An exposure index was generated from the optimized technique to guide operators when imaging hands. Homogeneous and anthropomorphic phantoms that simulated a patient's hand were imaged using a CR system at various tube voltages and current settings (40–55 kVp, 1.25–2.8 mAs), including those used in clinical routines (50 kVp, 2.0 mAs) to obtain an optimized chart. The homogeneous phantom was used to assess objective parameters that are associated with image quality, including the signal difference-to-noise ratio (SdNR), which is used to define a figure of merit (FOM) in the optimization process. The anthropomorphic phantom was used to subjectively evaluate image quality using Visual Grading Analysis (VGA) that was performed by three experienced radiologists. The technique that had the best VGA score and highest FOM was considered the gold standard (GS) in the present study. Image quality, dose and the exposure index that are currently used in the clinical routine for hand examinations in our institution were compared with the GS technique. The effective dose reduction was 67.0%. Good image quality was obtained for both techniques, although the exposure indices were 1.60 and 2.39 for the GS and clinical routine, respectively.

Introduction

Many disease processes are manifested in the small bones of the hands, wrists, and associated soft tissues [1,2]. Several diagnostic decisions depend on detecting the details and image contrast of interfaces in the hand and wrist. The early detection, diagnosis, and continuous evaluation of disease states are essential for successful treatment [1,2]. Radiography is the first choice for the evaluation of diseases of the hands, and other image techniques are rarely used to establish diagnosis and treatment. Therefore, the image quality of X-ray examinations is essential.

Homogeneous phantoms are widely used in image quality optimization to determine the optimal technique and establish protocols for clinical routines while ensuring maximal image quality with as low as reasonably achievable (ALARA) doses [3,4]. Such phantoms are constructed of tissue-equivalent materials to simulate the absorption and scatter of the X-ray beam in the body. These phantoms are generally made with polymethyl methacrylate (acrylic) and aluminum. Numerous homogeneous phantoms have been constructed for different anatomical regions, such as the chest, abdomen, lumbar spine, skull, and extremities [3–5].

With technical advances from analog to digital systems, techniques that have been traditionally considered optimum for analog systems may no longer be considered optimal for digital systems [6,7]. Operators base their choice of technique on trial and error because digital radiography can be manipulated in the display of the image to obtain the desired contrast [8].

Ideally, the objective optimization of digital radiographs is based on the signal difference-to-noise ratio (SdNR) [6]. A digital image with a high SdNR may provide inherently superior image quality compared with a lower SdNR [6]. Measurements of the SdNR are usually performed in a test object, such as a homogeneous phantom, in which the pixel value of a contrast object (signal) is compared with its surrounding area (background). However, the SdNR is of

* Corresponding author. Prof. Montenegro Avenue, Rubião Junior District, Botucatu, São Paulo 18618-970, Brazil. Tel.: +55 1438116088; fax: +55 1438159898.
E-mail addresses: analuiza@ibb.unesp.br (A.L.M. Pavan), allan@ibb.unesp.br (A.F.F. Alves), sbd@cbpf.br (S.B. Duarte), guigiacomini92@aluno.ibb.unesp.br (G. Giacomini), tsarden@fmb.unesp.br (T. Sardenberg), jmiranda@ibb.unesp.br (J.R.A. Miranda), drpina@fmb.unesp.br (D.R. Pina).

http://dx.doi.org/10.1016/j.ejmp.2015.06.010
1120-1797/

Medicine®

QUALITY IMPROVEMENT STUDY

OPEN

Quantification of Pulmonary Inflammatory Processes Using Chest Radiography: Tuberculosis as the Motivating Application

Guilherme Giacomini, PhD, José R.A. Miranda, PhD, Ana Luiza M. Pavan, MSc, Sérgio B. Duarte, PhD, Sérgio M. Ribeiro, PhD, MD, Paulo C.M. Pereira, PhD, MD, Allan F.F. Alves, MSc, Marcela de Oliveira, MSc, and Diana R. Pina, PhD

Abstract: The purpose of this work was to develop a quantitative method for evaluating the pulmonary inflammatory process (PIP) through the computational analysis of chest radiography exams in posteroanterior (PA) and lateral views. The quantification procedure was applied to patients with tuberculosis (TB) as the motivating application.

A study of high-resolution computed tomography (HRCT) examinations of patients with TB was developed to establish a relation between the inflammatory process and the signal difference-to-noise ratio (SDNR) measured in the PA projection. A phantom essay was used to validate this relation, which was implemented using an algorithm that is able to estimate the volume of the inflammatory region based solely on SDNR values in the chest radiographs of patients.

The PIP volumes that were quantified for 30 patients with TB were used for comparisons with direct HRCT analysis for the same patient. The Bland–Altman statistical analyses showed no significant differences between the 2 quantification methods. The linear regression line had a correlation coefficient of $R^2 = 0.97$ and $P < 0.001$, showing a strong association between the volume that was determined by our evaluation method and the results obtained by direct HRCT scan analysis.

Since the diagnosis and follow-up of patients with TB is commonly performed using X-rays exams, the method developed herein can be considered an adequate tool for quantifying the PIP with a lower patient radiation dose and lower institutional cost. Although we used patients with TB for the application of the method, this method may be used for other pulmonary diseases characterized by a PIP.

(*Medicine* 94(26):e1044)

Abbreviations: CR = computed radiography, CT = computed tomography, HRCT = high-resolution computed tomography, MFLIP = mean fractional length of inflammatory processes, PA = posteroanterior, PIP = pulmonary inflammatory process, PVC = polyvinyl chloride, ROI = region of interest, SDNR = signal difference-to-noise ratio, TB = tuberculosis, WHO = World Health Organization.

Editor: Ioannis Tsalafoutas.
Received: February 13, 2015; revised: May 22, 2015; accepted: May 29, 2015.
From Departamento de Física e Biofísica, Instituto de Biociências de Botucatu-IBB, UNESP—Univ Estadual Paulista, Botucatu/SP, Brazil (GG, JRM, ALMP, AFFA, MDO); Departamento de Doenças Tropicais e Diagnóstico por Imagem, Faculdade de Medicina de Botucatu, UNESP—Univ Estadual Paulista, Botucatu/SP, Brazil (SMR, PCMP, DRP); and Centro Brasileiro de Pesquisas Físicas-CBPF/MCT, Rio de Janeiro/RJ, Brazil (SBD).
Reprints: Diana Rodrigues Pina, PhD, Univ Estadual Paulista Júlio de Mesquita Filho—UNESP Botucatu, São Paulo, Brazil (e-mail: drpina@fmb.unesp.br).
The authors have no funding or conflicts of interest to disclose.

ISSN: 0025-7974
DOI: 10.1097/MD.0000000000001044

INTRODUCTION

Pulmonary diseases, including tuberculosis (TB) infection, cause an unacceptably large number of deaths, even given that most are preventable if people can access healthcare for proper diagnosis and treatment.[1,2] The launch of a new international strategy for TB care and control by the World Health Organization (WHO) in the mid-1990s allowed the development of new diagnostic and treatment methods.[1,2] While new treatments for TB are being developed, tools that are used to monitor the efficacy of TB treatments and quantify the disease remain limited and antiquated in both preclinical and clinical settings.[3]

Tuberculosis and others pulmonary diseases involve inflammation of the lung parenchyma, resulting in ongoing fibrotic scar formation of the pulmonary interstitium and alveoli.[4,5] Chest radiography and sputum bacilloscopy are the primary tools for medical examination and the routine diagnosis of TB, even in well-equipped medical centers where skin testing is available.[6,7] Physicians generally make decisions on TB cases mainly based on radiologic findings, combined with demographic and clinical data.[6,8] High-resolution computed tomography (HRCT) can be useful when chest radiographs are inconclusive or complications of TB are suspected.[9] However, this method results in higher radiation doses for the patients (ie, 2 orders of magnitude higher than radiographic examinations) and is associated with extremely high costs to the institution compared with chest radiography.[10–12] Moreover, in many cases the chest radiography is the only imaging examination in the diagnosis and follow-up of the patient.[6,8]

The quantification of TB by radiologists is commonly done on visual and subjective examination. An objective quantification tool is greatly important for the reliable and accurate assessment of TB's pulmonary inflammatory process (PIP).[3] Reliable assessment helps physicians with follow-up of the patient's disease.[3] The preliminary TB diagnosis is normally realized through chest radiography. However, the objective quantification of pulmonary diseases has been developed with HRCT scans[3,4,13–15] because of its higher resolution.[16]

The purpose of this work was to develop an objective method for PIP quantification using chest radiography. The viability of the quantification of PIP based on radiography is demonstrated, with a lower radiation dose and cost, without the loss of a secure medical diagnosis or treatment follow-up. Furthermore, this method allows assess objectively patients which have only X-rays exams.

Physica Medica 32 (2016) 123–132

Contents lists available at ScienceDirect

Physica Medica

journal homepage: http://www.physicamedica.com

Original Paper

Association between subjective evaluation and physical parameters for radiographic images optimization

A.F.F. Alves [a], M. Alvarez [a], S.M. Ribeiro [b], S.B. Duarte [c], J.R.A. Miranda [a], D.R. Pina [b,*]

[a] Department of Physics and Biophysics, Biosciences Institute of Botucatu, São Paulo State University, Distrito de Rubião Junior S/N, Botucatu, São Paulo, 18618-000, Brazil
[b] Department of Tropical Diseases and Diagnostic Imaging, Botucatu Medical School São Paulo State University, Distrito de Rubião Junior S/N, Botucatu, São Paulo, 18618-000, Brazil
[c] Brazilian Center of Physics Research – CBPF-MCT, Dr. Xavier Sigaud, 150, Rio de Janeiro, 22290-180, Brazil

ARTICLE INFO

Article history:
Received 22 July 2015
Received in revised form 28 October 2015
Accepted 30 October 2015
Available online 10 November 2015

Keywords:
Radiology
Computed radiography
Image quality
Dose

ABSTRACT

Purpose: The purpose of this study was to develop a methodology to optimize computed radiographic techniques to image the skull, chest, and pelvis of a standard patient.
Methods: Optimization was performed by varying exposure levels with different tube voltages to generate images of an anthropomorphic phantom. Image quality was evaluated using visual grading analysis and measuring objective parameters such as the effective detective quantum efficiency and the contrast-to-noise ratio. Objective and subjective evaluations were compared to obtain an optimized technique for each anatomic region.
Results: Gold standard techniques provided a significant reduction in X-ray doses compared to the techniques used in our radiology service, without compromising diagnostic accuracy. They were chosen as follows 102 kVp/1.6 mAs for skull; 81 kVp/4.5 mAs for pelvis and 90 kVp/3.2 mAs for chest.
Conclusion: There is a range of acceptable techniques that produce adequate images for diagnosis in computed radiography systems. This aspect allows the optimization process to be focused on the patient dose without compromising diagnostic capabilities. This process should be performed through association of quantitative and qualitative parameters, such as effective detective quantum efficiency, contrast-to-noise ratio, and visual grading analysis.

Introduction

Optimization of radiographic techniques aims to balance image quality and exposure dose to the patient and is outlined in the As Low As Reasonably Achievable (ALARA) principle [1–3]. Dose levels are related to image quality, but it should not be minimized to a degree that compromises diagnostic capabilities [1,2,4–6].

Image quality can be estimated subjectively using a Visual Grading Analysis (VGA), which is a direct analysis of the image by radiologists and can be performed in anthropomorphic phantom radiographs [7]. However, particularly with digital systems, sometimes VGA is not sufficient to make distinctions between different techniques.

In this case, objective parameters are extremely useful to investigate image quality and numerous attempts were made to optimize digital radiography systems. For example, some authors investigated the association of signal-to-noise ratio (SNR) and clinical observer evaluations to optimize images [8]. Additionally contrast-to-noise ratio (CNR) was used to optimize beam quality for regions of different attenuation such as the lung, heart, and abdomen [9].

Other metrics such as the detective quantum efficiency (DQE) and the effective DQE (eDQE) have been used to assess image quality in digital radiography systems [10,11]. The eDQE seems adequate to characterize system performance in a relevant clinical context, although it lacks the incorporation of the risk to the patient, which is evidenced by the effective dose measurement. The effective dose efficiency (eDE) managed to incorporate the effective dose into the eDQE metric and has been evaluated in chest radiographs [12].

However, in our understanding the incorporation of the effective dose value into the eDQE metric could influence the choice of an optimal technique over another with better performance in radiography systems. Therefore, in this present study we chose to analyze the eDQE and the effective dose separately and balance those two parameters to choose radiographic techniques with lower risk for the patient.

* Corresponding author. Prof. Montenegro Avenue, Rubião Junior District, Botucatu, São Paulo, 18618-970, Brazil. Tel.: +55 14 38801281; fax: +55 14 38801674.
E-mail addresses: allan@ibb.unesp.br (A.F.F. Alves), matheus@ibb.unesp.br (M. Alvarez), sribeiro@fmb.unesp.br (S.M. Ribeiro), sbd@cbpf.br (S.B. Duarte), jmiranda@ibb.unesp.br (J.R.A. Miranda), drpina@fmb.unesp.br (D.R. Pina).

http://dx.doi.org/10.1016/j.ejmp.2015.10.095
1120-1797/

Physica Medica 32 (2016) 1019–1024

Contents lists available at ScienceDirect

Physica Medica

journal homepage: http://www.physicamedica.com

Technical note

Occupational radiation exposure in vascular interventional radiology: A complete evaluation of different body regions

Fernando Antonio Bacchim Neto [a], Allan Felipe Fattori Alves [a], Yvone Maria Mascarenhas [b], Patrícia Nicolucci [c], Diana Rodrigues de Pina [d,*]

[a] Instituto de Biociências de Botucatu, Departamento de Física e Biofísica, UNESP — Universidade Estadual Paulista, Distrito de Rubião Junior S/N, Botucatu, 18618-000 São Paulo, Brazil
[b] Sapra Landauer, Rua Cid Silva César, 600, São Carlos, 13562-400 São Paulo, Brazil
[c] CIDRA – Centro de Instrumentação, Dosimetria e Radioproteção, Faculdade de Filosofia, Ciências e Letras de Ribeirão Preto, USP — Universidade de São Paulo, Av. Bandeirantes, 3900 Bairro Monte Alegre, Ribeirão Preto, 14040-901 São Paulo, Brazil
[d] Departamento de Doenças Tropicais e Diagnóstico por Imagem, Faculdade de Medicina de Botucatu, UNESP — Universidade Estadual Paulista, Distrito de Rubião Junior S/N, Botucatu, 18618-000 São Paulo, Brazil

ARTICLE INFO

Article history:
Received 8 April 2016
Received in Revised form 10 June 2016
Accepted 29 June 2016
Available online 21 July 2016

Keywords:
Radiation protection
Interventional radiology
Occupational exposure

ABSTRACT

Purpose: To perform a complete evaluation on radiation doses, received by primary and assistant medical staff, while performing different vascular interventional radiology procedures.
Materials and methods: We evaluated dose received in different body regions during three categories of vascular procedures: lower limb angiography (Angiography), lower limb percutaneous transluminal angioplasty (Angioplasty) and stent graft placement for abdominal aortic aneurysm treatment (A. A. A. Treatment). We positioned the dosimeters near the eye lens, thyroid, chest, abdomen, hands, and feet of the interventional physicians. Equivalent dose was compared with annual dose limits for workers in order to determine the maximum number of procedures per year that each physician could perform. We assessed 90 procedures.
Results: We found the highest equivalent doses in the A. A. A. Treatment, in which 90% of the evaluations indicated at least one region receiving more than 1 mSv per procedure. Angioplasty was the only procedural modality that provided statistically different doses for different professionals, which is an important aspect on regards to radiological protection strategies. In comparison with the dose limits, the most critical region in all procedures was the eye lens.
Conclusions: Since each body region of the interventionist is exposed to different radiation levels, dose distribution measurements are essential for radiological protection strategies. These results indicate that dosimeters placed in abdomen instead of chest may represent more accurately the whole body doses received by the medical staff. Additional dosimeters and a stationary shield for the eye lens are strongly recommended.

1. Introduction

Interventional radiology (IR) is an area of radiology that exposes medical staff to the highest doses of radiation [1–3]. The scattered radiation to which medical staff are usually exposed to comes mainly from the patient, therefore professionals who remain close to the patient receive highest levels of radiation [4]. Many other factors can influence the levels of exposure for medical staff, including the professional height, positioning in the room, the X-ray tube position relatively to table and patient, the use of radiological protection equipment, the total exposure time during the procedure and the condition of fluoroscopy and image acquisition [1–3].

Several studies have evaluated radiation exposure in IR to both describe medical staff exposure and improve radiological protection strategies [1,4,5]. However, these studies concentrated on a specific procedure or specific body region. Dosimetry is usually acquired under artificial conditions or neglects important body regions such as the abdomen [1,5,6].

The aim of our study was to investigate radiation exposure profiles in medical staff during different vascular IR procedures. We

* Corresponding author.
E-mail addresses: bacchim@ibb.unesp.br (F.A. Bacchim Neto), allan@ibb.unesp.br (A.F.F. Alves), yvone@sapra.com.br (Y.M. Mascarenhas), nicol@usp.br (P. Nicolucci), drpina@fmb.unesp.br (D.R.d. Pina).

http://dx.doi.org/10.1016/j.ejmp.2016.06.014
1120-1797/

Physica Medica 37 (2017) 58–67

Contents lists available at ScienceDirect

Physica Medica

journal homepage: http://www.physicamedica.com

Original paper

Efficiency of personal dosimetry methods in vascular interventional radiology

Fernando Antonio Bacchim Neto [a], Allan Felipe Fattori Alves [a], Yvone Maria Mascarenhas [b], Guilherme Giacomini [a], Nadine Helena Pelegrino Bastos Maués [a], Patrícia Nicolucci [c], Carlos Clayton Macedo de Freitas [d], Matheus Alvarez [e], Diana Rodrigues de Pina [f,*]

[a] São Paulo State University (UNESP), Instituto de Biociências de Botucatu, Departamento de Física e Biofísica, Botucatu 18618-000, São Paulo, Brazil
[b] Sapra Landauer, Rua Cid Silva César, 600, São Carlos 13562-400, São Paulo, Brazil
[c] Universidade de São Paulo (USP), Faculdade de Filosofia, Ciências e Letras de Ribeirão Preto, Centro de Instrumentação, Dosimetria e Radioproteção (CIDRA), Av. Bandeirantes, 3900 Bairro Monte Alegre, Ribeirão Preto 14040-901, São Paulo, Brazil
[d] São Paulo State University (UNESP), Faculdade de Medicina de Botucatu, Departamento de Neurologia, Psicologia e Psiquiatria, Botucatu 18618-000, São Paulo, Brazil
[e] Consult, Rua Sinharinha Frota, 1064, Matão 15990-060, São Paulo, Brazil
[f] São Paulo State University (UNESP), Faculdade de Medicina de Botucatu, Departamento de Doenças Tropicais e Diagnóstico por Imagem, Botucatu 18618-000, São Paulo, Brazil

ARTICLE INFO

Article history:
Received 30 January 2017
Received in Revised form 3 April 2017
Accepted 11 April 2017

Keywords:
Effective dose
Personal dosimetry
Interventional radiology
Anthropomorphic phantom

ABSTRACT

Purpose: The aim of the present study was to determine the efficiency of six methods for calculate the effective dose (*E*) that is received by health professionals during vascular interventional procedures.
Methods: We evaluated the efficiency of six methods that are currently used to estimate professionals' *E*, based on national and international recommendations for interventional radiology. Equivalent doses on the head, neck, chest, abdomen, feet, and hands of seven professionals were monitored during 50 vascular interventional radiology procedures. Professionals' *E* was calculated for each procedure according to six methods that are commonly employed internationally. To determine the best method, a more efficient *E* calculation method was used to determine the reference value (reference *E*) for comparison.
Results: The highest equivalent dose were found for the hands (0.34 ± 0.93 mSv). The two methods that are described by Brazilian regulations overestimated *E* by approximately 100% and 200%. The more efficient method was the one that is recommended by the United States National Council on Radiological Protection and Measurements (NCRP). The mean and median differences of this method relative to reference *E* were close to 0%, and its standard deviation was the lowest among the six methods.
Conclusions: The present study showed that the most precise method was the one that is recommended by the NCRP, which uses two dosimeters (one over and one under protective aprons). The use of methods that employ at least two dosimeters are more efficient and provide better information regarding estimates of *E* and doses for shielded and unshielded regions.

1. Introduction

Physicians who perform interventional X-ray procedures are exposed to the highest radiation doses compared with all other health professionals [1]. Several studies have shown that such physicians are exposed to non-uniform radiation levels throughout their bodies during interventional procedures [2–4].

The effective dose (*E*) is a physical quantity that is used to measure the detriment that is caused by radiation in the human body, thus providing important information for radiological protection purposes. The *E* value depends on equivalent doses that are measured in different organs and tissues of the body, which are usually the most sensitive to stochastic effect induction [5]. During each procedure, professionals use a personal dosimeter on the chest or abdomen to estimate the *E* that is received [5].

Different methods are used to estimate *E* during interventional procedures [6]. In Europe, a single personal dosimeter that is positioned on the anterior chest below the radiological protective apron was previously considered a good estimate of *E* [5,6].

* Corresponding author at: Departamento de Doenças Tropicais e Diagnóstico por Imagem, Faculdade de Medicina de Botucatu – FMB, Universidade Estadual Paulista "Júlio de Mesquita Filho" – UNESP, P.O. BOX 576, 18618-000 Botucatu, São Paulo, Brazil.
E-mail addresses: bacchim@ibb.unesp.br (F.A. Bacchim Neto), allan@ibb.unesp.br (A.F.F. Alves), yvone@sapra.com.br (Y.M. Mascarenhas), giacomini@ibb.unesp.br (G. Giacomini), nadine.maues@gmail.com (Nadine Helena Pelegrino Bastos Maués), nicol@usp.br (P. Nicolucci), cclayton@fmb.unesp.br (C.C.M. de Freitas), matheus@ibb.unesp.br (M. Alvarez), drpina@fmb.unesp.br (D.R.d. Pina).

http://dx.doi.org/10.1016/j.ejmp.2017.04.014
1120-1797/

Radiation Protection Dosimetry (2018), pp. 1–7 doi:10.1093/rpd/ncy181

ABDOMEN–PELVIS COMPUTED TOMOGRAPHY PROTOCOL OPTIMIZATION: AN IMAGE QUALITY AND DOSE ASSESSMENT

Nadine Helena Pelegrino Bastos Maués[1], Allan Felipe Fattori Alves[1], Ana Luiza Menegatti Pavan[1], Sergio Marrone Ribeiro[2], Seizo Yamashita[2], André Petean Trindade[2], Yvone Maria Mascarenhas[3], Patrícia Nicolucci[4] and Diana Rodrigues de Pina[2,*]
[1]São Paulo State University (UNESP), Instituto de Biociências de Botucatu, Departamento de Física e Biofísica, Botucatu 18618-000, São Paulo, Brazil
[2]São Paulo State University (UNESP), Faculdade de Medicina de Botucatu, Departamento de Doenças Tropicais e Diagnóstico por Imagem, Botucatu 18618-000, São Paulo, Brazil
[3]Sapra Landauer, Rua Cid Silva César, 600, São Carlos 13562-400, São Paulo, Brazil
[4]Universidade de São Paulo (USP), Faculdade de Filosofia, Ciências e Letras de Ribeirão Preto, Centro de Instrumentação, Dosimetria e Radioproteção (CIDRA), Av. Bandeirantes, 3900 Bairro Monte Alegre, Ribeirão Preto 14040-901, São Paulo, Brazil

*Corresponding author: drpina@fmb.unesp.br

Received 24 March 2018; revised 20 September 2018; editorial decision 21 September 2018; accepted 19 October 2018

Computed tomography (CT) has a high level of sensitivity and specificity for the diagnosis and follow-up of pathologies of the abdomen–pelvis region. Some features, such as automatic tube current modulation (ATCM), permits the acquisition of quality images with low radiation doses. This study evaluated the image quality and radiation dose of abdomen–pelvis CT protocols with ATCM technique. Were performed five CT protocols using 16-slice and 64-slice scanners, an anthropomorphic phantom for dosimetric measurements, an analytical phantom and retrospective examinations for image quality analysis. Were found significant reduction in effective dose. The highest absorbed doses were found in the stomach and spleen (56.1 and 47.2 mGy, respectively). Objective parameters as noise, low contrast and spatial resolution did not significantly differ between the protocols ($p > 0.05$). All protocols received the range of 'Optimum/Acceptable' in patient's image quality analysis. This methodology can be reproduced in any clinical routine to optimize CT protocols.

INTRODUCTION

Computed tomography (CT) has a high level of sensitivity and specificity and is widely used for the diagnosis and follow-up of pathologies of the abdomen–pelvis region[1, 2]. It is highly sensitive for the diagnosis of ureteric calculus, appendicitis, bone metastases, and bowel and mesenteric injuries, with sensitivities of 92, 100, 71–100 and 82%, respectively[1]. In 2008 and 2014, respectively, the French Speaking Society of Medical Emergencies and European Association of Urology recommended CT as the first-line imaging modality to investigate suspected cases of renal colic[2]. In the follow-up cases of ovarian cancer and nearly all pancreatic diseases, CT is considered the gold-standard imaging modality[3, 4].

The possibility of acquiring a large number of images in a short scanning time substantially has increased the number of CT exams that are performed in clinical routines. This has consequently increased the radiation doses that are received by patient populations, which has become a public health concern[4, 5]. Published data indicate that 70% of the radiation doses that are received by patients who undergo medical imaging is attributable to CT examinations[1, 6]. Furthermore, 31% of the annual radiation doses that are received from different imaging modalities is attributable to abdomen–pelvis CT exams[4]. This creates a concern about the high radiation doses that are received by patients, especially pediatric patients, and the well-known association between the risk of cancer and radiation exposure[5, 7, 8].

Based on the ALARA principle (As Low As Reasonably Achievable), radiology examinations must achieve a balance between radiation doses and image quality, with the continual goal of reducing the doses that are received by patients[2, 9]. With advances in CT scanners, some features (e.g. automatic tube current modulation [ATCM]) permit the acquisition of high-quality images with low radiation doses[10]. ATCM automatically adjusts the tube current (mA) during each gantry rotation according to the patient's size and attenuation body area[1, 3] to achieve a specific degree of image quality[11], which reduces radiation exposure compared with fixed tube current techniques[1, 10]. Previous studies found that ~60% of the radiation dose can be reduced with ATCM[1, 2, 12, 13].

Am J Otolaryngol 39 (2018) 431–435

Contents lists available at ScienceDirect

Am J Otolaryngol

journal homepage: www.elsevier.com/locate/amjoto

Cochlear implants: Insertion assessment by computed tomography☆

Ana Luiza Menegatti Pavan[a], Allan Felipe Fattori Alves[a], Guilherme Giacomini[a], João Maurício Carrasco Altemani[b], Arthur Menino Castilho[b], Raquel Andrade Lauria[b], Vagner Antonio Rodrigues da Silva[b], Alexandre Caixeta Guimarães[b], Diana Rodrigues de Pina[c,*]

[a] Instituto de Biociências de Botucatu, Universidade Estadual Paulista (IBB-UNESP), Botucatu, São Paulo, Brazil
[b] Hospital de Clínicas, Universidade Estadual de Campinas (HC-UNICAMP), Campinas, São Paulo, Brazil
[c] Faculdade de Medicina de Botucatu, Universidade Estadual Paulista (FMB-UNESP), Botucatu, São Paulo, Brazil

ARTICLE INFO

Keywords:
Cochlear implants
Computed tomography
Insertion measurements
Image reconstruction

ABSTRACT

Background and objectives: Imaging exams play a key role in cochlear implants with regard to both planning implantation before surgery and quality control after surgery. The ability to visualize the three-dimensional location of implanted electrodes is useful in clinical routines for assessing patient outcome. The aim of this study was to evaluate linear and angular insertion depth measurements of cochlear implants based on conventional computed tomography.

Methods: Tools for linear and angular measurements of cochlear implants were used in computed tomography exams. The tools realized the insertion measurements in an image reconstruction of the CIs, based on image processing techniques. We comprehensively characterized two cochlear implant models while obviating possible changes that can be caused by different cochlea sizes by using the same human temporal bones to evaluate the implant models.

Results: The tools used herein were able to differentiate the insertion measurements between two cochlear implant models widely used in clinical practice. We observed significant differences between both insertion measurements because of their different design and construction characteristics (p = 0.004 and 0.003 for linear and angular measurements, respectively; t-test). The presented methodology showed to be a good tool to calculate insertion depth measurements, since it is easy to perform, produces high-resolution images, and is able to depict all the landmarks, thus enabling measurement of the angular and linear insertion depth of the most apical electrode contacts.

Conclusion: The present study demonstrates practical and useful tools for evaluating cochlear implant electrodes in clinical practice. Further studies should measure preoperative and postoperative benefits in terms of speech recognition and evaluate the preservation of residual hearing in the implanted ear. Such studies can also determine correlations between surgical factors, electrode positions, and performance. In addition to refined surgical techniques, the precise evaluation of cochlear length and correct choice of cochlear implant characteristics can play an important role in postoperative outcomes.

1. Introduction

Cochlear implants (CIs) functionally restore hearing in individuals with profound hearing impairment [1–4]. An array of electrodes is introduced into the cochlea, and electrical pulses are applied across the array to stimulate residual populations of dendritic and spiral ganglion nerve bodies. Most individuals are able to obtain 40–80% correct postoperative word recognition with their CI compared with zero or only modest scores preoperatively [5]. Although the implantation procedure is safe and reliable, complications occur in approximately 16% of patients [6]. Following cochlear implantation, there is the possibility that residual hearing can be lost because of the surgical procedure itself or progression of the underlying pathology [7,8]. A greater focus has been placed on minimizing insertion trauma and preserving preexisting hearing [9,10]. For electroacoustic stimulation to be the most effective, the patient's residual hearing should be preserved during CI surgery [4,7,10–12]. Thus, selecting the optimal insertion depth should be patient-specific and based on the corresponding

☆ Conflict of Interest: The authors declare that they have no conflict of interest.

* Corresponding author at: Faculdade de Medicina de Botucatu, Departamento de Doenças Tropicais e Diagnóstico por Imagem, Universidade Estadual Paulista—UNESP, Distrito de Rubiao Junior S/N, Botucatu 18618-000, São Paulo, Brazil.
E-mail address: drpina@fmb.unesp.br (D.R. de Pina).

https://doi.org/10.1016/j.amjoto.2018.04.009
Received 13 March 2018

J Pediatr (Rio J). 2018;xxx(xx):xxx–xxx

Jornal de Pediatria
www.jped.com.br

ORIGINAL ARTICLE

Radiographic predictors determined with an objective assessment tool for neonatal patients with necrotizing enterocolitis☆

Allan Felipe Fattori Alves[a,1], Ana Luiza Menegatti Pavan[a,1], Guilherme Giacomini[a], Caio Cesar Quini[a], Sergio Marrone Ribeiro[b], Rozemeire Garcia Marquez[b], Maria Regina Bentlin[b], André Petean Trindade[b], José Ricardo de Arruda Miranda[a], Diana Rodrigues de Pina[b,*]

[a] *Universidade Estadual Paulista (UNESP), Instituto de Biociências de Botucatu (IBB), Botucatu, SP, Brazil*
[b] *Universidade Estadual Paulista (UNESP), Faculdade de Medicina de Botucatu (FMB), Botucatu, SP, Brazil*

Received 25 February 2018; accepted 17 May 2018

KEYWORDS
Necrotizing enterocolitis;
Abdominal radiography;
Image processing;
Texture analyses, wavelet

Abstract

Objectives: The objective of this study was to develop and validate a computational tool to assist radiological decisions on necrotizing enterocolitis.

Methodology: Patients that exhibited clinical signs and radiographic evidence of Bell's stage 2 or higher were included in the study, resulting in 64 exams. The tool was used to classify localized bowel wall thickening and intestinal pneumatosis using full-width at half-maximum measurements and texture analyses based on wavelet energy decomposition. Radiological findings of suspicious bowel wall thickening and intestinal pneumatosis loops were confirmed by both patient surgery and histopathological analysis. Two experienced radiologists selected an involved bowel and a normal bowel in the same radiography. The full-width at half-maximum and wavelet-based texture feature were then calculated and compared using the Mann–Whitney U test. Specificity, sensibility, positive and negative predictive values were calculated.

Results: The full-width at half-maximum results were significantly different between normal and distended loops (median of 10.30 and 15.13, respectively). Horizontal, vertical, and diagonal wavelet energy measurements were evaluated at eight levels of decomposition. Levels 7 and 8 in the horizontal direction presented significant differences. For level 7, median was 0.034 and 0.088 for normal and intestinal pneumatosis groups, respectively, and for level 8 median was 0.19 and 0.34, respectively.

☆ Please cite this article as: Fattori Alves AF, Menegatti Pavan AL, Giacomini G, Quini CC, Marrone Ribeiro S, Garcia Marquez R, et al. Radiographic predictors determined with an objective assessment tool for neonatal patients with necrotizing enterocolitis. J Pediatr (Rio J). 2018. https://doi.org/10.1016/j.jped.2018.05.017

* Corresponding author.
E-mail: drpina@fmb.unesp.br (D. Rodrigues de Pina).
[1] These authors contributed equally to this work.

https://doi.org/10.1016/j.jped.2018.05.017

Allan Felipe FATTORI ALVES

Traitement d'images pour le rehaussement de l'AVC ischémique sur des examens de tomographie

Résumé : L'Accident Vasculaire Cérébral (AVC) est l'une des principales causes de décès dans le monde. Le scanner et l'Imagerie par Résonance Magnétique (IRM) sont les deux principales techniques d'imagerie utilisées pour détecter les AVC. L'examen par scanner reste donc la principale méthode de diagnostic. Dans la plupart des cas, l'évaluation de la région cérébrale compromise est effectuée de manière subjective et peut entraîner des difficultés pour déterminer la région atteinte. Ce travail de thèse propose une approche basée sur un algorithme permettant de mettre en évidence les régions atteintes d'AVC ischémique dans les examens de scanner rétrospectifs. Différentes méthodes de traitement des images ont été utilisées pour réhausser les régions des tissus ischémiques. Afin de permettre aux médecins moins expérimentés de détecter de manière fiable les signes précoces AVC, une nouvelle approche est proposée pour améliorer la perception visuelle de l'accident ischémique cérébral. Une série de 41 images scanner rétrospectifs ont été utilisées, réparties en 25 cas d'AVC ischémiques et 16 patients normaux. Les cas d'AVC ont été obtenus dans les 4,5 heures suivant l'apparition des symptômes. Après la sélection des coupes importantes, une moyenne d'image est effectuée pour réduire le bruit. Ensuite, un modèle de décomposition variationnelle est appliqué afin de conserver la composante pertinente de l'image. Enfin, un algorithme d'espérance-maximisation est appliqué. Un test est proposé afin d'évaluer la performance des observateurs dans un environnement clinique avec et sans l'aide d'images rehaussées. La sensibilité globale de l'analyse de l'observateur a été améliorée de 64,5% à 89,6% et la spécificité de 83,3% à 91,7%. Ces résultats montrent l'importance d'un outil informatique d'aide à la décision en neuroradiologie, notamment dans les situations critiques telles que le diagnostic d'accident ischémique cérébral.

Mots clés: Accident vasculaire cérébral. Cerveau. Algorithmes. Scan tomographique. Diagnostic précoce.

Image Processing for Enhancement of Ischemic Stroke in Computed Tomography Examinations

Abstract : Stroke is one of the highest causes of death worldwide. Non-enhanced computed tomography (CT) and nuclear magnetic resonance imaging (MRI) are the two main imaging techniques used to detect stroke. CT has a lower cost and greater accessibility of the population, so it is still the main method used. In most cases, the assessment of the compromised brain area is performed subjectively and may lead to difficulties in diagnosis. This research proposes an approach based on a computational algorithm, highlighting regions of ischemic stroke. Different image processing methods were used to enhance ischemic tissues. A set of 41 retrospective CT scans from Botucatu Medical School (Brazil) was used, divided into 25 cases of acute ischemic stroke and 16 normal patients. Stroke cases were obtained within 4.5 h of symptom onset. After selection of CT slices, image averaging was performed to reduce the noise. This was followed by a variational decomposition model and the expectation maximization method was applied to generate enhanced images. We determined a test to evaluate the performance of observers in a clinical environment with and without the aid of enhanced images. The overall sensitivity of the observer's analysis was 64.5 % and increased to 89.6 % and specificity was 83.3 % and increased to 91.7 %. These results show the importance of a computational tool to assist neuroradiology decisions, especially in critical situations such as the diagnosis of ischemic stroke.

Keywords: Stroke. Brain. Algorithms. Computed Tomography. Early diagnosis.

Instituto de Biociências de Botucatu, Departamento de Física e Biofísica, UNESP – São Paulo State University, P.O. BOX 510, Distrito de Rubião Junior S/N, Botucatu, São Paulo 18618-000, Brazil

Laboratory I3MTO – University of Orleans, 5 Rue de Chartres, BP 6744, 45072 Orléans, France